STUDY OF MULTI-SCALE PLANT-GROUNDWATER INTERACTIONS

A Dissertation

by

SI GOU

Submitted to the Office of Graduate and Professional Studies of
Texas A&M University
in partial fulfillment of the requirements for the degree of

DOCTOR OF PHILOSOPHY

Chair of Committee,	Gretchen Miller
Committee Members,	Anthony Cahill
	Huilin Gao
	Binayak Mohanty
Head of Department,	Robin Autenrieth

August 2014

Major Subject: Civil Engineering

ABSTRACT

Groundwater serves as one of the main and reliable water sources for human-being and groundwater dependent ecosystems (GDEs). GDEs are threatened by insufficient groundwater supply, due to increasing groundwater extraction and climate change. Sustainable groundwater management should address the water needs for both human and ecosystems, which requires a better understanding of the complex interactions between GDEs and groundwater. This dissertation examines plant-groundwater interactions and their implications at a range of scales.

At the plant scale (~1 m^2), a physically-based model was developed to explore the hydraulic mechanisms of plant groundwater use. New functions of root water uptake and hydraulic redistribution (HR) in the model were driven by the potential gradients along the groundwater-soil-plant-atmosphere continuum, and a new water stress function was based on the linear relationship between stomatal conductance and root hydraulic conductance. These functions were further incorporated into a groundwater-land surface model, ParFlow.CLM, to develop a spatial distributed ecohydrological model at the stand scale (~1000 m^2). The modified ParFlow.CLM was used to conduct a 8-year simulation with half hourly time step at a AmeriFlux oak savanna site in California. It performed well when simulating daily, hourly, and spatial changes of water and energy dynamics. It captured the seasonal shift of plant water source from soil water during the wet season to groundwater during the dry season. The model simulated both hydraulic

lift and hydraulic descent during oak active and dormant seasons. The model suggested that HR at this site was a mechanism for oaks to compete for water with annual grasses.

At the regional scale (~1000 km^2), a method was proposed to identify vegetative GDEs using remote sensing data and to generate a detailed GDEs map for the Edwards aquifer region in Texas. This method used Landsat ETM+ and MODIS images to track the changes of NDVI for each vegetation pixel under different precipitation conditions. The NDVI dynamics were used to identify the vegetation with high potential to use groundwater. The method produces a detailed map of potential GDEs, which represents the first step towards sustainable water management associated with these ecosystems.

ACKNOWLEDGEMENTS

Firstly, I would like to thank my advisor, Dr. Gretchen Miller, for all her guidance, encouragement and help. I really thank Dr. Miller for showing trust in me by allowing me to conduct research freely and independently. She encouraged me to go further and dig deeper in research, when I tended to give up without thinking about other possibilities. She encouraged me to pursue an academic career and became a great role model for me. Within my four-year PhD study, I learned a lot from her—how to maintain a balance between life and research, how to conduct research and teaching, how to build a research group, how to improve writing and presentation skills…I believe I will keep benefiting from these experiences. I will continue to abide by the words of wisdom she gave to me, "Don't let perfection become the enemy of good," which relieved my stress during my study.

I am sincerely grateful to my committee members, Dr. Anthony Cahill, Dr. Huilin Gao, and Dr. Binayak Mohanty. They gave me many valuable suggestions to my research. They taught me how to think, through classes and our discussions. They were always patient and helpful whenever I approached them for questions and suggestions. I would also like to thank Dr. Ian Ferguson at U.S. Bureau of Reclamation and Dr. Reed Maxwell at Colorado School of Mines, who helped me a lot in learning ParFlow.CLM model.

I would like to acknowledge my two master advisors, Professors Hao Wang and Dayong Qin at China Institute of Water Resources and Hydropower Research. They

encouraged me to pursue Ph.D. abroad and provided me numerous support and encouragement. It is very delightful to share my research progress and Ph.D. life with them frequently. Sadly, Professor Qin was unable to see me graduate. He had fought against blood cancer for ten years. He taught me how to be brave.

I want to acknowledge all my colleagues in geoecohydrology group, Charles Bruc, Andrea DuMont, Susana Gonzalez, Jenna Kromann, Monica Long, Boris Minot, Mark Pauls, Ben Smith, Catalina Suarez, Cody Saville, Jonathan Sanders, and Jingqiu Zhang, for their help, support and many inspiring discussions. In particular, I would like to thank Susana Gonzalez, who has contributed a lot to GIS data collection and analysis. I really enjoyed working with her. I am greatly indebted to my friends over these years, for companion and support from Yuhang Duan, Allison Guettner, Yuxin He, Xiaohui Li, Chaoyi Wang, Jingqiu Zhang, and Nana Zhao especially.

I would like to acknowledge funding from the Schlumberger Foundation in the form of a Faculty for the Future Fellowship, which supported my tuitions, fees, living expenses and conference travel since 2011. I would also like to acknowledge funding from the Texas Water Resources Institute in the form of a Mills Scholarship.

Finally, I would like to thank my parents, Zhongqing Gou and Liping Sun, for all the support and love they have given me throughout my life. I must thank my husband, Qiang Chen, for all his unwavering trust and support. He always encourages me to fulfill my dreams, helps me build my self-confidence, acts as my stress reliever, and provides invaluable suggestions to my life and research. His love and patience helped both of us get through these tough years. I am always learning how to love from him.

TABLE OF CONTENTS

Page

LIST OF FIGURES

Page

LIST OF TABLES

CHAPTER I

INTRODUCTION

Groundwater provides a reliable source for anthropogenic water use, and also serves as one of the main water sources for particular ecosystems. These ecosystems, known as groundwater dependent ecosystems (GDEs), rely on or partly rely on either the surface expression or subsurface presence of groundwater. The groundwater consumption of GDEs potentially influences regional groundwater recharges and baseflow in streams, and further impacts the water available for human consumption. GDEs are especially sensitive to the stressors caused by groundwater extraction, land use practices, and climate change. Therefore, it is necessary to address these ecosystems in sustainable water and land management. Several government agencies have already incorporated considerations of GDEs in management practices and on-going research activities, including the European Union Water Framework Directive, Australian National Groundwater Action Plan, and U.S. Geological Survey Great Basin Integrated Landscape Monitoring Pilot. However, studies of GDEs are still at very early stages. Therefore, this dissertation focuses on the vegetation dependent on groundwater to develop a better understanding of plant-groundwater interactions and their implications, at perspectives ranging from a small plant scale (~1 m^2), to a medium stand scale (~1000 m^2), and to a large regional scale (~1000 km^2). This dissertation addresses the plants belong to two distinct types of groundwater-dependent ecosystems [Eamus and Froend, 2006]: 1) lowland GDEs which rely on the surface expression of groundwater and are

typically found around springs, within groundwater-fed wetlands, and along streams; 2) upland GDEs which access deeper groundwater (>2m) by their deep root system. These GDEs require the subsurface presence of groundwater, and are known as phreatophytes. A third class of GDEs is the groundwater-inhabiting microbial communities found in the saturated zone. They are substantially different in their character compared to vegetative GDEs and are not considered in this dissertation.

At different scales, the following specific questions were addressed:

- At the plant scale, this study strives to explore the mechanism underlying plant-groundwater interactions: When and how much groundwater is withdrawn by plants? Why do plants switch water uptake between soil water and groundwater during wet/dry seasons? What role does groundwater uptake play in mitigating plant water stress? This dissertation developed a physically-based model at the plant scale using system dynamics modeling approach to answer these questions.
- At the stand scale, this dissertation aims to study the spatial and temporal impacts of plant-groundwater interactions, including: How does groundwater interact with land surface processes, such as soil moisture and ET, through plant groundwater uptake and HR? How do these plant-controlled groundwater-land surface interactions drive feedbacks on the climate system? How do multiple plant species compete for available water sources at different depths? How do the plant groundwater use and the heterogeneous vegetation cover, soil types and topography influence the distributions of ET, soil moisture, infiltration, runoff and groundwater recharge? And overall, how do these interactions lead to the

complex ecohydrological implications at the stand scale? The plant-scale model was incorporated into a spatial distributed groundwater-land surface model (ParFlow.CLM) to develop a fully-integrated ecohydrological model for groundwater dependent ecosystems to test these research questions.

- At the large scale, this dissertation intends to remotely identify GDEs to answer: Where are these GDEs located? This dissertation proposed a cost-efficient method to identify the vegetative GDEs using remote sensing. It produced the detailed map of potential GDEs, which represented the first step towards sustainable water management associated with GDEs. The information of GDEs distribution was provided for groundwater managers and researchers to assess GDEs in their study areas. The GDE map could also be used for stand scale modeling in the future. It could work as the input land cover data with GDEs and non-GDEs for model simulation, so that the model could simulate the role of GDEs in ecohydrological processes at large scale.

The structure of this dissertation progresses from small scale (Chapter II) to large scale (Chapter V). In Chapter II, the mechanisms of plant-groundwater interactions were explained by the model developed at plant scale. This new phreatophytic vegetation water uptake model was driven by the potential gradients along groundwater-soil-plant-atmosphere continuum (GSPAC). The model calculated water potential and water content changes in both soil and plant media simultaneously. Water flow could be into or out of vegetation depending on the direction of water potential gradient, allowing the model to simulate hydraulic redistribution (HR) [Amenu and Kumar, 2008]. A new

water stress function was introduced that adjusts transpiration depending on the loss of hydraulic conductance along GSPAC pathway. To the best of our knowledge, it is the first time that the linear relationship between stomatal conductance and plant hydraulic conductance [Domec et al., 2006; Sperry et al., 2003] was used in model simulations of plant water stress. The differential equations developed were implemented in a system dynamics framework and were solved iteratively. The simulation methodology allows for the quantitative analysis of nonlinear systems with complex feedbacks [Forrester, 2007]. The model was applied to simulate the groundwater dependent blue oaks (Quercus douglasii) at a California oak savanna site . It performed well in capturing soil moisture dynamics, transpiration and leaf water potential of the blue oaks. This model resolved the challenge of explicitly simulating plant groundwater uptake, hydraulic redistribution, and water stress.

Plant-groundwater interactions at the plant scale can impact large scale water and energy dynamics. Therefore, the study in Chapter III integrated the representation of GDEs in Chapter II into a spatial distributed groundwater-land surface model (ParFlow.CLM). The modified model was tested at a semiarid oak savanna site and performed well, capturing the daily, hourly, and spatial water and energy patterns in a 8-year model simulation with a half-hourly time step. The model matched groundwater uptake results estimated from diurnal water table fluctuations. The simulations highlighted that the groundwater uptake from deep roots coordinated tightly with the soil water uptake from shallow roots to support transpiration and HR. It captured the seasonal shift of plant water source from soil water during the wet season to

groundwater during the dry season. It revealed an interesting finding that the time of this shift occurred when surface soil water content dropped around the point of inflection in soil water retention curve. The model simulated both hydraulic lift and hydraulic descent during the oak active and dormant seasons. It indicated that hydraulic lift promoted oak transpiration and hydraulic descent served as another pathway of downward soil water movement rather than percolation. The model also revealed that HR at this site is a competitive mechanism for oaks, allowing them to compete water with annual grasses. In Chapter IV, four scenario tests were conducted to further explain the findings from the plant scale and stand scale models in Chapter II and III. These scenarios addressed how groundwater, soil types, HR and root distribution controlled the dynamics of the whole GSPAC system.

In Chapter V, the dissertation further expanded its scope from the stand scale to the state to regional scale, placing the studies of plant-groundwater interactions into a GDE and groundwater management context. The first step effort towards GDE management was to develop a method to cost effectively identify the distribution of GDEs at scales appropriate for management. The detailed GDEs distribution produced by remote sensing may be useful for managers attempting to prioritize conservation and restoration efforts in sustainable groundwater management. It also provides researchers a guiding tool for the study of GDEs, including field-based assessment and monitoring. In the future, the product of GDE map generated from this remote sensing based method can be used as the input land cover data with GDEs and non-GDEs for the model developed in Chapter III. With these date, the model can simulate how the GDEs

impacts regional groundwater recharge and streamflow. The remote sensing based method proposed in Chapter V also highlighted the potential in documenting the changes in GDE distribution over time, which could also provide the historical land cover inputs for model simulation in the studies of water and energy changes caused by land cover changes.

CHAPTER II

MODELING PLANT WATER STRESS, UPTAKE, AND HYDRAULIC REDISTRIBUTION*

Introduction

Groundwater serves as one of the main and reliable water sources for phreatophytic vegetation; it can buffer the impacts of prolonged droughts and support the continued existence of vegetation in otherwise dry regions [*Eamus et al.*, 2006; *Orellana et al.*, 2012]. Groundwater uptake by phreatophytic vegetation has important implications for the study of the complex interactions and feedbacks in groundwater-soil-plant-atmosphere continuum (GSPAC). At the stand scale, it influences plant water use patterns and plant survival strategies under severe water limitations. At the watershed and landscape scales, it influences water and energy balance of the land surface [*Ferguson and Maxwell*, 2010; *Kollet and Maxwell*, 2008], groundwater recharge, and baseflow in streams [*Huxman et al.*, 2005; *Wilcox*, 2002a].

Several experimental approaches are available for quantifying groundwater uptake. Using diurnal water table fluctuations, the White-Loheide method [*Loheide et al.*, 2005; *White*, 1932] calculates daily groundwater consumption by phreatophytic vegetation in riparian zones [*Butler Jr et al.*, 2007; *Lautz*, 2008; *Loheide*, 2008; *Martinet*

* Reprinted with permission from "A groundwater-soil-plant-atmosphere continuum approach for modeling water stress, uptake, and hydraulic redistribution in phreatophytic vegetation" by Gou, S., and G. Miller, 2013. *Ecohydrology*, doi: 10.1002/eco.1427, Copyright 2013 by John Wiley and Sons.

et al., 2009], shallow water table areas [*Vincke and Thiry*, 2008], and even regions with relatively deep groundwater [*Miller et al.*, 2010b]. The water balance closure method is commonly used to estimate the proportion of annual water use derived from groundwater [*Scott et al.*, 2008b; *Steinwand et al.*, 2006]. Other methods, which combine stable isotope analysis of xylem and source waters with mixing models, have been used to determine spatial and temporal variations in the uptake of soil water and groundwater by phreatophytic vegetation [*Busch et al.*, 1992; *Dawson*, 1996; *Dawson and Pate*, 1996; *Meinzer et al.*, 2001]. Groundwater uptake rates also can be measured by some direct monitoring methods, such as sap flow measurements on roots [*Doody and Benyon*, 2011].

The tight linkage between plant water use patterns and spatial and temporal soil water content variation and groundwater fluctuations [*Newman et al.*, 2006] makes root water uptake modeling a challenging, but critical area. Previous efforts have focused on coupling soil water dynamics with water use by vegetation [*Feddes et al.*, 2001; *Wang and Smith*, 2004], but rarely have included plant groundwater uptake from the saturated zone. A stochastic model has been developed to analytically describe the probability distribution of root water uptake by groundwater dependent ecosystems [*Tamea et al.*, 2009] and associated long-term groundwater dynamics [*Laio et al.*, 2009]. In contrast, we develop equations that explicitly depict root water uptake processes and estimate actual groundwater uptake rates, appropriate for inclusion in process-based, land surface and vadose zone models.

The special characteristics of phreatophytic vegetation present several challenges for modeling groundwater uptake. First, a realistic model should include physically-based functions to specify the water and potential status within GSPAC. Potential gradients drive water movements through GSPAC, controlling when the dominant sources for transpired water switch between the unsaturated and saturated zones. Specific parameters of plant and soil properties are needed for these physically-based functions (Table 2.1), but some of these parameters (e.g., root distribution) are difficult to measure directly. Second, a model must simulate hydraulic redistribution (HR) across the root system, which frequently occurs at sites hosting phreatophytic vegetation [*Amenu and Kumar*, 2008; *Scott et al.*, 2008a]. HR has important implications in plant water use, namely supporting transpiration and plant growth during dry season, promoting plant water conservation by redistributing water into deeper soil, or increasing the water uptake of shallow roots by lifting water into shallow soil layers [*Caldwell et al.*, 1998; *Dawson*, 1993; *Dawson and Pate*, 1996; *Ryel et al.*, 2004; *Scott et al.*, 2008a]. Scott et al. [2008a] suggested that HR be incorporated into many ecohydrologic models due to the significant hydrologic and ecologic effects of HR and its frequent occurrence in many ecosystems. Third, modeling the influence of groundwater on plant water stress is critical for accurately simulating overall root water uptake rates.

The most commonly used approaches to simulate vegetation water stress are based on the soil moisture conditions; transpiration decreases linearly as a function of soil moisture, once the "onset of water stress" point has been reached [*Feddes et al.*,

1978; *Federer*, 1979; *Laio et al.*, 2001; *Porporato et al.*, 2001]. However, the impacts of groundwater on plant water stress status are not addressed in these approaches. In addition, roots experience various spatial and temporal soil moisture distributions that are not considered in these formulations. We hypothesize that some proportion of roots in dry layers may encounter severe water stress and nearly cease water uptake, while other roots in wet layers may still be able to access sufficient water storage to take water for transpiration. Therefore, a new water stress function is needed in order to incorporate the spatial and temporal influences of both groundwater and soil moisture on the water stress of phreatophytic vegetation.

Here, we propose a phreatophytic vegetation water uptake model, which combines a water potential gradient-based approach to simulate root water uptake from different sources with a new water stress function that adjusts transpiration depending on the loss of hydraulic conductance along the GSPAC pathway. The plant "vulnerability curve" concept is used to link the hydraulic conductance loss along the GSPAC with the water potential changes in saturated and unsaturated subsurface layers [*Sperry and Tyree*, 1988; *Sperry et al.*, 1993; *Sperry et al.*, 2003; *Sperry et al.*, 2002; *Tyree and Sperry*, 1989]. Soil and plant hydraulic conductivities are varied depending on soil and plant water potential status.

Table 2.1 Model Parameters

Parameters	Values	Units	Definition
Soil Properties			
Z_1	0.1	m	Thickness of soil layer 1
Z_2	0.2	m	Thickness of soil layer 2
Z_3	0.4	m	Thickness of soil layer 3
Z_4	8.3	m	Thickness of soil layer 4
h	9	m	Groundwater depth
ϕ	0.55	-	Porosity
f_{run}	0.94	-	Runoff coefficient (See Miller et al. 2012)
α_{soil1}	0.45	1/m	van Genuchten parameter of soil, reservoir 1
α_{soil2}	1	1/m	van Genuchten parameter of soil, reservoir 2
$\alpha_{soil3,\ 4}$	0.9	1/m	van Genuchten parameter of soil, reservoir 3 and saprolite reservoir
n_{soil1}	1.42	-	van Genuchten parameter of soil, reservoir 1
n_{soil2}	1.33	-	van Genuchten parameter of soil, reservoir 2
$n_{soil3,\ 4}$	1.35	-	van Genuchten parameter of soil, reservoir 3 and saprolite reservoir
$S_{res\ ,soil1}$	0.08	m/m	van Genuchten parameter, residual water content of soil, layer 1
$S_{res\ ,soil2}$	0.1	m/m	van Genuchten parameter, residual water content of soil, layer 2
$S_{res\ ,soil3,\ 4}$	0.13	m/m	van Genuchten parameter, residual water content of soil, layer 3 and saprolite reservoir
S_{sat}	1	m/m	van Genuchten parameter, saturated water content of all soil reservoirs
$K_{s,soil1}$	0.009	m/half an hour	Sat. hydraulic conductivity of soil, layer 1
$K_{s,soil2,\ 3,\ 4}$	0.06	m/half an hour	Sat. hydraulic conductivity of soil, layer 2, 3 and saprolite reservoir
$K_{s,gw}$	0.006	m/half an hour	Sat. hydraulic conductivity of groundwater aquifer
Plant Properties			
$K_{s\_root,i}$	0.002	m/half an hour	Hydraulic conductivity of lateral roots with 100% conductance in soil layer 1, 2, and 3
$K_{s\_root,gw}$	0.004	m/half an hour	Hydraulic conductivity of tap roots with 100% conductance reaching groundwater aquifer
K_{s_stem}	0.0004	m/half an hour	Hydraulic conductivity of stem and branch with 100% conductance
f_{s1}	0.21	fraction	Root fraction, soil layer 1
f_{s2}	0.28	fraction	Root fraction, soil layer 2
f_{s3}	0.36	fraction	Root fraction, soil layer 3

Table 2.1 Continued

Parameters	Values	Units	Definition
f_{s3}	0.36	fraction	Root fraction, soil layer 3
f_{gw}	0.15	fraction	Root fraction, groundwater aquifer
b/r	250	-	Ratio of distance between the nearby two roots (b) and root diameter (r)
r	0.002	m	Root diameter of lateral roots
l	0.2	m	Length of absorbing root part of lateral and tap roots
L	1	m	Horizontal length of transporting root part of lateral roots
$A_{t\_a\_root}$ /A_{leaf}	0.5	-	Ratio of total absorbing root surface area: leaf area without cavitation in roots

The model calculates water potential and water content changes in both soil and plant media simultaneously. Water flow may be into or out of vegetation depending on the direction of water potential gradient, allowing the model to simulate hydraulic redistribution [*Amenu and Kumar*, 2008]. The differential equations developed are implemented in a system dynamics framework. This type of simulation methodology allows for the quantitative analysis of nonlinear systems with complex feedbacks [*Forrester*, 2007], making it uniquely adept at describing the processes, patterns, and feedback loops inherent in the GSPAC.

Thus, the objective of this study was to develop a new model framework to simulate root water uptake of phreatophytic vegetation. The model was applied to a California oak savanna site, where our previous study [*Miller et al.*, 2010b] had determined that the blue oaks (*Quercus douglasii*) are obligate phreatophytes. We compared the model results against measured soil moisture, ET and leaf water potential data to test the model's performance. This paper discusses model formulation and case

study results, focusing on: a) the mechanisms of soil water-groundwater use pattern controlled by the dynamics of rhizosphere resistances, root resistances and potential gradients, b) the influence of hydraulic redistribution on plant water use patterns, and c) the feedback loops that link stomatal conductance with the water status of saturated and unsaturated layers in the subsurface.

Methods

Potential-based Function for Root Water Uptake and Hydraulic Redistribution

The system is conceptualized and illustrated using an electrical circuit analogy (Figure 2.1). The junction point between the root system and stem is set as the reference point, which is also at the same elevation of the ground surface. Each root is considered to have a transporting portion and an absorbing portion, i.e., the short absorbing zone behind the root tip [*Sperry et al.*, 1998]. Water is absorbed from unsaturated and saturated zones by the absorbing root portions, conveyed along the transporting root portions to converge at the reference point, and moved through the stem to the leaves. This uptake and transport is driven by potential gradients along the rhizosphere-leaf pathway (rhizosphere ↔ root ↔ reference point ↔ stem ↔ leaf).

Considering water absorbing and transporting of a single root within soil, we modify Gardner's equation [1960] to depict the process of absorbing water by a single root:

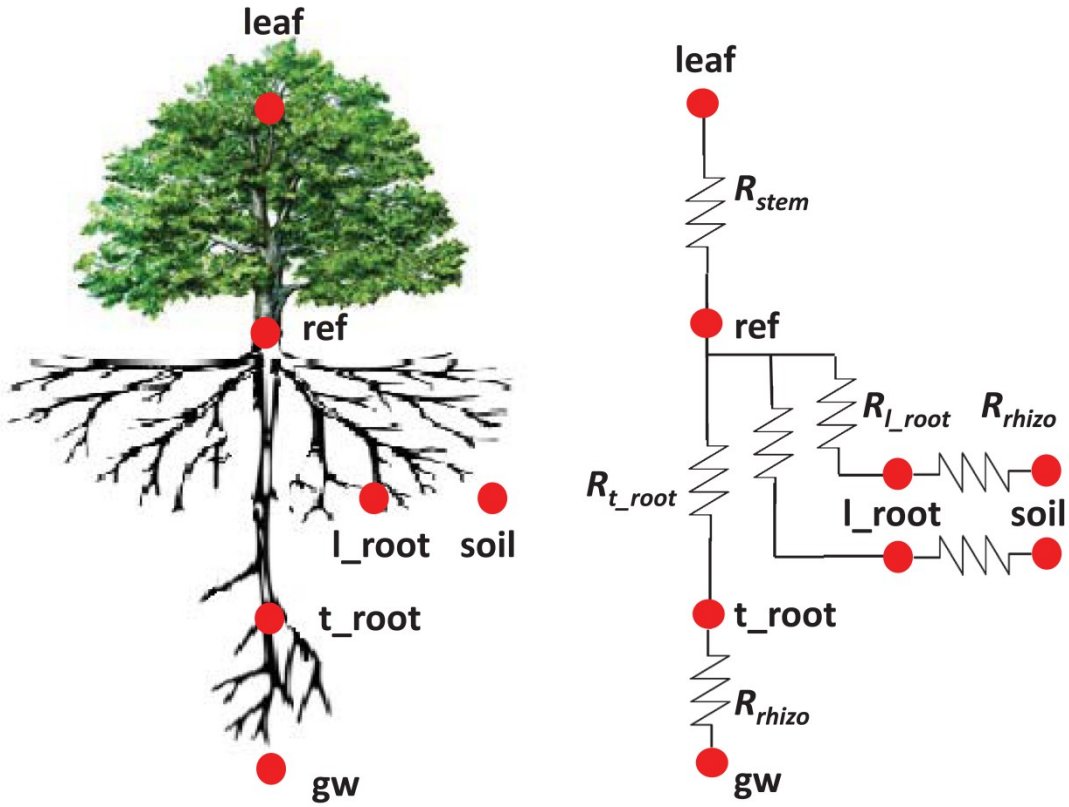

Figure 2.1 A Conceptual Diagram of Root Water Uptake Model Using Electrical Circuit Analogy. The red dots represent the water potential points within plant, soil and groundwater layers (gw, groundwater; l_root, lateral root in soil; t_root, tap root accessing groundwater; ref, reference point). These dots are connected by the resistances, which represents the different resistances along GSPAC path (R_{rhizo}, rhizosphere resistance; R_{l_root}, lateral root resistance; R_{t_root}, tap root resistance; R_{stem}, stem and branch resistance).

$$Q_{root} = 2\pi l K_{soil}(\psi_{soil}) \frac{\psi_{soil} - \psi_{root}}{\ln(\frac{b}{r})} \tag{2.1}$$

where Q_{root} is the root water uptake rate [L^3T^{-1}], Ψ_{soil} is the soil water potential, in units of hydraulic head [L] (soil and plant osmotic potentials are assumed to be negligible), Ψ_{root} is the root water potential [L], $K_{soil}(\Psi_{soil})$ is the hydraulic conductivity of the soil [LT^{-1}] which is assumed to be the same as the hydraulic conductivity of the rhizosphere zone, l is the length of the absorbing root portion [L], r is the root diameter [L], and b is the distance from the edge of the rhizosphere zone to the axis of the root [L] [*Gardner*, 1960; *Gardner*, 1965; *Gardner and Ehlig*, 1962]. We assume the water potential within rhizosphere zone is the same as the soil water potential at the outer edge of the zone. The b value defines the outer radius of the "zone of influence" for each root. Gardner's equation [1960] was derived for steady state flow conditions [*Cowan*, 1965; *Gardner*, 1960; *Newman*, 1969], but is used to approximate the transient case by assuming that the zone of influence for each root does not vary with as water uptake rates change.

The root water storage term is negligible; absorbed water is continuously moved through the transporting root portion from root to the reference point:

$$Q_{root} = \pi r^2 K_{root}(\psi_{root}) \frac{\psi_{root} - \psi_{ref} - z}{0.5l + L + z} \tag{2.2}$$

where Ψ_{ref} is the potential at the reference point [L], $K_{root}(\Psi_{root})$ is the hydraulic conductivity of the absorbing and transporting root portions [LT^{-1}], L is the horizontal length of the transporting root portion [L], and z is the vertical length of the transporting

root portion [L], which is also equal to the vertical depth from the soil layer to the reference point.

Combining equations 2.1 and 2.2, we find:

$$Q_{root} = A_{a\_root} \frac{\psi_{soil} - \psi_{ref} - z}{\Gamma_s + \Gamma_r} \tag{2.3}$$

where $A_{a\_root} = 2\pi rl$ is the area of the absorbing root surface [L^2], $\Gamma_s = \frac{r \ln(b/r)}{K_{soil}(\psi_{soil})}$ represents the resistance of the rhizosphere zone per unit absorbing root surface area [$TL^{-1}L$], and $\Gamma_r = \frac{2l(0.5l + L + z)}{rK_{root}(\psi_{root})}$ represents the resistance of the root per unit absorbing root surface area [$TL^{-1}L$].

Equation 2.3 demonstrates that root water uptake is a function of the potential gradient between the soil and the reference point. When $\Psi_{soil} - \Psi_{ref} - z > 0$, the potential gradient drives water absorption from the soil and moved upward towards the reference point. In this case, Q_{root} is a positive value, which implies water uptake by the root. If $\Psi_{soil} - \Psi_{ref} - z < 0$, the potential within root system is higher than the potential of surrounding soil. In this case, Q_{root} becomes negative, implying that water is released from the root to the soil. This release is important, as soil water content can vary significantly with depth. The roots within wet zones can be driven to uptake water by the potential gradient towards the plant, while the roots in dry areas may be driven to release water by the potential gradient towards the dry soil. Thus, Equation 2.3 also estimates hydraulic redistribution rates. We assume that root hydraulic conductivity is non-hysteretic.

Next, we divide the root zone into several soil layers and one groundwater layer. The roots in the same layer are assumed to have the same geometric and hydraulic properties. For simplicity, the model ignores root growth and assumes a "static" rooting profile during the model simulation period, although the redistribution of root may respond quickly to water table fluctuations and variations in soil moisture [*Naumburg et al.*, 2005].

Water flow from the ith soil layer is represented as:

$$Q_{s,i} = nf_{root,i} A_{a\_root,i} \frac{\psi_{soil,i} - \psi_{ref} - z_i}{\Gamma_{s,i} + \Gamma_{r,i}} \tag{2.4}$$

where $Q_{s,i}$ is the soil water uptake from or release to ith soil layer [L^3 T^{-1}], $f_{root,i}$ is the root fraction in the ith layer. The root fraction $f_{root,i}$ can be obtained from experimental data or estimated using the standard exponential model [*Jackson et al.*, 1996]. We assume all roots are first-order roots which directly connect to the reference point. The total number of the first-order roots in the whole plant is given by n. Water extracted from the groundwater layer is written using a similar formula:

$$Q_{gw} = nf_{root,gw} A_{a\_root,gw} \frac{\psi_{gw} - \psi_{ref} - h}{\Gamma_{s,gw} + \Gamma_{r,gw}} \tag{2.5}$$

where Q_{gw} is the groundwater uptake or recharge [L^3T^{-1}] and h is the depth to groundwater from the reference point [L].

The total net water uptake from all the soil and groundwater layers equals the transpiration of the phreatophytic vegetation, on the assumption that the plant water storage change is negligible:

$$T = \frac{A_{t\_a\_root}}{A_{leaf}} \left(\sum_{i=1}^{m-1} f_{root,i} \frac{\psi_{soil,i} - \psi_{ref} - z_i}{\Gamma_{s,i} + \Gamma_{r,i}} + f_{root,gw} \frac{\psi_{gw} - \psi_{ref} - h}{\Gamma_{s,gw} + \Gamma_{r,gw}} \right) \tag{2.6}$$

where, T is the plant transpiration rate [LT^{-1}] and $A_{t\_a\_root}/A_{leaf}$ is the ratio of the total absorbing root surface area to the total leaf area. We also assume that the absorbing root surface area is the same for every root, thus $A_{a\_root} = A_{a\_root,i} = A_{a\_root,gw}$ and $A_{t\_a\_root} = nA_{a\_root}$. Equation 2.6 then becomes the governing equation for the simulation of potential-based root water uptake and hydraulic redistribution. Two unknown variables, T and Ψ_{ref}, remain, requiring another equation to calculate the plant transpiration rate according to the potential ET and a water stress function (Section 2.2).

The water flux within the soil media is calculated by the Richards' equation, and the lateral soil water flux is assumed negligible in the model:

$$\frac{\partial \theta}{\partial t} = \frac{\partial}{\partial z} \left[K_{soil}(\psi_{soil}) \left(\frac{\partial \psi_{soil}}{\partial z} + 1 \right) \right] - S \tag{2.7}$$

where θ is the soil water content [L^3L^{-3}], t is time [T], S is the sink/source term [T^{-1}] that corresponds to the water uptake by roots or the water release from roots due to hydraulic redistribution. The equations for other hydrologic processes, such as infiltration, groundwater recharge and surface runoff, are similar to those presented by Miller et al. [2012].

Phreatophyte Water Stress Function based on Plant Hydraulic Conductivity Loss

The van Genuchten [1980] curve for unsaturated soil conductivity is used to describe soil water characteristics in the model. We also use a functionally similar

relationship, known as the vulnerability curve, to depict the relationship between xylem hydraulic conductivity and xylem water potential [*Sperry and Tyree*, 1988; *Tyree and Sperry*, 1989]. Vulnerability curves can be measured using experimental methods [*Pockman et al.*, 1995; *Sperry et al.*, 1988; *Sperry et al.*, 2003; *Tyree*, 1997]. In a typical vulnerability curve (Figure 2.2), xylem hydraulic conductivity declines non-linearly as xylem pressure decreases. Previous studies have also revealed that roots are more vulnerable to cavitation than stems and shoots, making them the weakest links in the GSPAC [*Jackson et al.*, 2000; *Saliendra et al.*, 1995; *Sperry and Saliendra*, 1994]. The loss of hydraulic conductance in the root system limits the whole plant's ability to uptake water to support transpiration.

Stomata sense the changes of plant water status and adjust their conductance accordingly. Sperry et al. [2003] reviewed the previous studies and indicated that "there is a strong and often linear relation between the diffusive conductance of stomata to water vapor and the hydraulic conductance of SPAC." This relationship suggests three important interactions and feedbacks between the loss of hydraulic conductance and transpiration rate: 1) the stomata respond linearly to the loss of hydraulic conductance by adjusting transpiration rate, 2) the change of transpiration rate regulates plant water potential, and 3) the altered plant water potential further influences plant hydraulic conductance to prevent catastrophic hydraulic failure of plant [*Sperry*, 2000; *Sperry and Tyree*, 1988; *Tyree and Sperry*, 1989].

Based on these findings, we introduce a new water stress function for use in root water uptake modeling of phreatophytic vegetation. For the whole root system, the loss of hydraulic conductivity is given as:

$$\xi = \frac{\frac{r_{gw}^{\ 2}}{L_{t\_gw}} K_{root,gw}(\psi_{root,gw}) f_{root,gw} + \sum_{i=1}^{m-1} \frac{r_{s,i}^{\ 2}}{L_{t\_s,i}} K_{root,i}(\psi_{root,i}) f_{root,i}}{\frac{r_{gw}^{\ 2}}{L_{t\_gw}} K_{s\_root,gw}(\psi_{root,gw}) f_{root,gw} + \sum_{i=1}^{m-1} \frac{r_{s,i}^{\ 2}}{L_{t\_s,i}} K_{s\_root,i}(\psi_{root,i}) f_{root,i}} \tag{2.8}$$

where ξ is the fractional loss of hydraulic conductivity of the whole root system. For the roots within the ith soil layer, $K_{s\_root,i}$ is the saturated root hydraulic conductivity [LT^{-1}], $r_{s,i}$ is the root diameter [L], and $L_{t\_s,i}$ is the total length of one single root [L]. This nomenclature is continued for the roots within the groundwater layer, which is labeled with the subscript "gw." The variable root hydraulic conductivity $K_{root,i}(\Psi_{root,i})$ and $K_{root,gw}(\Psi_{root,gw})$ are determined from the root xylem vulnerability curves for the species of interest.

In the model, we assume that the hydraulic conductivity loss of roots can represent the hydraulic conductivity loss of the whole GSPAC path, and the stomata respond linearly to the hydraulic conductivity loss of the whole root system. Thus, the value of ξ in Equation 2.8 directly impacts transpiration rate, and serves as the water stress in Equation 2.9:

$$T = ET_{pot}\xi \tag{2.9}$$

where ET_{pot} is the potential ET [LT^{-1}], as calculated by the Penman-Monteith equation. In addition, we assume the loss of root hydraulic conductivity recovers immediately

when the root potential increases. Therefore, the model does not incorporate the thresholds of the permanent root hydraulic conductivity loss and ignores the possible hysteresis of the vulnerability curve [*Sperry et al.*, 2003]. By combining Equations 2.6 and 2.9, the model is capable of simulating root water uptake of phreatophytic vegetation.

Model Case Study

Study Site

The Tonzi Ranch site was chosen as a test site. The site is an oak savanna located in the foothills of the western Sierra Nevada in California (latitude: 38.4311^{o}N, longitude: 120.966^{o}W, altitude: 177m). The climate is Mediterranean with a wet, cold winter and a dry, hot summer, and the mean annual precipitation is around 560 mm [*Baldocchi et al.*, 2004; *Chen et al.*, 2008; *Ma et al.*, 2007]. The dominant woody vegetation type is deciduous blue oak *(Quercus douglasii)*, and the grasses are a mix of non-native annual species [*Baldocchi et al.*, 2010]. The savanna at the site has limited annual water supply and undergoes seasonal temperature and soil water depletion extremes [*Baldocchi and Xu*, 2007]. The site is underlain by a shallow soil layer which is approximately 60-100 cm of silt loam to rocky silt loam, followed by a 4-8 m saprolite zone and then the fractured greenstone bedrock. The water table varies from 7 to 12 m below the ground surface [*Miller et al.*, 2010b].

In 2001, two eddy covariance towers were established to measure the latent heat flux at the site every half an hour, and data collection has occurred continually since [*Baldocchi et al.*, 2010]. The overstory and understory towers are 23 m and 2 m high, respectively. The difference in latent heat flux measured at the two towers can be used to estimate the transpiration of woody vegetation at the site [*Chen et al.*, 2008; *Miller et al.*, 2010a]. Soil moisture at 5, 20 and 50 cm depths was monitored at half-hourly intervals using theta probes (Delta-T Devices, Cambridge, UK). During the oak growing season, the midday and predawn leaf water potentials of blue oak leaves (sampled at a height of 2-3 m) were measured every 10-14 days [*Miller et al.*, 2010b; *Osuna*, 2011].

Estimates from diurnal water table fluctuation data and stand-scale water balances showed that during the dry season, when soil water is depleted, a significant amount of groundwater is used by the blue oaks (4 to 25mm per month). Water potential measurements suggested that groundwater uptake is energetically favorable over soil water use during June, July, and August [*Miller et al.*, 2010a].

Model Structure and Parameters

Vensim (Ventana Systems Inc., Harvard, MA), a software package designed to simultaneously solve sets of differential equations, was used to create the system dynamics model. Our model simulates the dynamics of both water and water potential systems. The water system is represented by the stock-flow loops in the system dynamics model—the stocks represent the changes of water within different "reservoirs" of roots, soil and groundwater layers, while the flows represent the water fluxes among

the reservoirs and the water fluxes out of model boundary, such as the precipitation, infiltration and runoff. The water potential status of each component is represented by its state variable (e.g., root water potential, soil water potential, leaf water potential) which links to the stock-flow loops of water to drive water flowing among the reservoirs. The water potential variables change simultaneously with the water status in the reservoirs. While we chose to use this framework to test our theoretical model, the differential equations developed may be used, with only minor adaptations, in a range of Earth system models.

We adapted our system dynamics model to simulate the water uptake of the blue oaks at the Tonzi Ranch site. The shallow soil layer was divided into three soil water reservoirs, from 0 to 10 cm, from 10 to 30 cm, and from 30 to 70 cm. The saprolite zone, from 70 cm to 9 m, was considered as the 4th water reservoir. The bedrock zone was viewed as the groundwater reservoir with the depth from 9 to 20 m. The depth to groundwater was considered constant at 9 m. The model simulation was conducted with the half-hourly time step. Meteorological data from the site were used to calculate the potential ET and to force the model with actual rainfall events.

Xylem cavitation parameters for *Quercus* species [*Cochard and Tyree*, 1990; *Matzner et al.*, 2001; *Tyree et al.*, 1993] were used to generate vulnerability curves for the blue oaks. Matzner et al. [2001] showed that the roots of greenhouse-grown live oak seedlings lose 50% of conductance at -1.4 MPa pressure, 81.9% at -3.0 MPa and 93.9% at -5.0 MPa. We created a vulnerability curve with a slightly higher maximum conductance value than those determined by Matzner et al [2001], since the xylems of

older trees have higher cavitation resistance than the seedling xylems (Figure 2.2). We used the same vulnerability curve for all roots and stems, although some studies show that the smaller roots may be more vulnerable to cavitation [*Jackson et al.*, 2000; *Sperry et al.*, 2003; *Sperry et al.*, 2002].

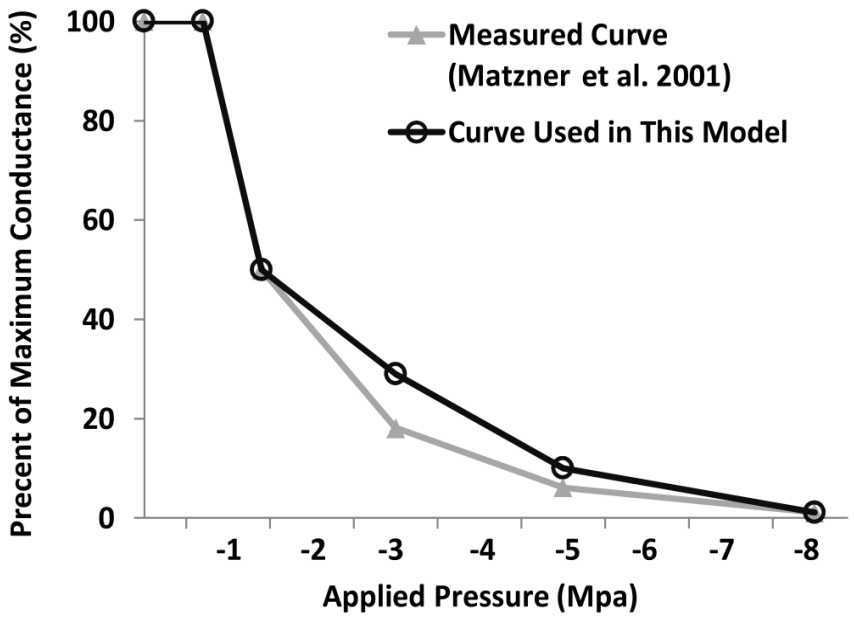

Figure 2.2 Vulnerability Curve for Blue Oaks. The grey line represents the vulnerability curve of greenhouse-grown live oak seedling roots from the experiment results of Matzner et al. [2001], while the black line is the vulnerability curve used to simulate the xylem hydraulic conductance loss of mature blue oak.

To examine the model's performance, we compared the results it produced against the soil moisture, ET, and water potential measurements from the site. Since the soil moisture measurements are impacted by a combination of blue oak water uptake, grass water uptake, and soil evaporation, we added soil evaporation and grass

evapotranspiration components into the model (see Miller et al. [2012] for equations). Soil evaporation losses were limited to the top soil reservoir, while the grass obtained water from the three soil reservoirs, according to its root distribution. The phenological stages of blue oaks and grasses were applied in the model based on the observed data.

Model Calibration and Validation

The system dynamics model reported the results for every stock, flow and variable at each simulation time step. The model was calibrated against data measured in 2007, and validated against those collected in 2008. Soil moisture values produced by the model were strongly correlated with half-hourly measurements at depths of 5, 20, and 50 cm (r^2~ 0.85 in model validation) (Figure 2.3a). The model was able to precisely simulate the timing and rate of decline in soil moisture at the beginning of dry season (May to June). However, it slightly over-predicted the soil moisture at 5 cm during the dry period, from June to September (by 0.02 cm^3/cm^3), which resulted in a higher antecedent soil water content prior to the October onset of the rainy season and further led to the overestimation of soil water content in October. The model also effectively captured the daily transpiration dynamics of the blue oak (Figure 2.3b). In the model validation, the modeled and measured transpiration showed a positive correlation (r^2 = 0.69). The modeled soil moisture and transpiration rates showed the successful simulation of water dynamics within the GSPAC system.

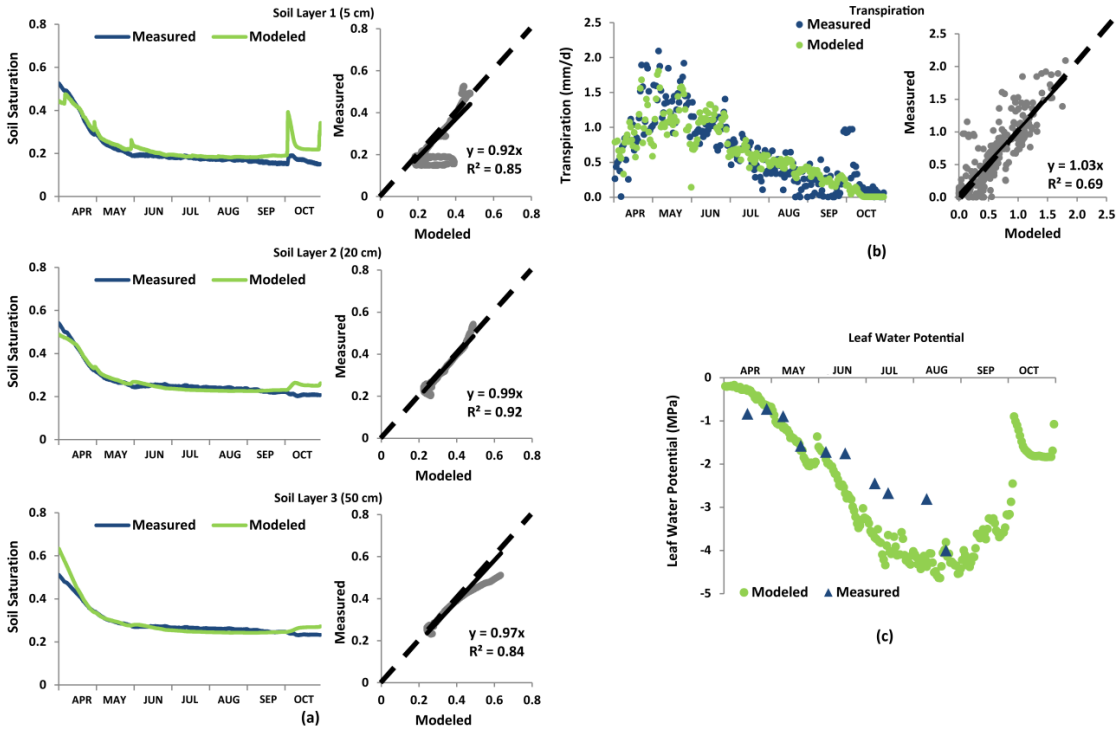

Figure 2.3 Model Validation Results in Oak Active Season (April-October of Year 2008). The model was calibrated against data measured in 2007 and validated against data from 2008. The soil moisture results are shown at a half-hourly time scale, and transpiration and leaf water potential are shown at a daily time scale. Most rainfall events occurred from April to May and there were no significant rainfall events during the prolonged dry period from June to the end of September. Winter precipitation came in October. The model had a good prediction for the soil moisture during the dry period, but overpredicted the soil water content especially in October. The model accurately captured the transpiration dynamics. However, there were big differences between measured leaf water potential and model results during the dry period. Taking account for the uncertainty of leaf water potential measurements (0.5~0.9 MPa) in the dry period, we considered the model was able to predict the general trend of leaf water potential changes.

The model also captured the general trend of leaf water potential (Figure 2.3c). The model matched the lowest leaf water potential measurement in August (-4 to -4.6 MPa) and the relatively high leaf water potential data at the beginning of the dry season in May and June (-0.7 to -1.7 MPa). However, the model failed to reproduce the leaf

water potential during the dry season from June to August. This error was not necessarily model induced; the measured values were also subject to considerable uncertainty due to tree-to-tree variability and imprecise instrumentation.

Each time, nine leaves were taken from three individual trees to conduct leaf water potential measurements. The nine measured values had lower variation during the wet period with the standard deviation of around 0.1 MPa. But the measurements were more dispersed during the dry period and the standard deviation reached as high as 0.9 MPa. The average standard deviation of leaf water potential measurements at this site was 0.38 MPa. The high uncertainty of the measured values during the dry season contributed to the mismatch between modeled leaf water potential results and measurements from June to August.

Results

Groundwater Uptake

The model results showed the different annual water use patterns of the blue oak at the site. During the oaks' active season (April-October) in Year 2007, precipitation was 122 mm and modeled groundwater uptake (79 mm) contributed to 48% of modeled transpiration (165 mm). During the oak active season in Year 2008, precipitation was only 30 mm and modeled groundwater uptake (99 mm) contributed to 71% of modeled transpiration (140 mm). Significantly lower precipitation input in Year 2008 did not result to a dramatic decrease in total transpiration. The model showed that in Year 2008

the time of groundwater uptake was earlier and a larger amount of groundwater was used to buffer the impacts of precipitation deficit on transpiration.

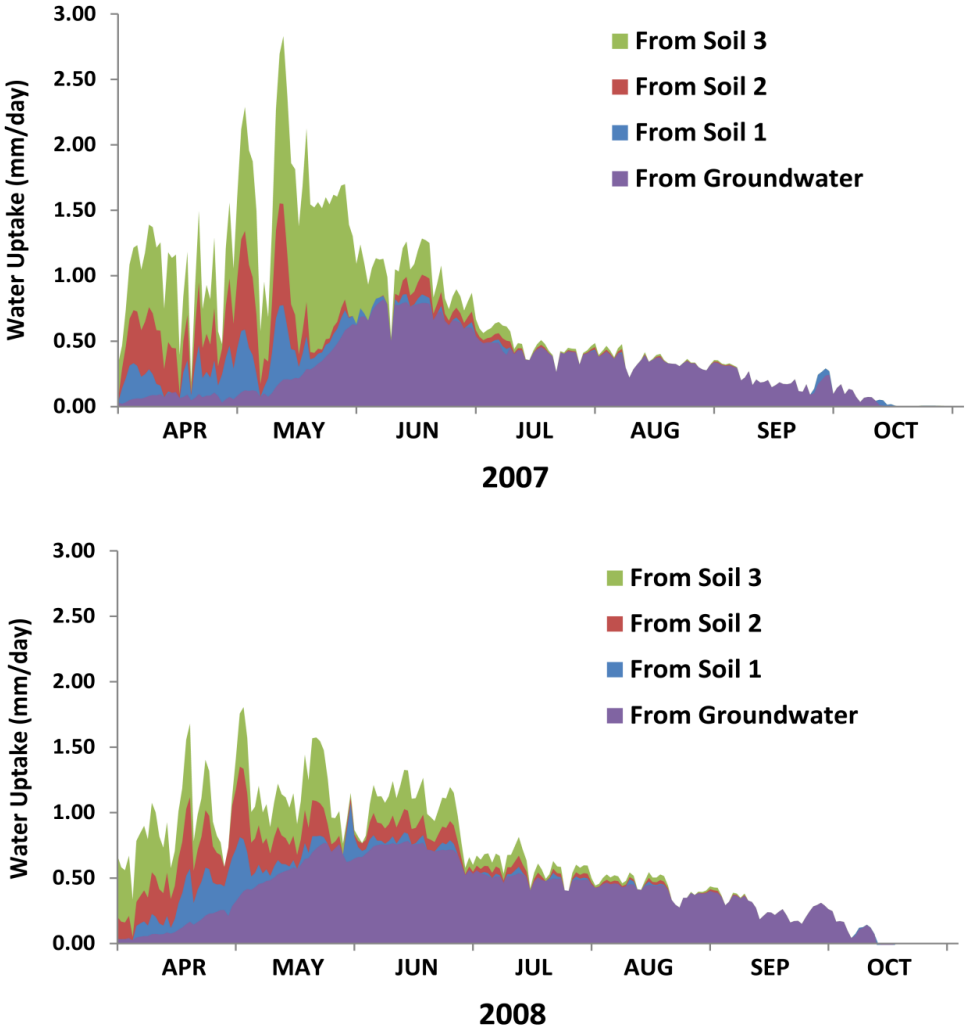

Figure 2.4 Plant Water Use Pattern. In these stacked area charts, the contributions from each source are additive. For example, in June of 2008, the total net water uptake was around 1.25 mm/d, which was divided into 0.75 mm/d from groundwater, 0.04 mm/d from soil reservoir 1, 0.16 mm/d from soil reservoir 2, and 0.30 mm/d from soil reservoir 3. For both years, groundwater uptake started in April, peaked in May, and declined steadily through the dry season. Overall groundwater uptake in 2008 was higher than in 2007 due to the significant decrease of precipitation in 2008.

The model results also revealed the seasonal water use patterns of the blue oak (Figure 2.4). At the beginning of the oaks' active season (April to May), the precipitation input and the antecedent soil moisture, built up over the wet winter, provided sufficient soil moisture for trees. During this period, the model showed that most water for transpiration was taken from soil. The rainy season ceased at the middle of May. Without the inputs of precipitation, the oaks quickly dried the soil water reservoirs. The soil water storage in the top layers was depleted most rapidly, and the soil water uptake rates from the deeper soil layers successively increased. To compensate, the modeled groundwater uptake rate started to increase. During the dry season (June to August), soil water reservoirs were depleted and soil water uptake only contributed to a small proportion of transpiration. The model results indicated that the proportions of transpired water from groundwater uptake in Year 2007 were 62% in June, 73% in July, and 84% in August, and 69%, 85% and 96% in June, July and August of 2008, respectively. The modeled groundwater uptake rate reached the maximum rate in June and slightly decreased as the dry month progressed.

The model showed the dynamics of water uptake throughout at the site: soil water uptake generally followed the Mediterranean precipitation regime, i.e., it was higher in wet season and much lower in dry season. Groundwater uptake worked in an opposite manner, complementing the deficit of soil water in dry season and buffering the impacts of drought on woody vegetation. It supplied most of the transpired water during the dry season, but this proportion decreased markedly during the wet season.

Hydraulic Redistribution

To illustrate the daily and seasonal dynamics of hydraulic redistribution, we plotted the average diurnal cycles of water uptake and release for three two-week time periods: 102^{th} to 115^{th} day during the wet season, 131^{th} to 144^{th} day during the transitional season, and 224^{th} to 237^{th} day during the dry season in Year 2007 (Figure 2.5). During the wet period, the highest proportion of transpired water was taken from the soil reservoirs, which were consistently wet due to regular rain events. For every reservoir, the modeled water fluxes approached zero in the nighttime, indicating that hydraulic redistribution was not significant. A minimal amount of groundwater was extracted during the daytime. During the transition period in late May, the rainy season ended and soil layers started to dry. In the daytime, the modeled maximum water uptake rate occurred in the soil layer 3, indicating that the trees directed water uptake to deeper and wetter soil layers when the top soil layers were dry. Hydraulic redistribution happened in the nighttime; water was removed from layer 3 and the groundwater, and transferred to the shallow soil layers (represented by layer 1 and 2). Soil water storage was nearly depleted during the dry period in August, making the saturated zone the only water source for hydraulic redistribution. During this time, the model indicated that groundwater was withdrawn during the night and released to all of the soil reservoirs, confirming that hydraulic redistribution was actively occurring.

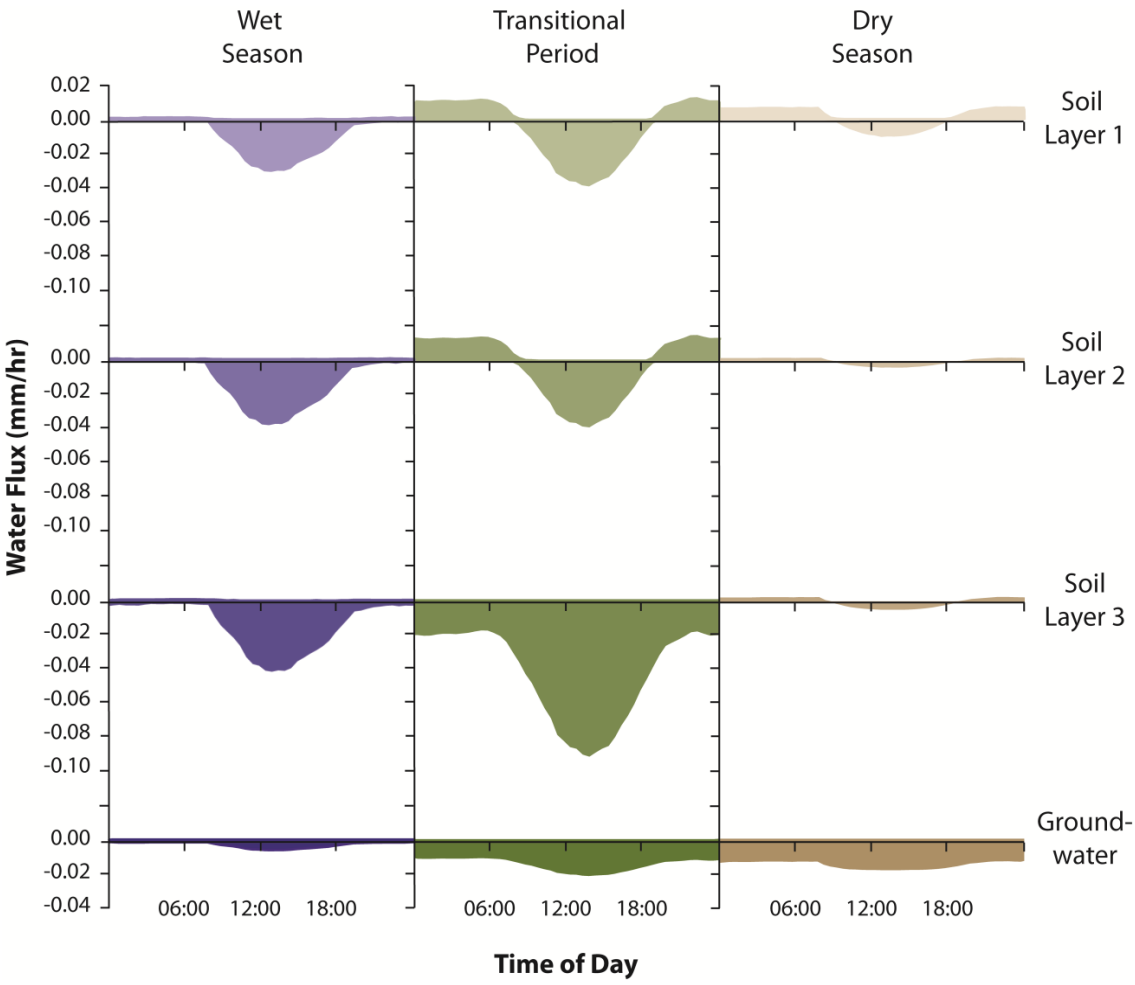

Figure 2.5 Daily and Seasonal Hydraulic Redistribution Dynamics. Three periods in the oak active season were chosen to indicate HR dynamics in variant moisture conditions: the wet period (Days 102 to 115), the transitional period (Days 131 to 144), and the dry period (Days 224 to 237). Positive water fluxes indicate a release of water to a reservoir, while negative values indicate uptake from a reservoir. During the wet period, the model predicted little to no hydraulic lift; water fluxes to all layers were negative throughout the day. This trend shifted during the transitional period, when soil layers 1 and 2 received additions of water at night, indicating hydraulic redistribution. The source of this water was the groundwater and soil layer 3, which had correspondingly negative fluxes at night. A similar pattern occurred during the dry period, except the only source of water for hydraulic redistribution was groundwater.

During the transition period, the daily patterns indicated that the total amount of water released to soil during the night was smaller than the total amount of water taken from soil during the day, for soil reservoirs 1 and 2. This finding implied that soil water previously stored in these reservoirs still contributed to transpiration in the transition period. However, in August, the total amount of water released to each soil layer during the night was nearly the same as the total amount of water taken from each soil layer during the day. Net water uptake from soil was almost zero, and soil water contributed little to transpiration. However, hydraulic redistribution still had important implications in plant water use during this dry period. It helped the soil layers maintain the minimum soil moisture level needed to avoid extremely low soil water potential caused by soil evaporation and further prohibited the hydraulic failure of the whole GSPAC system. Hydraulic redistribution also recharged lateral roots in top dry soil layers using groundwater during the night. As a result, it protected the further cavitation in lateral roots. In addition, water release curves showed that water release rate reached to a relatively constant value from 0200 to 0500, which implied the whole system approached an equilibrium state around the predawn period.

Water Potential

The modeled leaf water potential results generally followed the trend of biweekly measured leaf water potential data (Figure 2.3c). At the beginning of April, the antecedent soil moisture built up in soil layers was sufficient to support the plant transpiration. The modeled leaf water potential was as high as -0.2 MPa at this time.

During the wet season (April and May), soil water potential largely influenced leaf water potential, as most water was taken from soil layers. Leaf water potential decreased dramatically with the rapid decline of soil water potential and reached -2 MPa at the end of May. From late June to August, the highest proportion of transpired water came from groundwater uptake. However, the limited tap roots reaching groundwater constricted the plant groundwater uptake and transmission capacity. Although the blue oaks could access groundwater, the modeled leaf water potential dropped to -4 to -5 MPa during the dry season, indicating the blue oaks still experienced severe water stress when accessing the constant water source from the saturated zone. In late September, soil water potential increased quickly after several significant rain events, and subsequently leaf water potential increased to -1 to -2 MPa.

Blue oaks at the site are known to be drought tolerant, and predawn leaf water potentials of as low as -6 MPa have been measured during the dry period [*Baldocchi et al.*, 2010; *Xu and Baldocchi*, 2003]. In the model, leaf water potential during the dry period was primarily controlled by the groundwater depth and the hydraulic conductance of tap roots and their degree of cavitation. Therefore, both groundwater depth and plant characteristics affected the degree of water stress that the trees suffer during the dry season.

Discussion

Mechanism of Soil Water-Groundwater Uptake Pattern

The water uptake pattern of blue oaks is controlled by both resistance and potential gradient within GSPAC system. The resistance in root water uptake path consists of two components— rhizosphere resistance and root resistance. In the model, the changes of rhizosphere resistance are controlled by the change of soil conductivity in the rhizosphere zone; the changes of root resistance are caused by cavitation in the root system. When the soil is wet, the simulated root resistance is much higher than the simulated rhizosphere resistance. Thus, root resistance dominates the total resistance of water uptake path during the wet season, which is in agreement with previous research [*Federer*, 1979; *Gardner*, 1965; *Newman*, 1969; *Sperry et al.*, 1998]. When soil goes dry, rhizosphere resistance increases because of the declining soil hydraulic conductivity. Root resistance also rises and remains as the dominating resistance component, due to the higher degree of cavitation in the roots caused by the decline of root water potential. Under extremely dry conditions, rhizosphere resistance can reach the same magnitude as root resistance and start to exert a remarkable influence on water uptake.

Combining the changes of resistance with the dynamics of potential gradients throughout the wet-dry cycle, we can explain the soil water-groundwater uptake pattern of the blue oak. During the wet season, the soil water potential was on the same order of magnitude as the groundwater potential. However, transporting groundwater to the

reference point needed extra energy to overcome gravitational pressure due to the deep groundwater level. Thus, soil water uptake was more thermodynamically favorable than groundwater uptake when soil layers were wet. Although the hydraulic conductivity of tap root was higher than the hydraulic conductivity of lateral roots, the relatively low root density and long root length of the tap root resulted in a total tap root resistance on the same order as the total lateral root resistance. Therefore, the gravitational force on the stem water column was the critical factor that influenced plant water uptake during the wet season, when the oaks tended to take more water from soil layers than from saturated zone. During the dry season, the influence of gravity on water uptake was insignificant compared to the tremendous decline in soil water potential associated with soil drying. Groundwater uptake became thermodynamically favorable over soil water uptake when soil water potential was very low. Cavitation led to a maximum of 85% hydraulic conductivity loss of lateral roots in soil layers in August. The significant increase in both rhizosphere resistance and lateral root resistance in the soil layers led to a higher resistance in the soil-plant pathway as compared to the groundwater-plant pathway. Thus, in the model, both resistance and potential gradient were the key factors affecting plant water uptake during the dry season; the oaks tended to uptake more groundwater through the smaller hydraulic resistance pathway driven by the higher groundwater-plant potential gradient.

Tradeoffs

Blue oaks develop deep roots to access groundwater to support subsistence during the dry season. The model indicated that the root fraction accessing groundwater cannot represent more than 15% of the total roots. This observation begs the question: why not develop additional hydraulic capacity in the tap roots (more root fractions or higher maximum conductance) to access the reliable groundwater source from saturated zone? Four tradeoffs should be considered. One tradeoff is between the "carbon cost" of developing and maintaining deep roots and the "carbon benefit" of having a continual groundwater supply. Since the water table depth is around 7 to 12 meters in this case study, it is relatively costly for the oaks to develop more deep roots to penetrate the thick, but fractured, bedrock layer to access groundwater. The second tradeoff is between the risk of cavitation vulnerability and the benefit of high hydraulic sufficiency of roots [*Hacke et al.*, 2000; *Tyree and Sperry*, 1989]. The tap root with higher hydraulic conductance has bigger pores which make the root more vulnerable to cavitation. The third tradeoff is between the efficiency of soil water use and groundwater uptake. Additional or more highly conductive deep roots will form a relatively lower hydraulic resistance path to access groundwater. Therefore, the groundwater uptake rate will be higher and begin earlier, resulting in lower soil water use. The unused soil moisture reserves may be squandered through evaporation or co-opted by shallow-rooted grasses. Finally, insufficient nutrients may be available from the groundwater, and soil moisture use may be necessary to obtain nitrogen. This limited groundwater uptake capacity only allows the blue oak to survive rather than to flourish; thus the oaks still suffer from water

stress even though they can access groundwater. Considering these tradeoffs, the current configuration (lower deep root mass and capacity) may indeed represent the optimal use of the available water sources.

Performance of the New Water Stress Function

The new water stress function provides a physically-based approach to relate stomatal conductance with the water status in saturated and unsaturated zones. The critical assumption which lies behind this function is that stomata respond linearly to the changes of hydraulic conductance of the whole root system. Previous experiments have revealed the strong, linear relationship between stomatal conductance and hydraulic conductance of GSPAC [*Sperry et al.*, 2003]. Although the new water stress function in our model performed well, future field and modeling studies are still needed to determine if the relationship between stomatal conductance and hydraulic conductance of GSPAC is linear, and whether the hydraulic condition of root system can be used to represent the hydraulic condition of the whole GSPAC.

The new water stress function altered transpiration based on the variable influence of water status across the deep root zone, without assigning water stress parameters (e.g. stress point and wilting point) to each soil layer. The new function showed distinct advantages when simulating water stress in deep-rooted vegetation and could solve two previously unresolved issues: 1) modeling plant water stress when some fraction of the roots is encountering serious water deficits in dry layers while other roots are able to access sufficient water sources in wet layers; and 2) simulating plant water

stress when some fraction of the roots have ceased water uptake while other roots are still absorbing and transporting water for transpiration.

Conclusions

We proposed a physically-based model using system dynamics modeling approach to explore how phreatophytes manage soil water and groundwater resources throughout the growing season. The model was also able to capture the dynamics of hydraulic redistribution. A new water stress function was introduced to incorporate the influence on transpiration caused by the spatially variable levels of water availability throughout the saturated and unsaturated subsurface layers.

The model was applied to simulate water uptake of *Quercus douglasii* (blue oak) in a California savanna. The model results indicated that groundwater uptake can support around 50-70% of transpiration over the 6 month oak growing season. Based on our modeling observations, groundwater also protected the plants from extreme cavitation and hydraulic dysfunction by recharging lateral roots in top soil layers through hydraulic redistribution and maintaining the minimum soil moisture level during the dry season. Plant water stress in the wet season largely depended on water potential in shallow soil layers. However, during the dry season, the depth to groundwater and the plant hydraulic conductance together determined the water stress of plant. Blue oaks must make several tradeoffs to reach an optimum state—the trees maintained only a small portion of deep roots as a protection mechanism to mitigate the impacts of drought. The model results

indicated that, without a sufficient number of deep roots, the blue oaks would suffer severe water stress in the dry season.

The model illustrated the relationship between water and water potential status along GSPAC pathway. While this model was calibrated and validated against measured potential and water status data (transpiration, soil moisture and leaf water potential data), for future applications, we recommend the development and implementation of an integrated measurement system to monitor a high spatial and temporal resolution suite of potential and water statuses in soil, vegetation, and saturated zone. The integration of the model and the new data sets will provide crucial understanding of plant water use pattern and plant water stress.

The proposed model also improves our understanding of the influence of groundwater on land-surface processes. Without phreatophytes, the surface energy and mass fluxes are not sensitive to deep groundwater dynamics when the water level exceeds a critical depth range [*Ferguson and Maxwell*, 2010; *Kollet and Maxwell*, 2008]. However, phreatophytes can act as the linkage between deep groundwater and land surface processes. In our case study, even though the groundwater depth was 9 m, it could still influence land surface processes in two ways: 1) through hydraulic redistribution, groundwater uptake directly contributed to transpiration and influenced the moisture in the top soil layers; and 2) groundwater use patterns indirectly affected soil water use pattern and controlled the dynamics of soil water storage. In the future, the proposed model can be incorporated into the coupled land surface and groundwater models, such as ParFlow.CLM [*Maxwell and Miller*, 2005], to improve model

performance when studying the effects of groundwater uptake on ecohydrological processes at larger scales. The model also could have significant implications for improving climate prediction by considering the transpiration supported by groundwater.

CHAPTER III

INCORPORATING PLANT GROUNDWATER DYNAMICS INTO GROUNDWATER-LAND SURFACE MODEL

Introduction

Groundwater dynamics significantly influences land surface processes, such as soil moisture, evapotranspiration (ET), infiltration, runoff and groundwater recharge, which further impact the atmospheric boundary layer. These groundwater-land surface-atmosphere interactions have been addressed in a number of previous modeling studies aimed at incorporating water table dynamics into climate, hydrological and land surface models [*Chen and Hu*, 2004; *Fan et al.*, 2007; *Liang et al.*, 2003; *Maxwell and Miller*, 2005; *Maxwell et al.*, 2011; *G-Y Niu et al.*, 2007; *York et al.*, 2002]. However, vegetation-based groundwater dependent ecosystems (GDEs) significantly influence the groundwater-land surface-atmosphere connection through two mechanisms: groundwater evapotranspiration (ET_{gw}) and hydraulic redistribution (HR). Groundwater dynamics are directly linked to ET through plant groundwater uptake, while HR indirectly impacts the groundwater-land surface-atmosphere interaction by redistributing soil water and groundwater [*Dawson*, 1993; 1996; *Hultine et al.*, 2003; *Ludwig et al.*, 2003; *Orellana et al.*, 2012]. Groundwater dependent vegetation widely spread in the lowland areas along streams, around springs and within groundwater-fed wetland, and in the upland areas where the plants can access groundwater using their relative deep roots

[*Eamus and Froend*, 2006; *Eamus et al.*, 2006; *Orellana et al.*, 2012]. It is necessary to incorporate the dynamics of these plants into current models to improve ecohydrological, hydrogeological, and climate models.

Recent modeling studies have mainly focused on the impacts of shallow water table on water and energy fluxes at the land surface. These modeling efforts examined how shallow groundwater directly interacts with unsaturated zone, leading to wetter soil moisture and increased ET [*Chen and Hu*, 2004; *Fan and Miguez-Macho*, 2010; *Fan et al.*, 2007; *Liang et al.*, 2003; *Miguez-Macho and Fan*, 2012a; *G Y Niu et al.*, 2007; *York et al.*, 2002]. These changes may further enhance precipitation in some regions [*Anyah et al.*, 2008; *Jiang et al.*, 2009] and alter surface runoff and stream flow rates [*Gusev and Nasonova*, 2002; *Gutowski et al.*, 2002; *Miguez-Macho and Fan*, 2012b; *Yeh and Eltahir*, 2005]. However, the existences of groundwater dependent vegetation, especially the deep-rooted phreatophyte species, can link relatively deep groundwater dynamics (~ 10 m) with land-atmosphere system, since their roots can reach over 20 m [*Bleby et al.*, 2010; *Canadell et al.*, 1996; *Lewis and Burgy*, 1964]. The groundwater transpired by phreatophytes may contribute to a large portion of total plant transpiration [*Orellana* et al., 2012], significantly impacting the surface energy budget. Therefore, modeling efforts also need to address the impacts of relatively deep groundwater on water and energy fluxes at the land surface through the groundwater uptake of phreatophytes.

Hydraulic redistribution (HR) refers to the water movement from higher water potential layers to lower potential layers through plant roots [*Burgess et al.*, 1998; *Caldwell and Richards*, 1989; *Caldwell et al.*, 1998; *Dawson*, 1993; *Hultine et al.*,

2003]. It occurs worldwide, across a range of plant species, in both dry and wet regions [*Oliveira et al.*, 2005] and in both active and dormant vegetation [*Hultine et al.*, 2004; *Scott et al.*, 2008a]. HR has been frequently observed in groundwater dependent ecosystems [*Dawson*, 1993; 1996; *Hultine et al.*, 2003; *Ludwig et al.*, 2003; *Orellana et al.*, 2012]. It redistributes both soil water and groundwater, which impacts plant water use and changes the temporal and spatial patterns of water and energy fluxes at large scale [*Jackson et al.*, 2000; *Lee et al.*, 2005]. Due to the significant hydrological and ecological effects of HR, Scott et al. [2008a] suggested account HR into ecohydrological models. Most physically based HR modeling efforts were currently conducted at plant-scale [*Amenu and Kumar*, 2008; *Gou and Miller*, 2013; *Mendel et al.*, 2002]. The conceptual HR scheme of Ryel et al. [2002] was coupled into land surface models and climate models to simulate the potential hydrological and climatic impacts of HR at large scale [*Lee et al.*, 2005; *Wang*, 2011; *Zheng and Wang*, 2007]. However, the conceptual HR scheme did not describe the HR processes explicitly. More physically based HR schemes were needed in model simulations at large scale.

To address the influence of plants, especially phreatophytes, on the groundwater-land surface-atmosphere interactions, we previously developed a plant-scale model to simulate root water uptake, HR and water stress in phreatophytic vegetation [*Gou and Miller*, 2013]. This physically-based model performed well when simulating water and energy transfer along GSPAC. The root water uptake function proposed in this model was driven by the potential gradients along the groundwater-soil-plant-atmosphere continuum (GSPAC), which allowed it to simulate both root water uptake and HR

simultaneously. In addition, we introduced a new water stress function in the plant-scale model [*Gou and Miller*, 2013], which depended on "the linear relation between the diffusive conductance of stomata to water vapor and the hydraulic conductance of SPAC" [*Domec et al.*, 2006; *Sperry et al.*, 2003]. To the best of our knowledge, it is the first time that the linear relationship was used to simulate plant water stress.

The results from the study highlighted the seasonal shift in plant water sources– during the wet season, plant water uptake was predominantly from the upper, wet soil layers. As the dry season progressed and upper soil dried, trees exploited more water from deeper, wetter soil layers or increasingly tapped groundwater, and vise versa. The phenomenon of seasonal shift in plant water sources was widely observed in many species, especially in the species with deep roots or dimorphic root systems in water limited environments [*Bleby et al.*, 2010; *Dawson and Pate*, 1996; *Ehleringer and Dawson*, 1992; *Meinzer et al.*, 2001; *Meinzer et al.*, 1999; *Rose et al.*, 2003; *White et al.*, 1985]. Some studies found that plants can respond to the changes in soil water rapidly using sap flow measurements and stable isotope [*Bleby et al.*, 2010; *Ehleringer and Dawson*, 1992; *Hultine et al.*, 2004; *Scott et al.*, 2008a] so that the shift in plant water sources can also occur at daily scale. The shift in plant water sources suggests that the linkages between ET and soil moisture memories at different depths vary daily and seasonally, which can significantly impact the climate [*Koster and Suarez*, 2001]. However, few modeling efforts addressed this phenomenon in land surface models, hydrological and climate models [*Feddes et al.*, 2001], which may lead to significant biases especially in the model simulation with deep rooted vegetation.

The objective of this study was to develop a modeling tool to determine the influence of plants on the temporal and spatial interactions between groundwater, the land surface, and the atmosphere at stand to landscape scales. We implemented the functions developed by Gou and Miller [2013] into a distributed groundwater-land surface model, ParFlow.CLM [*Jones and Woodward*, 2001; *Kollet and Maxwell*, 2006; *Kollet and Maxwell*, 2008; *Maxwell and Miller*, 2005]. These revisions allowed the model to explicitly describe vegetation water use and HR by a range of plant species, which effects both surface and subsurface water flow and alters the water and energy balances at the land surface. The model was then applied to conduct a long term simulation of the water and energy dynamics in a savanna system at an AmeriFlux site in California. Specifically, the model was used to address (1) the contribution of groundwater to stand-scale ET and the strength of the link between soil water uptake and groundwater uptake; (2) the seasonal and daily shift in plant water sources; (3) the influence of both hydraulic lift and hydraulic descent on ET and soil moisture distribution during oak active and dormant seasons; and (4) how HR influences the water competition between oaks and grasses.

Method

A Plant Scale Phreatophytic Vegetation Water Use Model

Both root water uptake and HR in the phreatophytic vegetation water use model [*Gou and Miller*, 2013] are driven by the potential gradients along GSPAC. Water may

flow into or out of vegetation roots depending on the direction of water potential gradient between roots and surrounding soils, allowing the model to simulate HR. The net water uptake from all soil layers and groundwater equals to the transpiration, assuming that the plant water storage does not change. Equation 3.1 was the governing equation for the functions of plant water uptake and HR.

$$T = \frac{A_{t\_a\_root}}{A_{leaf}} \sum_{i=1}^{m} f_{root,i} \frac{\psi_{soil,i} - \psi_{ref} - z_i}{\Gamma_{s,i} + \Gamma_{r,i}} \tag{3.1}$$

where T is the plant transpiration rate [LT^{-1}], $A_{t\_a\_root}/A_{leaf}$ is the ratio of the total absorbing root surface area to the total leaf area. This model can be adopted to study the impacts of root to leaf area ratio on plant water use pattern [*Hacke et al.*, 2000; *Jackson et al.*, 2000; *Sperry et al.*, 1998]. $f_{root,i}$ is the root fraction in the i^{th} layer. $\Psi_{soil,i}$ is the soil water potential [L] in the i^{th} layer, z_i is the vertical length of the transporting root portion [L] in the i^{th} layer. A reference point is defined in the model, which referred to the junction point between root system and stem located at the same elevation of the ground surface. The potential of the reference point, Ψ_{ref} [L], was further used to estimate the leaf water potential by accounting the energy consumption of overcoming gravitational potential and resistance to transport water from the reference point to leaves. $\Gamma_{s,i}$ refers to the resistance of flowing from surrounding soil into roots and vice versa [$TL^{-1}L$], and $\Gamma_{r,i}$ refers to the resistance of transporting from root tip to the reference point [$TL^{-1}L$], which. The explicit equations for $\Gamma_{s,i}$ and $\Gamma_{r,i}$ were in Gou and Miller [2013]. Soil and plant hydraulic conductivities both varied depending on soil and plant water potential

status, respectively. When $\Psi_{soil,i} - \Psi_{ref} - z_i > 0$, the potential gradient drives the water uptake from surrounding soil to root in the ith layer, while when $\Psi_{soil,i} - \Psi_{ref} - z_i < 0$, the negative potential gradient implies the water releasing from roots to surrounding soils. Therefore, Equation 3.1 estimated both plant water uptake and hydraulic redistribution rates.

A new water stress function was introduced based on the linear relationship between stomatal conductance and root hydraulic conductivity was used to simulate plant water stress [*Domec et al.*, 2006]. The loss of hydraulic conductivity in the whole root system was calculated by Equation 3.2.

$$\xi = \frac{\sum_{i=1}^{m} \frac{r_{s,i}^{2}}{L_{t\_s,i}} K_{root,i}(\psi_{root,i}) f_{root,i}}{\sum_{i=1}^{m} \frac{r_{s,i}^{2}}{L_{t\_s,i}} K_{s\_root,i} f_{root,i}} \tag{3.2}$$

where x is the fractional loss of hydraulic conductivity of the whole root system. For the roots within the ith soil layer, $K_{s\_root,i}$ is the root hydraulic conductivity when caviatation does not occur [LT^{-1}], $K_{root,i}(\Psi_{root,i})$ is the root hydraulic conductivity in cavitated roots [LT^{-1}], which changes with the root water potential $\Psi_{root,i}$, $r_{s,i}$ is the root diameter [L], and $L_{t\_s,i}$ is the total length of one single root [L]. In this study, the stomatal conductance calculated in CLM linearly responded to x, which further limited transpiration.

ParFlow.CLM

ParFlow.CLM was developed to couple a variably saturated groundwater model (ParFlow) and a land surface model (CLM) together [*Kollet and Maxwell*, 2006; *Kollet and Maxwell*, 2008; *Maxwell and Miller*, 2005]. CLM was incorporated into ParFlow as a module [*Kollet and Maxwell*, 2008]. Thus, each soil column in ParFlow had one corresponding CLM module to calculate the water and energy fluxes at the land surface of this column under a specific land cover type. The subsurface formulations in CLM were replaced by ParFlow, which simulated soil water and groundwater movements and overland flow. The two models communicate with each other over the root zone at every time step: ParFlow passes the subsurface information (soil moisture and groundwater dynamics) to CLM; CLM considers the subsurface information into its calculation of infiltration and plant water uptake. These land surface fluxes were treated as sinks/sources in Richards' equation in ParFlow. The coupled ParFlow.CLM can describe the hydrological and ecological processes related to the vertical and horizontal heterogeneity of vegetation, topography, and hydrogeology [*Atchley and Maxwell*, 2011; *Ferguson and Maxwell*, 2010; *Kollet and Maxwell*, 2008; *Rihani et al.*, 2010].

Incorporating New Functions from the Phreatophytic Vegetation Water Use Model into ParFlow.CLM

First, the previous root water uptake function in CLM was replaced by the new one (Equation 3.1) from the phreatophytic vegetation water use model. In the previous function, the total transpiration was distributed over layers within root zone according to

the root fraction in each layer [*Dai*, 2001]. In the previous function, plants extracted water simultaneously from each layer at the same water uptake rate per unit root fraction. However, in the new function, the root water uptake from each layer was controlled by the layer's water potential, the plant's water potential, and the soil-root resistance (see Equation 3.1). It allowed the model to simulate root water uptake in a more physically-based approach, which captured the seasonal and daily shift in plant water source.

Second, the plant water stress function in CLM [*Dai*, 2001] was replace with Equation 3.2. The previous function in CLM was a most commonly used function which simulated plant water stress as a linear function of soil water condition between wilting point and stress point [*Feddes et al.*, 1978; *Federer*, 1979; *Laio et al.*, 2001; *Porporato et al.*, 2001]. However, the previous function has its limitations in simulating water stress of deep rooted plant. The root system expanded across various water content layers. Some roots in wetter and saturated layers may be more active (less cavitated) while other roots in drier layers maybe less active. The previous water stress function considers the aggregate water availability over the root zone based on the root fraction, but neglects the influence of root activity on plant water stress. The new function integrates the influence of various soil water contents, groundwater and root activity on plant water stress. After the replacement of the new function, the stomatal conductance calculated by CLM was linearly limited by the plant water stress x in Equation 3.2.

One critical assumption was made in these modifications of ParFlow.CLM. In the original functions [*Gou and Miller*, 2013], the root hydraulic conductivity in

cavitated roots $K_{root,i}(\Psi_{root,i})$ changed with the root water potential $\Psi_{root,i}$ (see Equation 3.3), making $K_{root,i}(\Psi_{root,i})$ a critical variable in the calculation of plant water uptake/release rate and transpiration. However, the root water potential $\Psi_{root,i}$ was also related to the plant water uptake/release rate and transpiration. Therefore, whe whole model was solved iteratively in the study of Gou and Miller [*Gou and Miller*, 2013]. In this study, we assumed the root hydraulic conductivity in cavitated roots $K_{root,i}$ changed with the water potential of surrounding soil Ψ_{soil} (i.e. $K_{root,i}(\Psi_{soil,i})$), rather than the root water potential Ψ_{root} (i.e. $K_{root,i}(\Psi_{root,i})$). This assumption avoids model iteration, increasing simulation efficiency.

In addition, a new vegetation type, winter grass, was added into the model. The original ParFlow.CLM model only contained the grass type that was active based on the soil temperature [*Dai*, 2001]. The green-up and senescence of the new winter grass type were controlled by the soil moisture of the top soil layer in the model, which represented some specific grass types active with rain. In the modified ParFlow.CLM, only the old functions in CLM were replaced by our new functions. All functions in ParFlow remained the same. Therefore, these new functions could be incorporated into other land surface models, such as the stand-alone version of CLM in the Earth System Modeling Framework.

Model Application

Study Site

The model application aimed to test the model performance in capturing the spatial and temporal water and energy dynamics at a savanna site known. The study site was Tonzi Ranch site, a blue oak savanna in the lower foothills of the western Sierra Nevada (latitude: 38.4311^{o}N, longitude: 120.966^{o}W). The Mediterranean climate leads to wet, mild winters and dry, hot summers [*Baldocchi et al.*, 2004; *Chen et al.*, 2008; *Ma et al.*, 2007]. The mean annual precipitation is about 560 mm, which mainly occurs between October and May (wet season) [*Chen et al.*, 2008]. Previous study had determined that deciduous blue oaks *(Quercus douglasii),* the dominant woody vegetation type at this site, are obligate phreatophytes and that plant groundwater use supports most transpiration during the dry season [*Miller et al.*, 2010b]. Blue oak phenology is tightly related to temperature; they leaf out at the end of March and senesce around the beginning of October. In contrast, the grasses at the site are the annual species which only depend on the soil water [*Ma et al.*, 2007]. The active season of the grass is linked to soil water availability; they typically green up in November and senesce in May of the next year [*Ma et al.*, 2007]. The site has a shallow soil layer consistently of rocky silt loam approximately 60-100 cm deep, underlain by a 4-8 m saprolite zone followed by fractured, metamorphic bedrock. The water table depth ranges from 7-12 m [*Miller et al.*, 2010b].

A suite of measurements have been collected at the site for over thirteen years. Two eddy covariance towers, placed in the overstory (23 m height, above tree canopy) and the understory (2 m height, under tree canopy), measure fluxes of CO_2, water vapor, and sensible heat using the eddy covariance method [*Baldocchi et al.*, 2010]. Continuous soil moisture measurements have been collected at half-hourly intervals using theta probes at 5, 20 and 50 cm depths under a blue oak tree. In addition, time domain reflectometry (TDR) probes were installed at nine locations (five under tree canopy and four in the open spaces) to weekly or biweekly measure soil moisture under trees and grasses [*Chen et al.*, 2008]. The biweekly measurements of the midday and predawn leaf water potentials of blue oak leaves (sampled at a height of 2-3 m) were monitored in the oak active season [*Miller et al.*, 2010b; *Osuna*, 2011]. The root distribution in the soil layer was measured with ground penetrating radar in 2011 [*Baldocchi*, 2012]. Three observation wells were drilled to manually measure water table depth at biweekly intervals since the end of 2006, and the half-hourly groundwater depth was automatically recorded in one well since May 2007 [*Miller et al.*, 2010b]. Other variables, such as leaf area index, stomatal conductance and plant height, have been periodically monitored [*Baldocchi*, 2012].

Model Setup

A 200 m × 200 m area with a depth of 15 m was chosen for model simulation. Previous LIDAR images showed 43% coverage by blue oak, 52% by grass, and 5% by pine (Figure 3.1) [*Chen et al.*, 2008]. The model domain was discretized into 100 x 100

x 28 cells, with a lateral resolution of 2 m ($\Delta x = \Delta y = 2$ m) and variable vertical resolutions (Δz) ranging from $\Delta z = 0.2$ m for soil layers and layers within the range of water table fluctuations to $\Delta z = 0.8$ m for saprolite layers. The bottom of the computational domain was set as a no-flow boundary. Four lateral boundaries were defined as monthly-changed constant head boundary conditions according to the groundwater depth measurements from nearby three wells. Vegetation distribution and land surface elevation (ranging from 166 m to 170 m) were obtained from the LIDAR imagery and a DEM created from it [*Chen et al.*, 2008]. Only the blue oaks in the model simulation were considered as the phreatophytes, with tap roots reaching groundwater table. The grasses and pines in the model simulation solely relied on soil water. Only one vegetation cover type was assigned to each surface model cell, neglecting grasses occurring under the tree canopy. Four soil types were applied for the top soil layer, the deeper soil layers, the saprolite layers and the bedrock layers. The van Genuchten parameters of these four soil types were based on previously obtained site data [*Miller*, 2009]. Most parameter values of blue oak properties were the same as the ones used in Gou and Miller [*Gou and Miller*, 2013], except the root distribution with 45% of roots in 0-20 cm top soil layer, 30% of roots in 20-40 cm soil layer, 15% of roots in the soil layers ranging from 40 to 60~100 cm depth, and the remaining 10% of roots accessing groundwater.

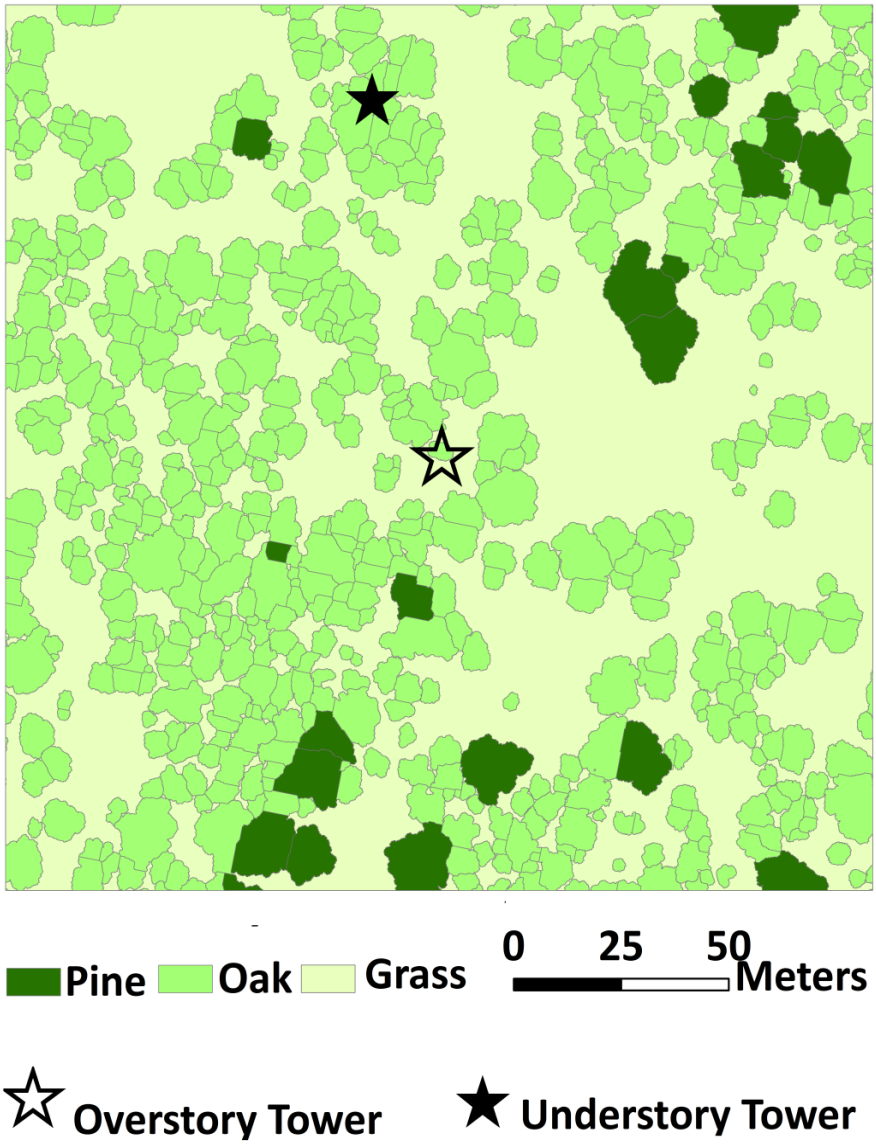

Figure 3.1 Modeling Study Site Showing the Three Dominant Plant Species. 1) Blue oaks, which were believed to use both soil water and groundwater with the active season from March to October; 2) annual winter grasses, which only depended on soil water and had an active season from November to May of the subsequent year; and 3) evergreen grey pines, which were considered to use soil water only in model simulation. Two eddy covariance systems were located at this site: one on a 23-m high overstory tower and another on a 2-m high understory tower.

Model Simulation

Conditions at the site were simulated for 8 years (2002 to 2009), with a half-hourly time step. The whole model was forcing with incoming radiation, wind speed and direction, surface air temperature, precipitation, pressure and humidity. The model performance was tested by comparing the model results and measurements for daily and hourly timescales and at different spatial locations. First, the half-hourly model results were summarized into daily results to compare against the 8-year measurements of overstory ET, understory ET, soil moisture at different depths at a single location, and available predawn leaf water potential. Second, the half-hourly model results for latent heat were compared against the half-hourly measurements from 23 m overstory eddy covariance tower, to test if the model captured diurnal changes of latent heat in different seasons/years. Third, the model simulation from Year 2004 (drier year) and 2005 (wetter year) were chosen to analyze the spatial patterns of soil moisture dynamics under different vegetation covers, as measured by the spatially distributed TDR probes. We further analyzed the model results to determine if the model captured the seasonal plant groundwater use and the hourly dynamics of HR.

Comparison to Field Data

Comparison between Measurements and Simulation Results at a Daily Time Scale

Micrometeorological conditions at the site were typical of savannas in Mediterranean climates (Figure 3.2a). During the 2001-2009 interval, Years 2004 and

2008 were the driest, while Years 2005 and 2006 were the wettest. Net radiation (Rn), measured above the canopy, averaged 3.15 GJ/m^2/year. The energy balance was computed based on the latent heat (LE), sensible heat (H) and soil heat (G) flux measurements (Figure 3.2a), neglecting storage in the canopy air space and biomass , as per Wilson et al. [*Wilson et al.*, 2002]. The comparison between measured Rn and measured LE+H+G implied that significant energy imbalance occurred during all winters and the dry summers in wet years of 2005, 2006 and 2009. The days with significant energy imbalance (when daily |(Rn-LE-H-G)/Rn|>30%) counted 24% of total days. While this site provided reliable data with high degree of energy balance closure [*Baldocchi et al.*, 2004; *Wilson et al.*, 2002], the issue is important as it can significantly influence on model calibration and validation [*Foken*, 2008].

The model produced results at half-hourly time interval for the 8-year simulation from 2002 to 2009, which were further aggregated into daily sums and averages for comparison to the field data. We assumed that the energy and water fluxes from the domain (200 m × 200 m) were representative of the fluxes from the footprints of both overstory and understory eddy covariance towers. Thus, the total ET (ET_{total}) measured by the overstory tower was compared to the total ET averaged over the entire model domain (Figure 3.2b).

Initially, the modeled ET_{total} was higher than the measured value, and the modeled and measured results showed a positive correlation, with r^2=0.71 (Figure 3.2f). Typically, the model failed to match the measured ET_{total} during the winter periods when significant energy imbalance occurred (Figure 3.2a). Significant energy imbalance in

early spring during 2005 and 2006 (Figure 3.2a) also corresponded with clear mismatches between modeled and measured ET_{total} at the same time (Figure 3.2b). We removed the results for days with poor energy budget closure (i.e., when daily |(Rn-LE-H-G)/Rn|>30%), or 24% of total days. This correction improved the agreement between modeled and measured data, with r^2=0.87 (Figure 3.2g).

The measured understory ET (ET_{under}) (Figure 3.2c) was estimated from the measurements from the understory eddy covariance tower (2 m height), which captured the fluxes under the tree canopy, i.e. the fluxes from grasses and soil. The measured ET_{under} from the understory tower was compared to the modeled ET_{under} averaged from ET of grass covered areas and the soil evaporation under the tree canopy over the entire model domain (Figure 3.2c). The model ignored the grasses under the tree canopy, since the CLM code only allows one plant functional type in each grid cell. This limitation led to the underestimation of ET_{under}, restricting its ability to study water competition and facilitation between trees and grasses. Energy balance closure problems in measured data are still an issue in ET_{under} simulation, with significant mismatches between measured and modeled results during winter periods when large energy imbalances occurred.

In the model, the critical soil water potential to control the activity of winter grass was set to -1.2 Mpa. In the model simulation, the winter grass was active in the winter when soil water potential in the top 20 cm depth of soil exceeded -1.2 Mpa, while the grass senescent when soil water potential at top soil layer dropped below -1.2 Mpa. This relationship helped to capture the changes of ET_{under} (Figure 3.2c) with soil

moisture (Figure 3.2e), especially the fast decrease in ET_{under} after the rains ceased. According to this relationship, the average grass green-up date was the 314th day of year, and the average grass senescence date was the 143th day of year, which were within 24 days of those observed on site [*Ma et al.*, 2007].

A new feature of this model allowed the simulation of leaf water potential, which could be used to explore the water stress of plants. Leaf water potential measurements for blue oaks were available in Years 2002, 2003, 2007 and 2008 from wet season to dry season when blue oak was active [*Osuna*, 2011] (We noted that the measurements in 2008 were less reliable than the others due to an equipment malfunction.). Modeled predawn leaf water potential results were averaged of all blue oaks within model domain. The model successfully captured the predawn leaf water potential dynamics (Figure 3.2d). For each year, the predawn water potential was high (~0.2 MPa) during the wet season when soil water potential was high. It decreased dramatically following the rapid decrease of soil water potential from May to June. During the dry season from June to September, the predawn leaf water potential dropped to -4 to -6 MPa, even though the blue oaks were mainly relying on groundwater at this time. Even with access to deep groundwater, the blue oaks still suffered water stress due to the limitations of plant hydraulic structure (e.g., xylem hydraulic conductance and cavitation in tap roots). The predawn leaf water potential bounced up and reached ~-0.2 MPa during September and October when winter rains commenced. It quickly responded to the soil water potential dynamics. For the inter-annual changes, the predawn leaf water potentials

during the dry seasons were lower in dry years (Year 2004 and 2008) and higher in wet years (Year 2005 and 2006).

We chose the modeled soil moisture results at the location where the soil moisture sensors (theta probes) were installed to compare against measurements at different depths (Figure 3.2e). The model generally matched the measurements, but it failed to exactly reproduce the soil moisture from May to August when soil was dry. The soil evaporation simulation in CLM tends to be overestimated [*Lawrence et al.*, 2007], possibly resulting in the rapid decrease of soil moisture at the beginning of dry season in May. Therefore, the modeled soil moisture reached low soil water content rapidly rather than decreasing gradually during dry season as the measurements show. In addition, lacking of the understanding of water movement in the fractured saprolite zone, the saprolite zone underlying the shallow soil layers was simply treated as low permeable soil, which may also effect the soil moisture simulation of upper soil layers.

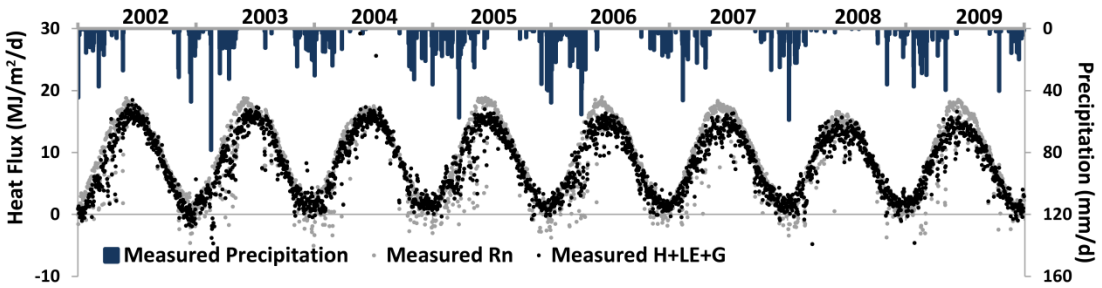

(a)

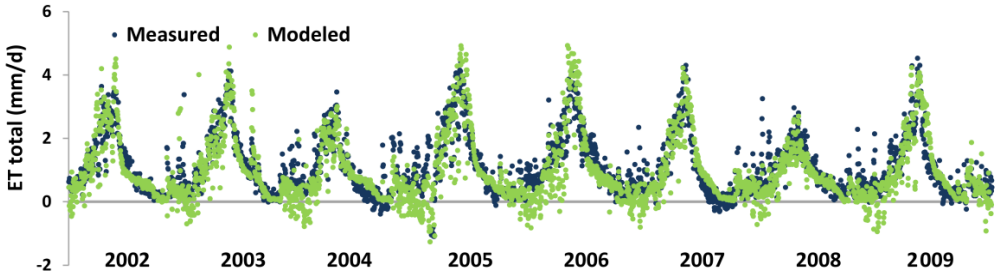

(b)

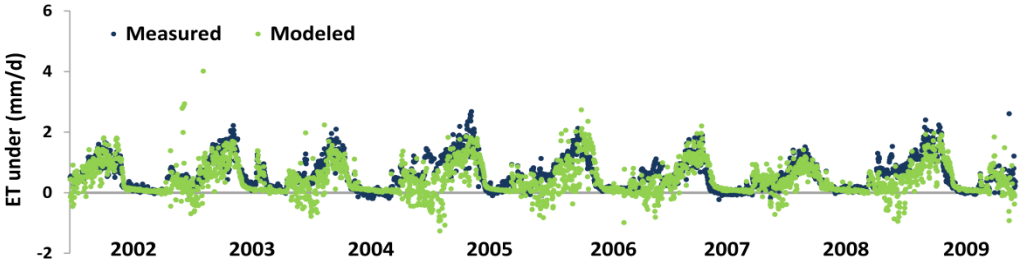

(c)

Figure 3.2 Daily Aggregated Modeling Results for a 8-year-long Simulation. Measured Rn and H+LE+G from the overstory eddy covariance tower showed the energy imbalance problem in measured data (a).Model results compared well with the measured ET from the overstory tower (b) and the understory tower(c). The model captured the measured predawn leaf water potential of blue oaks (d). Modeled soil moisture results compared with the measurements at different depths measured by theta probes(e); Removing measurements with poor energy budget closure from the analysis improved the model's fit with total ET (g vs. f).

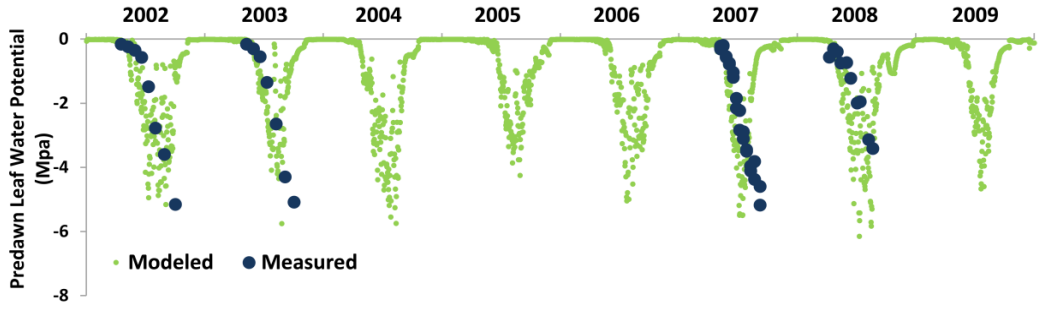

(d)

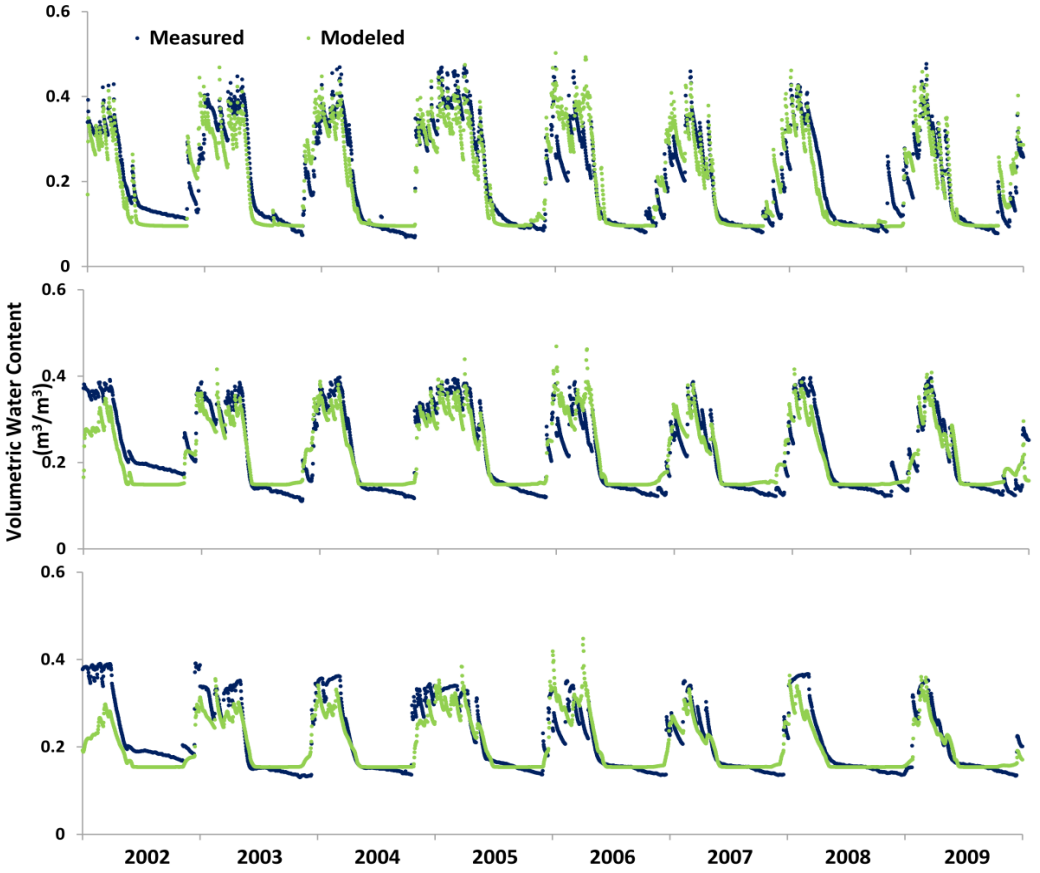

(e)

Figure 3.2 Continued.

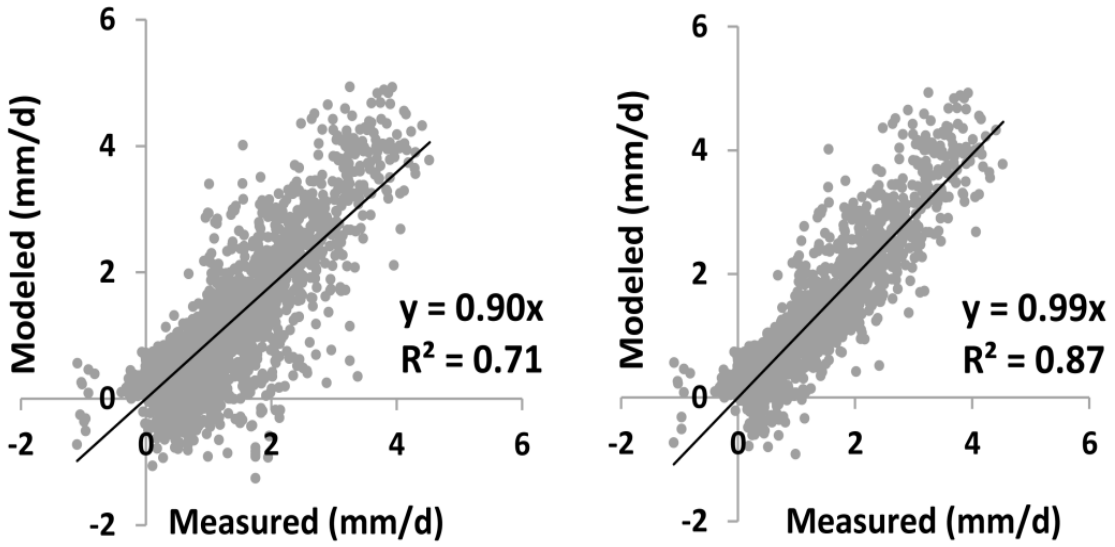

(f)

Figure 3.2 Continued.

Comparison between Measurements and Simulation Results at a Diurnal Scale

We further examined the model performance in simulating the diurnal changes of latent heat. We chose the results from four biophysically representative time periods: the wet season during winter when the oaks were dormant and the grasses were active (wet, January), the wet season during spring (wet, April) and the transitional period between wet and dry seasons (transitional, May) when both the oaks and grasses were active, and the dry season during summer when the oaks were active and the grasses were senescent (dry, August) (Figure 3.3). During each time period, we took the half-hourly average over a five-day period to display the diurnal cycle of latent heat. These five days were chosen from the days with high degree of energy closure measurements.

Modeled latent heat generally followed the diurnal patterns found in the measured results, albeit with some notable exception. Modeled values tended to be lower during nighttime, especially during the winter wet season (January in Figure 3.3). One possible cause: the model can simulate dew while the measurements from eddy covariance tower did not capture dew during the night. This phenomenon became more obvious in winter nights when temperature was low. Both overestimations (e.g. May 2005 and 2009) and underestimations (e.g. May 2002 and 2003) of midday latent heat were shown in Figure 3.3. These mismatches did not show any seasonal or annual biases that they may occur in any seasons in both wet and dry years. We suspect one reason of these mismatches was that the model domain did not represent the footprint of the eddy covariance tower [*Miller*, 2009]. Since the spatial dimension of the flux footprint was not fixed and it changed with the atmospheric conditions [*Wilson et al.*, 2002], the modeled results from the fixed model domain may overestimate or underestimate the measured flux captured in the dynamic footprint.

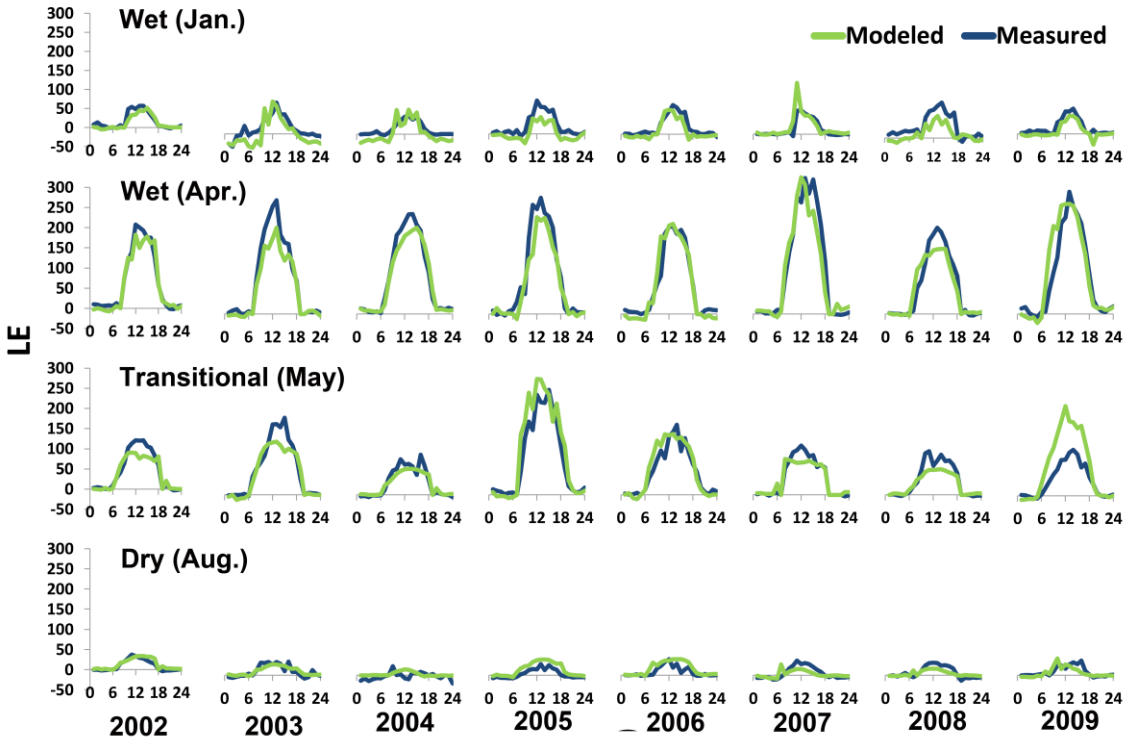

Figure 3.3 Model Performance. When simulating 5-day average diurnal changes of latent heat from the overstory tower, the results were broken down by plant physiological stage and season.

Comparison between Spatial Patterns in Measurements and Simulation Results

We chose the modeled soil moisture results at nine locations where the nine sets of TDRs were installed to compare against the measurements under different oak and grass covers at 10 cm depth in Year 2004 and 2005 (Figure 3.4). The modeled results generally captured the soil moisture changes under different vegetation cover. During the wet winter seasons, the soil moisture values under oak and grass were similar because canopy interception and ET were low. After major precipitation events ceased in May, soil moisture decreased rapidly and the soil water content under oak and grass were differentiated due to unequal plant water uptake and soil evaporation rates ; the soil moisture under grass decreased more slowly than the soil moisture under oaks did. This pattern became more obvious when comparing the model results of seasonal changes in soil moisture at different depths (Figure 3.5). For example, soil moisture in January 2004 was wetter and more homogeneous across the model domain than soil water in April and May. In the model simulation, individuals of the same species were assigned the same species specific parameters. For example, every oak tree had the same leaf area index and root distribution. Therefore, the soil moisture results under the same species were very similar and only slightly altered by topographic factors. However, the differences of soil moisture under different species (Figure 3.1) could be easily distinguished (Figure 3.5).

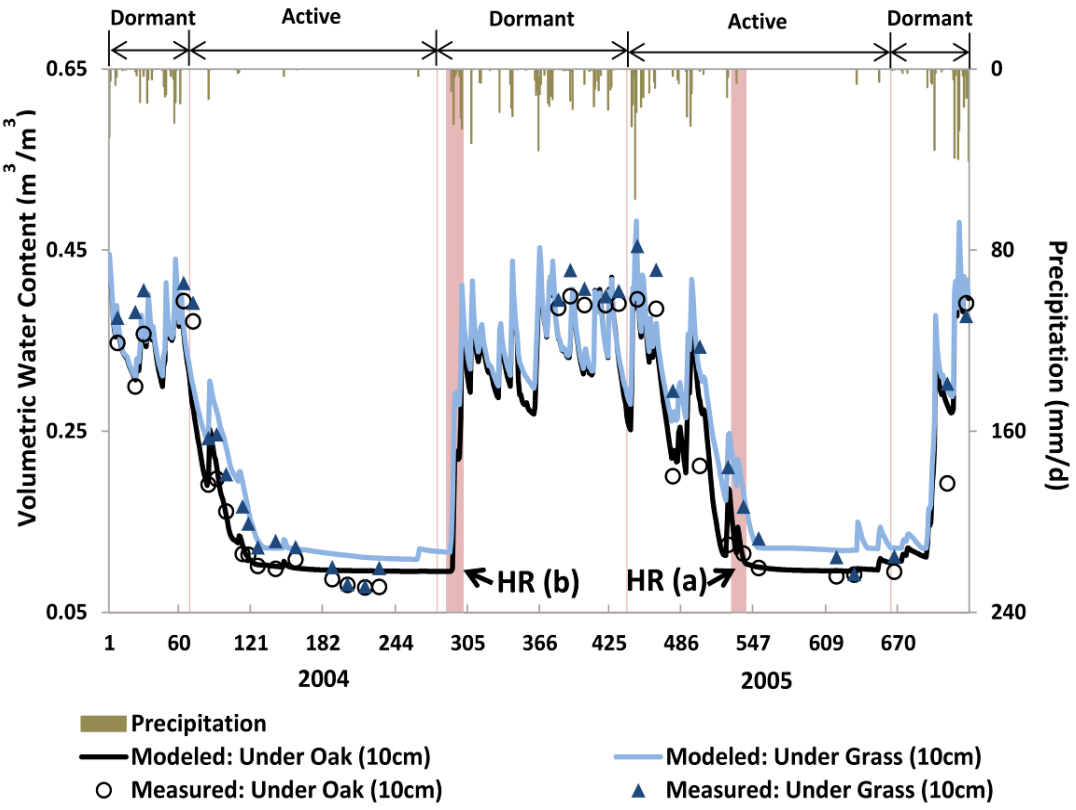

Figure 3.4 Soil Moisture Under Oak and Grass Covers at 10 cm Depth in 2004 (A Dry Year) and 2005 (A Wet Year). The black circles were the averaged measurements collected by TDRs under oak canopies, and the blue triangles were the averaged measurements from TDRs in the grass. The pink columns indicated the periods which were chosen to highlight the HR dynamics in Figure 3.8.

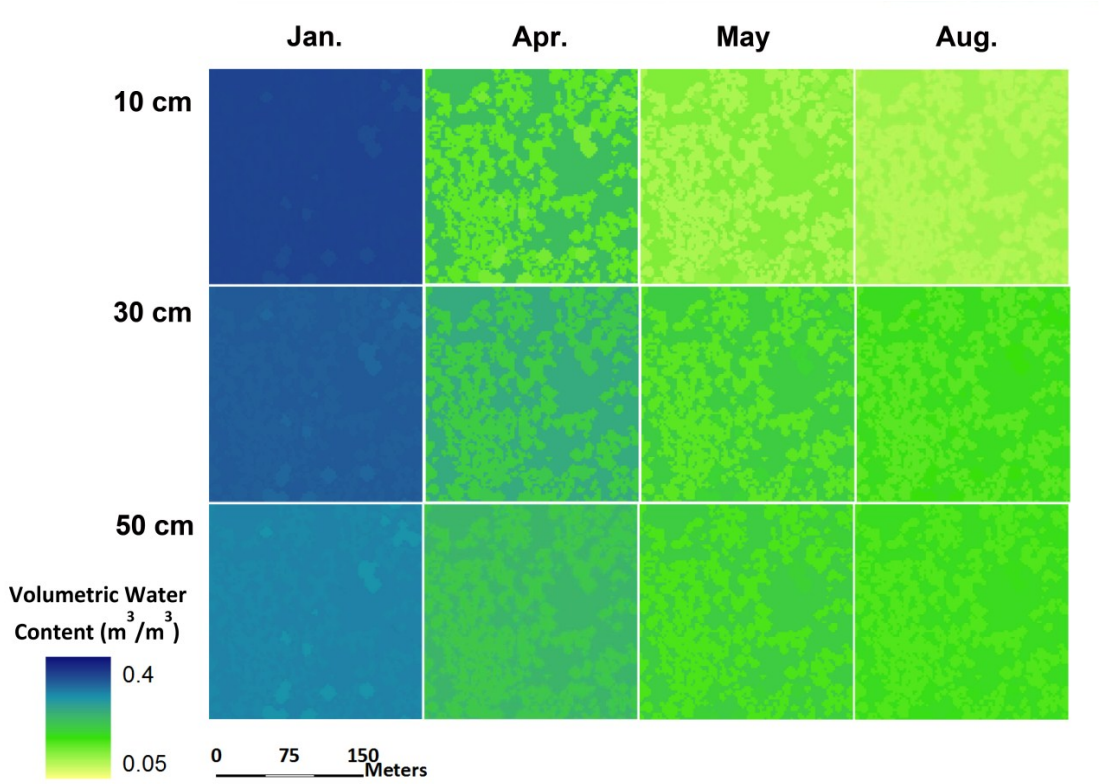

Figure 3.5 Monthly Average Soil Moisture Modeled at Different Depths During 2004.

Results and Discussion

Groundwater Uptake and the Shift in Plant Water Sources

The seasonal shift in plant water sources was also found at our study site. Miller et al. [2010] presented a suite of direct and indirect methods to examine the groundwater uptake by blue oak at this site. The results indicated that the blue oaks switched to take more water from saturated zone when soil water was depleted in dry season. We followed the White-Loheide method [*Loheide et al.*, 2005; *White*, 1932] reported in the study of Miller et al. [2010] using diurnal water table fluctuation data to estimate groundwater consumption by the blue oaks at this site. Continuous groundwater measurements with half hourly time interval were collected since May 2007. The daily groundwater uptake rate was estimated from May 2007 to December 2009 with two major measurement gaps from January 2008 to March 2008 and from August 2008 to September 2008 (Figure 3.6, estimated groundwater uptake). Considerable uncertainty and errors in this estimation were subjected to the measurements, the assumptions, the parameter value selection and the method itself (see discussions in Miller et al. [2010]). The estimated results (Figure 3.6) showed that groundwater uptake started increasing in May when soil water was decreasing and reached the maximum rate around June when net radiation was maximum (Figure 3.2a). The total ET measured from the overstory eddy covariance tower was decreasing at the same time. It indicated that soil water uptake was decreasing rapidly and plant water source switched from soil water to groundwater. Groundwater uptake decreased after June with the decreasing in net

radiation. Comparing to the wetter year 2009, the estimated groundwater uptake in the drier year 2008 started increasing earlier and had a greater contribution to total ET. It indicated that the time and duration of groundwater uptake tightly related to precipitation and as Bleby et al. [2010] found.

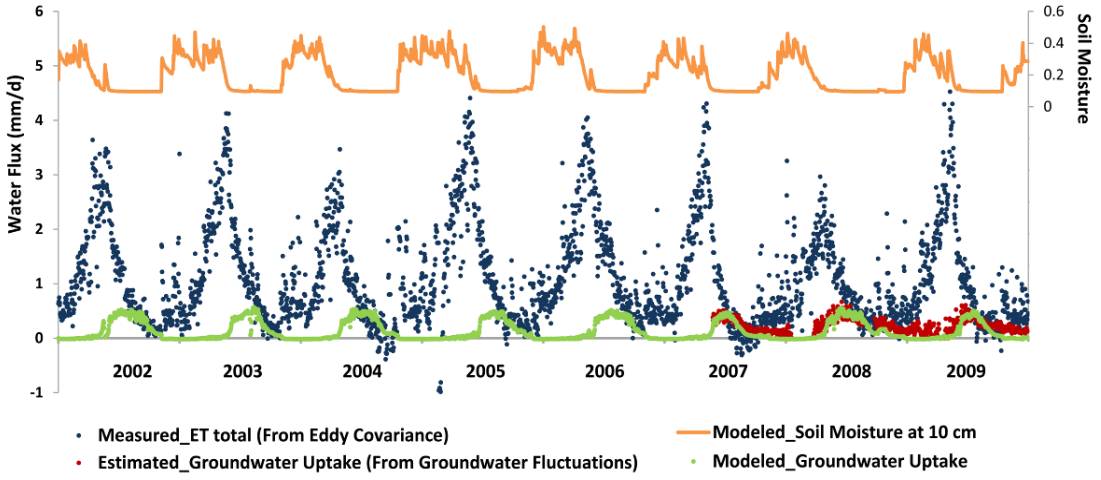

Figure 3.6 The Model Captured the Plant Groundwater Uptake, as Estimated from An Analysis of Diurnal Water Table Fluctuations.

The new root water uptake function in our model was based on the dynamics of potential gradients and resistances in the groundwater-soil-plant-atmosphere continuum. Therefore, it was capable of capturing the daily and seasonally shifts in plant water source. Figure 3.6 showed a good agreement between the modeled groundwater uptake and the estimated values from the groundwater fluctuation data from May 2007 to December 2009. Because only the blue oaks were considered to reach groundwater in the model simulation, the modeled groundwater uptake dropped to nearly zero when

blue oak canopy was dormant from around mid-October to mid-March next year. However, the estimated groundwater uptake continued to occur with a low rate after the blue oaks litter fell which may due to groundwater use by the evergreen grey pines at this site [*Miller et al.*, 2010b]. Therefore, the modeled groundwater uptake results were slightly lower than the estimated values from water table fluctuation. The model generally matched the trend of increasing and decreasing in groundwater uptake from May to September and captured the seasonal shift in plant water source.

The modeled groundwater uptake in the 8-year simulation showed that the groundwater uptake by blue oaks supported most dry season ET at the site. During the dry seasons, over 60% of total ET during June, July, August and September came from groundwater uptake. The highest groundwater contribution to dry season total ET occurred in Year 2008 (76%) and the lowest happened in Year 2005 (42%). It implied the oaks used more groundwater during dry season in drier year (Year 2008) to buffer the impacts of drought, while they used more soil water in the wetter year (Year 2005). The modeled maximum groundwater uptake rates were almost the same in each year, with the rate of 0.61 mm/day. It was mainly limited by the ability of tap root to transport water (tap root hydraulic conductivity and cavitation) and tightly related to the groundwater depth.

Considering the dynamics of soil moisture of the top 20 cm depth, Figure 3.6 revealed that the time when groundwater uptake started increasing (groundwater uptake started to exceed 10% of total plant water uptake) corresponded to the time when the volumetric soil water content dropped to around 0.11 m^3/m^3. Figure 3.7 showed the van

Genuchten curves used in model simulation for the top soil layer, which described the relationships of volumetric soil water content, soil water potential and soil hydraulic conductivity. The critical soil water content value 0.11 m^3/m^3 (the red dot shown in Figure 3.7) approached to the point of inflection (when soil water content equals to 0.107 m^3/m^3) in both curves. When soil moisture dropped below a threshold soil water content of 0.11 m^3/m^3, corresponding to a soil water potential of -0.26 Mpa, past which a slight decrease in soil water content would lead to dramatic decrease in soil water potential and soil hydraulic conductivity. Under that situation, when plant extracts a small amount of water from the soil water, it needs to overcome a large amount of negative potential and resistance. It is at this point that groundwater uptake starts to become more thermodynamically favorable than soil water uptake and the plants subsequently increased their groundwater uptake. This relationship may help to explain the phenomena found in other studies whereby deep roots are tightly coordinated with shallow roots to supply plant water use and HR [*Bleby et al.*, 2010]. A threshold approach could also help make future applications of the model more computationally tractable.

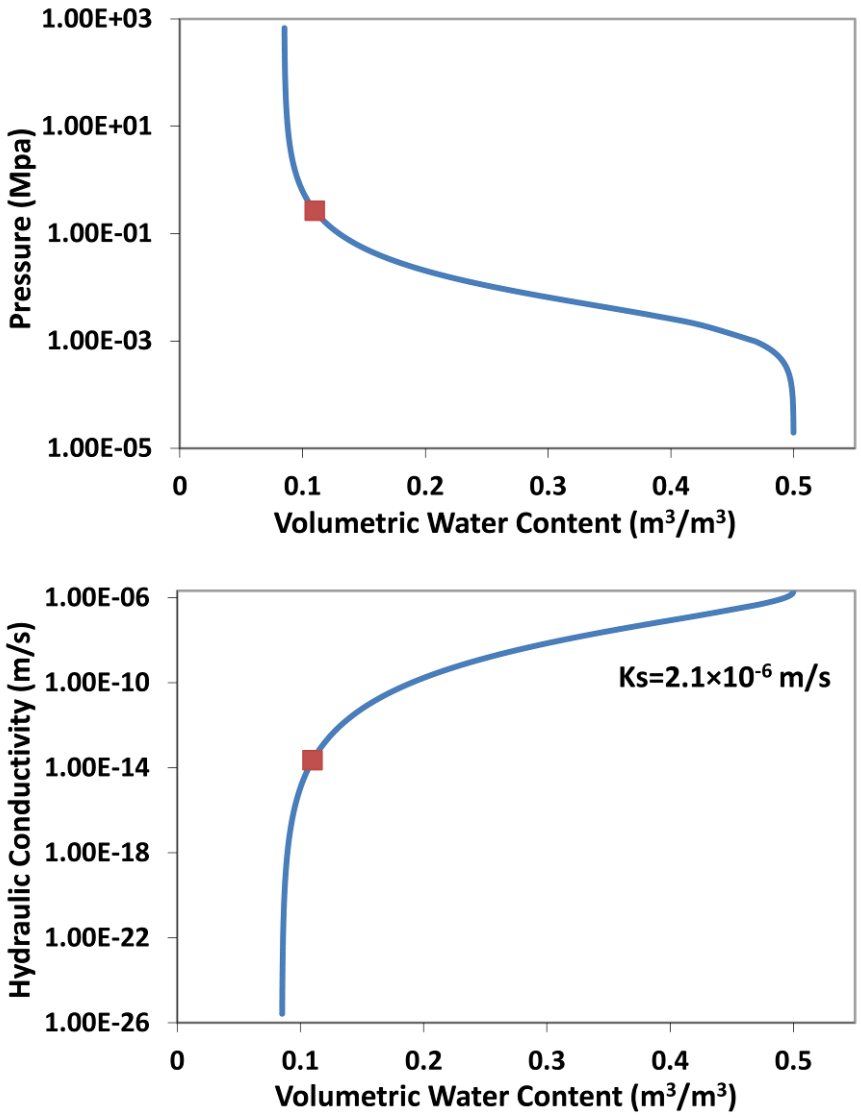

Figure 3.7 van Genuchten Curves Used for the Top Soil Layer in Model Simulation. The red dots indicated the critical soil water content point (0.11 m^3/m^3). When soil moisture dropped below this point, groundwater uptake became thermodynamically favorable than soil water uptake, and plants switched to extracting more groundwater.

Hydraulic Redistribution

While no observations of sap flow in roots or conclusive stable isotope data at this site [*Miller et al.*, 2010b] were available to measure HR directly, the diurnal fluctuation in soil moisture measurements at different depths under the blue oak canopy indicated that HR likely occurred [*Miller*, 2009]. The model results revealed that HR (both hydraulic lift and hydraulic descent) occurred throughout the year, even during the periods when blue oak canopy was dormant (Figure 3.4). Hydraulic lift mainly arose in nighttime during the dry season when blue oaks were active. During these periods, the upper soil layer dried, and a water potential gradient formed between the upper dry soil and the deeper wet soil or/and groundwater. For example, in 2004, daily hydraulic lift ranged from 0.04 to 0.2 mm/day, with the average of 0.07 mm/day. The water lifted by HR during the night contributed to 5-47% of oak transpiration next day, with the average of 10%. Hydraulic lift during 2005 was similar, with daily ranges from 0.03 to 0.22 mm/day and an average of 0.06 mm/day. It contributed to 4 to 19% of next day oak transpiration, with the average of 8%. Hydraulic lift became noticeable at Day 120 in Year 2004 and at Day 174 in Year 2005. Generally, hydraulic lift occurred earlier and had larger effects to increase transpiration in dry year (Year 2004) than did in wet year (Year 2005). Hydraulic descent occurred following the rainfall events. The precipitation stored the shallow soil layers was taken by the lateral roots and transferred downward into the deeper, drier layers. It formed a likely more favorable pathway to transfer precipitation into deep soil layers than did infiltration through the soil pores. The model results showed that hydraulic descent was larger than hydraulic lift. Hydraulic descent

ranged from 0.08 to 1.89 mm/day, with the average of 0.2 mm/day. The magnitudes of both hydraulic lift and hydraulic descent fell into the ranges reported in Neumann and Cardon's review of HR [*Neumann and Cardon*, 2012].

Figure 3.8a showed both hydraulic lift and hydraulic descent in blue oak active season in Year 2005. Upper Soil Water uptake, Middle Soil Water Uptake, Lower Soil Water Uptake, and GW uptake in Figure 3.8a indicated the root water uptake from upper soil layer (0-20 cm), middle soil layer (20-40 cm), lower soil layers (40-60~100 cm), and groundwater, correspondingly. The positive value indicated the water was taken from the soil layers and saturated layers into the roots, while the negative value implied the water was released from the roots to the surrounding layers. From Day 530 to 532 before the small rainfall events, the soil layers were drying. During the daytime, the water taken from the dry soil layers decreased while the water used from deep groundwater increased. During the nighttime, the root water uptake from groundwater was positive while the water uptake from soil layers were negative, which implied hydraulic lift occurred that water was taken from groundwater and released into the dry soil layers. At the end of Day 532, small rainfall events commenced and the upper soil layer became wetter. Hydraulic descent occurred at approximately Day 533 (i.e., June 16, 2005) when the lateral roots took water from the wetter, upper soil layer and transferred the water downward into the drier, middle and lower soil layers. At the same time, the saturated layer and the soil layers did not reach equilibrium during Day 533. Therefore, the groundwater uptake values were still positive in nighttime of Day 533, indicating a small amount of hydraulic lift from groundwater to soil layers still occurred. These model

results revealed that hydraulic lift and hydraulic descent could theoretically happen at the same time. From Day 535 to 540, as the soil layers gradually dried, nighttime hydraulic lift from groundwater to soil layers became more apparent again. The drier the soil layer (i.e. upper soil layer in this case), the larger amount of water was released into the layer through hydraulic lift. Figure 3.8a also showed that the daily shift in plant water source during the daytime that groundwater uptake was increasing when soil water was depleting (from Day 530 to Day 532 before the rain, and from Day 533 to Day 540 after the rain), and it decreased rapidly after the rain in Day 533. The soil water uptake functioned oppositely as the groundwater uptake did.

When the canopy was leafless, there were no strong diurnal fluctuations in root water uptake, compared to the obvious diurnal changes during the active season (Figure 3.8b vs. Figure 3.8a). Slight diurnal fluctuations in root water uptake occurred during Day 288 and 289 due to soil evaporation. The roots in the wetter, middle and lower soil layers lifted a small amount of water to the drier, upper soil layer, which compensated for some water loss from soil evaporation. Groundwater was continuously lifted into soil layers due to the disequilibrium between dry soil layers and groundwater. In Day 290 (i.e., October 16, 2004), the incoming precipitation led to obvious hydraulic descent whereby the roots moved water from upper soil layer and transported it into deeper soil layers. The root water uptake from groundwater diminished immediately after the rainfalls. Hydraulic descent continued after the rainfalls and it occurred during both daytime and nighttime. During the rainy days from Day 290 to 299, soil evaporation was very small and no apparent diurnal fluctuations were found during these days. In Day

298, a large rainfall event happened. However, the magnitude of hydraulic descent caused by this large rainfall was much smaller compared to the hydraulic descent amount in Day 290 following the small rainfalls. Before Day 290, all soil layers were dry. The incoming rainfalls in Day 290 caused a significant soil water potential gradient between the top soil layer and the rest soil layers, which led to a large magnitude of hydraulic descent. From Day 290 to 297, precipitation was gradually distributed into different soil layers through hydraulic descent and percolation. The soil water potential gradients among these soil layers decreased. Even a large rainfall occurred at Day 298, the small soil water potential gradients only resulted to a small magnitude of hydraulic descent. The similar phenomenon was shown in Figure 3.8a that the small rainfalls at Day 532 led to significant hydraulic descent. Therefore, the magnitude of hydraulic descent did not only depend on precipitation amount, but also depended on the water potential gradients among layers.

The downward water movements in soil layers through hydraulic descent had different mechanisms compared to the downward soil water movements through infiltration and percolation. For example, during Day 532 and 533 in Figure 3.3b, the total amount of the small rainfalls was only 6 mm, while the saturation of the upper 20 cm soil layer was only 31% before the rains. These small rainfalls were not enough to trigger percolation. However, the occurrence of hydraulic descent moved these small rainfalls down into middle and lower soil layers. If hydraulic descent did not occur, the small precipitation would be confined in the top soil layer and may be wasted through soil evaporation later. Therefore, hydraulic descent could help the plants take advantages

of small rainfalls, which may have important ecological and hydrologic impacts especially for the plants in arid areas.

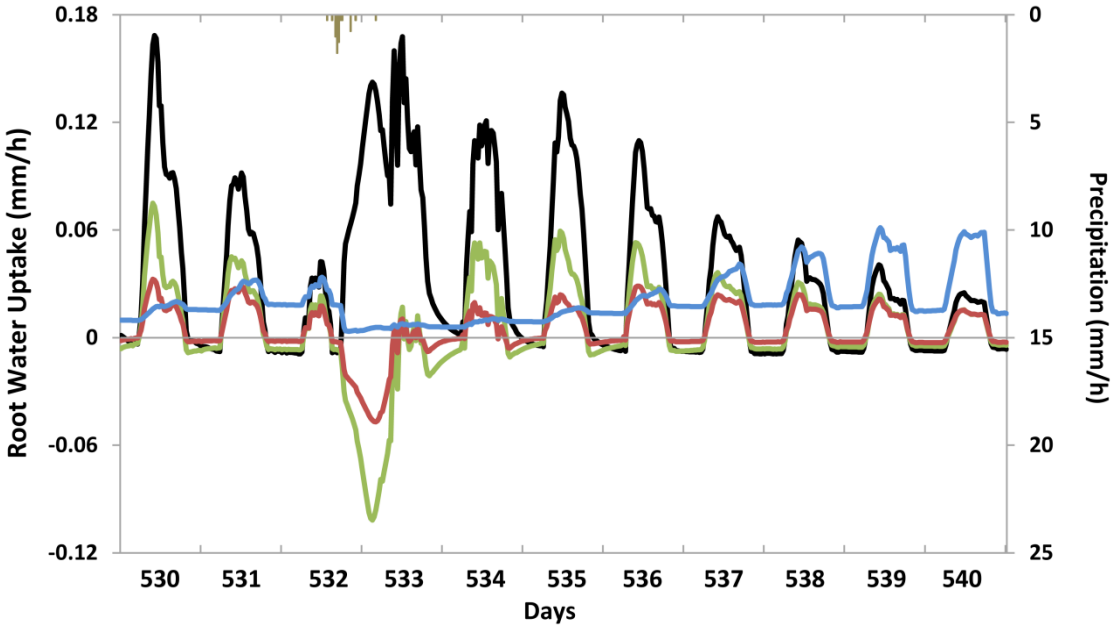

(a)

Figure 3.8 Two HR Examples. (a) HR when blue oak canopy was active in Year 2005 during the dry season. (b) HR when blue oak canopy was dormant in Year 2004 at the beginning of wet season in winter. Upper, Middle and Lower Soil Water Uptake and GW uptake indicated the water was taken by the roots in upper soil layer (0-20 cm), middle soil layer (20-40 cm), the remaining lower soil layers (40-60~100 cm), and groundwater, correspondingly. The positive water uptake values indicate that the water was removed from the soil layers and saturated layer by the roots, while the negative values implied the water was released from the roots to the surrounding layers.

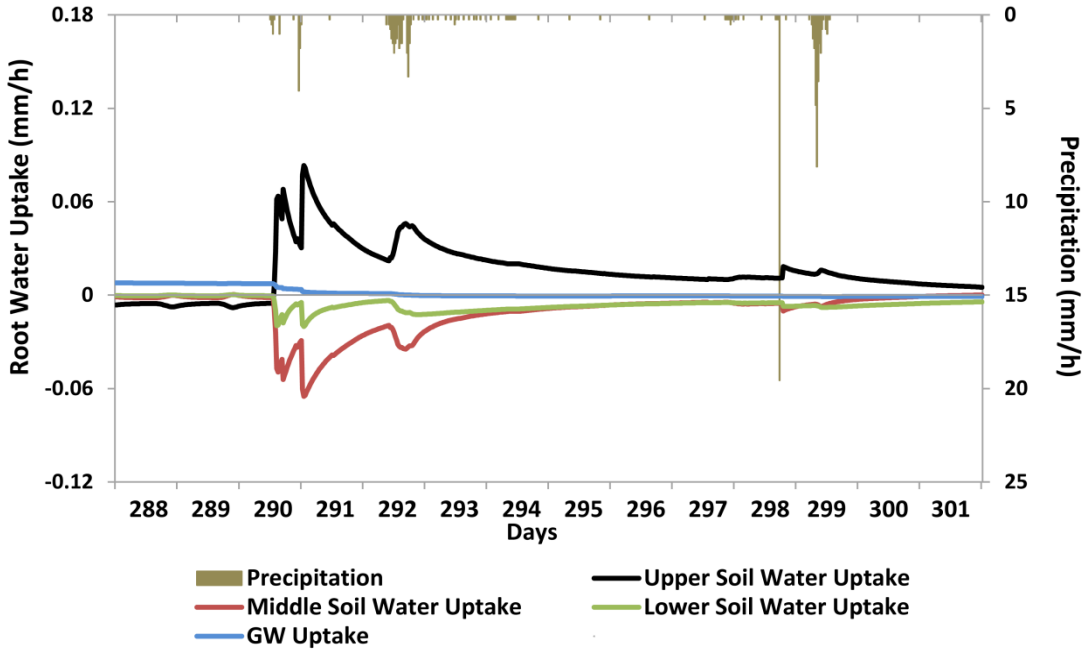

(b)

Figure 3.8 Continued.

In addition, we found both hydraulic lift and hydraulic descent of the blue oaks at this site served as the competitive mechanism between trees and annual grasses. Hydraulic lift became obvious at Day 120 in Year 2004 and at Day 174 in Year 2005. At that time, the surface soil layers were dry and the grasses had almost senescenced. Hydraulic lift of blue oaks occurred too late in the dry summer to benefit the surrounding annual grasses. It only improved the water use for blue oaks themselves. The similar conclusion was found in Ishikawa and Bledsoe's study [2000] in a California blue oak woodland; hydraulic lift did not appear until June and was unlikely to facilitate annual grasses. During the wet winter when the grasses were active and the trees were dormant,

hydraulic descent by blue oaks moved surface soil water into deeper layers, away from the reach of shallow rooted grasses. Such water would be stored in deeper layers and utilized later by the blue oaks when they were active. Therefore, the HR of the blue oaks at this site only benefited the oaks themselves, rather than profited the shallow rooted grasses. This finding was different from some findings at various sites that the shallow rooted plants could benefit from HR by using significant portion of water lifted by deep rooted plants [*Dawson*, 1993; *Koster and Suarez*, 2001; *Ludwig et al.*, 2003].

Conclusions

We integrated new functions for modeling uptake by phreatophytic plants [Gou and Miller, 2013] into the spatial distributed groundwater-land surface model, ParFlow.CLM [*Maxwell and Miller*, 2005] to improve its performance in simulating plant root water uptake, hydraulic redistribution, and plant water stress. The modified model was tested at a semiarid, oak savanna site and performed well, capturing the daily, hourly and spatial water and energy patterns in a 8-year model simulation. The energy balance closure problem in the measured data from the eddy covariance tower resulted to significant influence in our model testing. Future modeling efforts using similar datasets should address this issue in model calibration and validation.

The new plant water stress function used for the blue oak simulation was based on the linear relationship between the changes of stomata conductance and the changes of hydraulic conductance in roots [*Meinzer et al.*, 2001; *Sperry et al.*, 2003]. This new

plant water stress function was again capable of capturing the latent heat dynamics in our model tests and proved to be valuable for simulating deep rooted trees and groundwater dependent vegetation. It also had advantages in the simulation of plants in arid and semiarid areas where the plants may suffer periodic cavitation in roots. In addition, the model predicted leaf water potentials which are not available in most land surface models although they serve as a critical indicator of plant water status. In future study, the new feature of leaf water potential simulation will allow the model to estimate the potential impacts on plants introduced by groundwater overpumping or climate change.

The analysis of diurnal water table fluctuation data indicated that the trees took most water from soil water during the wet season and switched to mainly depend on groundwater during the dry season at this site. This seasonal shift of plant water source was captured by our model. The model revealed that deeper soil water and groundwater contributed to tree transpiration later when top soil layer was depleted. It indicated that the soil moisture memories at different depths and groundwater linked to atmosphere through transpiration during different time periods. This phenomenon is currently ignored in many land surface models. The plant water uptake functions in previous versions of CLM extracted water from different layers simultaneously, potentially leading to biases in the modeling of land surface-atmosphere interactions, especially in long term simulations.

The simulation of plant water uptake in our model also highlighted how groundwater uptake from deep roots coordinated tightly with the soil water uptake from

shallow roots in order to support transpiration and HR. The critical soil water content value was found to be near the point of inflection of the soil water retention curve. When surface soil water content dropped below the critical point, groundwater uptake became thermodynamically favorable than soil water uptake and plants switched to use groundwater. This critical point was tightly related to the soil water characteristics. Thus, soil types should have significant impacts on the critical point value. Also, the cavitation of plant roots was also impacted by surrounding soil. It would further change the resistance of GSPAC and root water uptake. Therefore, the hydraulic characteristics of both soil (depicted by soil water retention curve) and plant (depicted by xylem vulnerability curve) should be considered together to analyze the complex root water uptake dynamics in future studies.

The model predicted both hydraulic lift and hydraulic descent during blue oak active and dormant seasons. The timing of HR suggested that HR helps the blue oaks compete for water with the annual grasses at this site. Hydraulic lift became obvious during the dry season when oaks were active and grasses had senescenced, potentially enhancing oak transpiration without benefiting grasses. The simulations for 2004 and 2005 showed that the water lifted by hydraulic lift during the night contributed to 4-47% of next day oak transpiration. Hydraulic descent was more detectable than hydraulic lift, and ranging from 0.08 to 1.89 mm/day. Hydraulic descent occurred after rains, but large rainfall events did not always trigger significant hydraulic descent, as the magnitude of hydraulic descent also depended on water potential gradients between layers. Hydraulic descent served as another pathway of downward soil water migration, supplementing or

even eclipsing percolation. Our model allows simulation of the impacts of hydraulic redistribution on the spatial and temporal patterns of soil moisture and ET and can be used to determine their further impacts on regional energy and water dynamics.

CHAPTER IV

IMPACTS OF HYDRAULIC REDISTRIBUTION, SOIL TYPE, GROUNDWATER DEPTH AND ROOT DISTRIBUTION ON ECOHYDROLOGICAL PROCESSES

Introduction

The two models developed in Chapter II and III were capable of capturing a series of key ecohydrological processes acting along the groundwater-soil-plant-atmosphere continuum (GSPAC) at a range of scales. Various factors, such as climate, soil type, groundwater depth, and plant physiology, may influence these ecohydrological processes and lead to changes in water and energy dynamics at larger scale. Therefore, in Chapter IV, four scenario tests were conducted using the models discussed in Chapters II and III, to address how hydraulic redistribution, soil texture, groundwater depth and root distribution impacts the dynamics of the whole GSPAC system.

Previous studies have found many ecohydrological impacts of HR. Hydraulic lift increases dry season transpiration by lifting water up into the dry top soil layer where most root biomass located [*Caldwell and Richards*, 1989; *Caldwell et al.*, 1998; *Emerman and Dawson*, 1996; *Ryel et al.*, 2002; *Scott et al.*, 2008a]; Hydraulic lift recharges the shallow roots in dry season, prolonged the life span of these roots, and helped them maintain hydraulic contact with the surrounding dry soil [*Bauerle et al.*, 2008; *Domec et al.*, 2004], all of which could further promote plant nutrient and water

uptake; Hydraulic descent distributed precipitation into deep soil and promoted plant water conservation [*Hultine et al.*, 2004; *Scott et al.*, 2008a]; And HR serves as an important mechanism for trees competing with shallow-rooted species for water, or facilitating the water use of whole ecosystem [*Dawson*, 1993; *Ludwig et al.*, 2003; *Quijano et al.*, 2012]. The last impacts of HR had been discussed in previous Chapter III. In this chapter, Scenario 1 was constructed to test the first three impacts of HR by comparing the two cases with/without HR.

The results in Chapter III indicated that soil characteristics directly influenced plant soil water uptake, while indirectly impacting the timing and amount of plant groundwater use. Sperry and Hacke [2002] proposed the hypotheses that the plants in finer textured soils in arid climates experienced lower plant and soil water potential during drought, had higher xylem cavitation resistance, and developed shallower root systems than the plants in coarser soils. These hypotheses were supported by field study, model simulation and literature review of global rooting depth [*Hacke et al.*, 2000; *Jackson et al.*, 2000; *Jackson et al.*, 1996; *Sperry and Hacke*, 2002; *Sperry et al.*, 1998]. In this chapter, Scenario 2 was designed to explore how various soil textures influenced plant water use, and provide reasonable explanations of the impacts of soil texture on plant characteristics in the hypotheses of Sperry and Hacke [2002].

With the increasing demand for human water use and the changing climate regime, decreasing water tables caused by groundwater over-exploration and drought, may introduce severe stresses to groundwater dependent ecosystems. Sustainable groundwater management needs to address the water demand of human while

maintaining a low risks to GDEs [*Eamus and Froend*, 2006]. Information on the relationship between GDE health and groundwater depth is needed [*Eamus et al.*, 2006; *Orellana et al.*, 2012]. Therefore, Scenario 3 was conducted to test how the whole GSPAC system responded to different groundwater depths, and provided information of the influences of groundwater depth on groundwater-land surface-atmosphere interactions and the water use of GDEs.

Root distribution is considered as a critical factor in root water uptake simulation from local to global scales in many hydrological, land surface and climate models [*Feddes et al.*, 2001; *Jackson et al.*, 2000; *Zeng*, 2001; *Zeng et al.*, 1998]. Plant roots provide the linkage from soil water and groundwater to the atmosphere through root water uptake and transpiration, which directly impacts the atmospheric boundary layers and is closely related to climate prediction [*Feddes et al.*, 2001; *Zeng et al.*, 1998]. Feddes et al. [2001] reviewed the root water uptake simulation in a number of hydrological and climate models, and summarized two broad classes of root parameters used: the bottom-up or microscopic models with detailed description of plant root distribution and functions, and the top-down or macroscopic modeled with simply parameterized root properties. The models in Chapter II and III belonged to the first category of bottom-up model. Such models allow the explicit description of root influences on plant water use. In Scenario 4, cases with a range of root distributions were compared to address its impacts on ecohydrological processes.

Method

All scenarios in Chapter IV used the modified ParFlow.CLM model in Chapter III. Scenario 1 examined the water and energy changes of blue oak with and without HR at the Tonzi site, aiming to illustrate the implications of HR in the whole system. A 1-D model was created that the soil column had shallow soil depth from 0 to 60 cm, underlain by a 8 m saprolite zone and then the fractured bedrock. The soil column was divided into 28 uneven layers, including three shallow soil layers with 20 cm thickness for each layer. All the parameters related to soil characteristics were the same values as those used in Chapter III. The vegetation cover of this 1-D model was blue oak, represented by the deciduous broadleaf forest type in CLM with the newly modified phreatophtic vegetation functions and the blue oak specific vegetation parameters. The water table depth was set to 9 m below ground. For the case with HR, all the functions in CLM were the same as those in Chapter III, allowing water release from root to soil and bi-direction water movement in roots. For the case without HR, the HR function in CLM was turned off so that there was no water leaking from the roots to the soil, and water was only transported from root tip to stem. Other functions and model settings were the same in both cases. Both simulation cases were forced by the measured meteorological data at Tonzi site used in Chapter III, including short wave radiation, long wave radiation, precipitation, air temperature, wind speed, atmospheric pressure, and specific humidity. The scenario tests were conducted at a half-hour time step for 8-year simulation, from 2002 to 2009.

Scenario 2 testing included twenty-one simulations with different soil textures to explore the effects of soil characteristics on the GSPAC system. The model settings were almost identical to those in the 1-D model used in Scenario 1, except shallow soil texture was altered for each simulation. The computer program ROSETTA [*Schaap et al.*, 2001] was used to predict the van Genuchten parameters [*van Genuchten*, 1980] needed for model simulation, based on the percentages of sand, clay and silt. All twenty-one simulations were conducted at half-hour time step with one year meteorological forcing of Year 2002. Soil texture also impacted soil evaporation. Scenario 2 only focused on the impacts of soil texture on plant water use. Therefore, the soil evaporation under the blue oak canopy was set to zero. Although soil texture could influence plant characteristics, such as root distribution, xylem cavitation resistance and root to leaf area ratio, the parameters related to plant characteristics were kept the same in all twenty-one simulations due to a lack of reliable data for these parameter values.

Scenario 3 testing had four simulations with various groundwater depths (3 m, 5 m, 7 m and 9 m). Scenario 3 helped interpret how the groundwater disturbed the vegetation water use. The model settings in Scenario 3 were the same as those used in Scenario 1, except that the groundwater depth changed in each simulation.

Scenario 4 had five simulations with the root fractions in groundwater increasing from 10% to 50% of total roots, in order to examine the influence of root distribution on the whole system dynamics. The root fractions in soil layers were decreased correspondingly. The model settings in Scenario 4 were also the same as those used in Scenario 1, except the changes of tap roots in each simulation. All simulations in

Scenario 3 and 4 were conducted at half-hour time step using the forcing data of Year 2002.

Results and Discussion

Scenario 1: With/Without Hydraulic Redistribution

Neumann and Cardon [2012] reviewed the empirical and modeling studies of HR and found the magnitude of HL represented 2-80% of transpiration. Figure 4.1 shows the transpiration difference of blue oak between two cases with/without HR. The averaged annual transpiration was 7% (15 mm) greater with HR (Table 4.1 (a)). HR promoted transpiration, especially in dry years of Year 2004 and 2008, which implied that the ecohydrological impacts of HR were more significant in dry years/seasons. In Chapter III, the model simulation showed that significant HL occurred during the transitional period and the dry season. Therefore, in Figure 4.1, the difference in transpiration between the two cases with/without HR became obvious mainly in the transitional and dry period from May to October. Table 4.1 (b) showes there were nearly no transpiration difference in wet season until May and the difference becomes obvious from May to October. HR increased dry season transpiration by 11%. Therefore, the contribution of HR to the land-atmosphere water flux was significant only in the dry season.

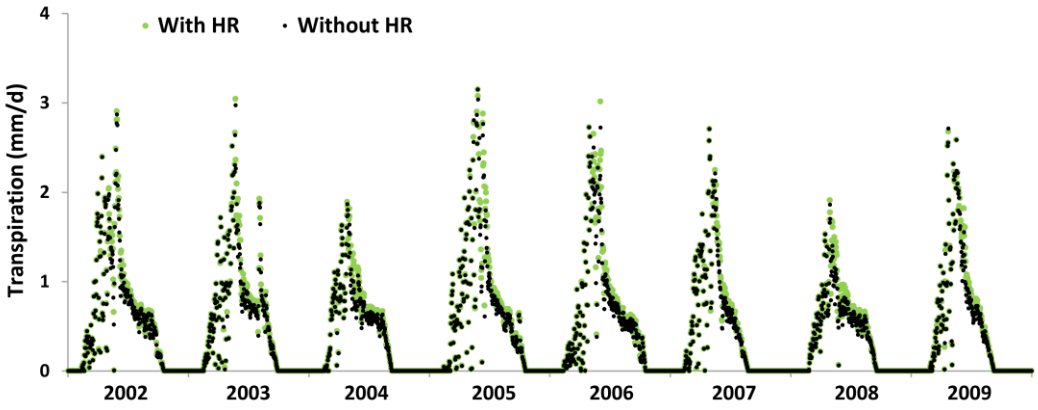

Figure 4.1 Impacts of HR on Transpiration. The black dots showed daily transpiration when HR did not occur in blue oak, while the grey dots showed the results of the case with HR. HR slightly promoted transpiration, especially during the dry season. The transpiration differences between two cases were more obvious in the dry years 2004 and 2008.

However, the impacts of HR on land surface processes may also be significant in wet season, since hydraulic descent (HD) occurred following rainfall events even through the trees were dormant. HD moved precipitation down into deeper soil layers, which may largely change soil moisture distribution in different depths. Figure 4.2 (a) showed the difference of soil moisture in the top soil layer at 10 cm. Hydraulic lift during the dry seasons did not lead to obvious difference in soil moisture at 10 cm, because most water lifted to top soil layer by HL was contributed to transpiration and soil evaporation. However, although the lowest soil water content during the dry season seemed nearly the same in two cases, the soil water potential was slightly higher in the case with HR. As a result, soil moisture rebounded faster after rain in the HR case. At

the end of dry season in October, soil moisture in the HR case was slightly higher than the results in the No-HR case (Figure 4.2 (a)).

Table 4.1 Transpiration Differences With/Without HR

(a) Annual averaged difference ((With HR-Without HR)/With HR)

Year	Transpiration Difference	
	(mm/yr)	(%)
2002	12	6
2003	10	6
2004	12	9
2005	13	6
2006	15	8
2007	9	6
2008	14	11
2009	11	7
Average	12	7

Table 4.1 Continued.

(b) Monthly averaged difference

Month	Transpiration Difference	
	(mm/month)	(%)
Jan	0	0.0
Feb	0.003	0.2
Mar	0.006	0.2
Apr	0.078	0.2
May	2.85	6.3
Jun	4.68	16.1
Jul	2.127	10.9
Aug	1.278	8.8
Sep	0.516	8.7
Oct	0.099	9.5
Nov	0	0
Dec	0	0

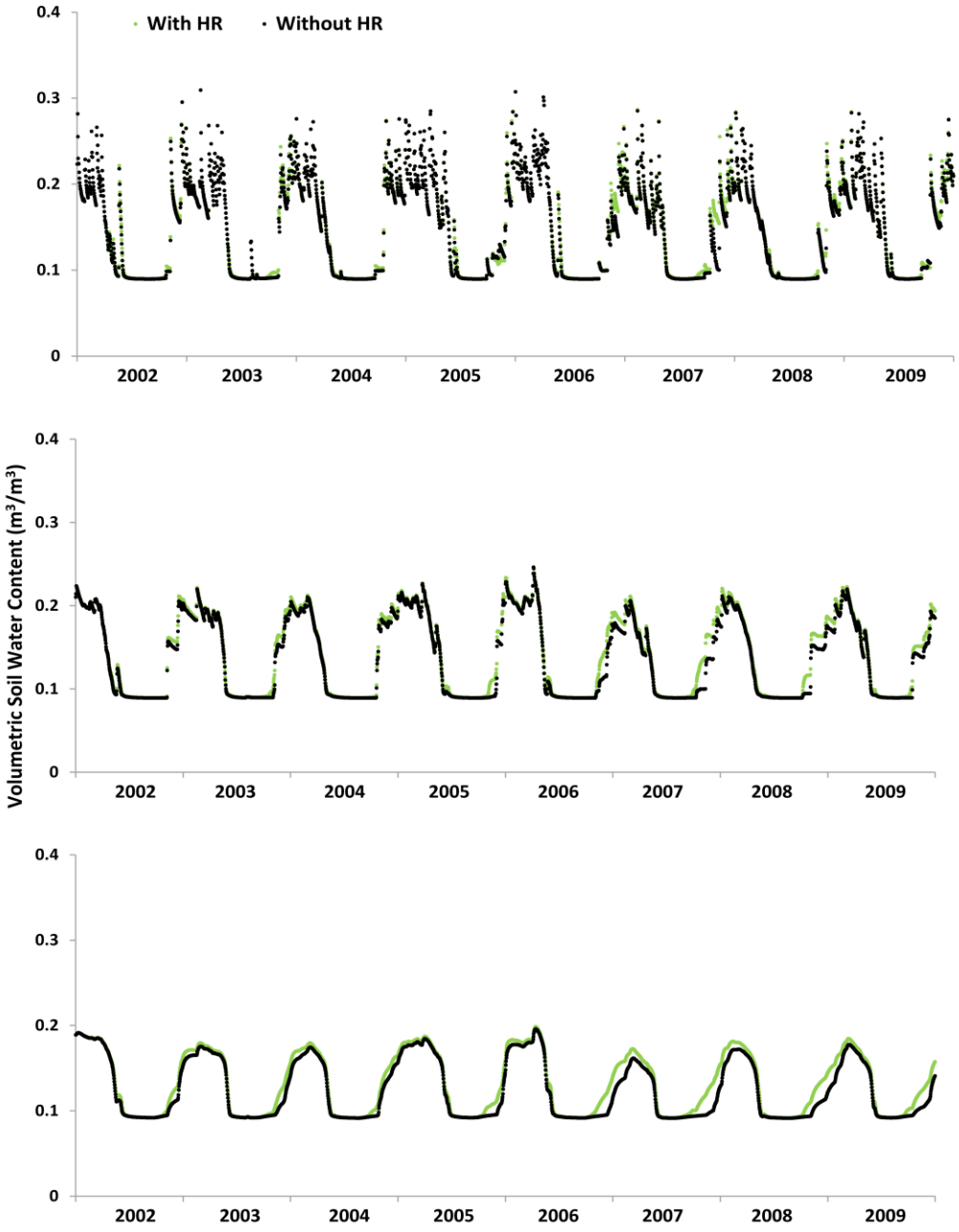

Figure 4.2 Impacts of HR on Soil Moisture. From the top to the bottom, the figures are soil moisture at 10 cm depth in the upper soil layer, at 30 cm depth in the middle soil layer, and at 50cm depth in the deep soil layer. The deeper soil layer was, the more obvious differences between two cases were during the wet season.

Although the soil moisture difference was small in top soil layer, it was interesting that the difference became more obvious in deeper soil layers (Figure 4.2 (b) and (c)). These differences were mainly due to hydraulic descent, which formed alternative pathway to distribute water into deeper layers. As a result, the soil moisture of deeper soil layers after the dry season was significant higher in the case with HR. The difference at 50 cm (Figure 4.2 (c)) was most significant. The deeper the layer was, the more obvious the difference was. When rainfall commenced after the dry season, the soil moisture in deep layers in the HR case increased earlier, which indicated that the precipitation that was moved downward through hydraulic descent reached the deep layers earlier than that was percolated.

In addition, HR also acted as the mechanism to recharge top dry soil layers and the roots in these layers in dry season. HR helped the top soil layers keep a certain potential to avoid further cavitation in lateral root. Without HR, the soil water potential in the dry season was slightly lower since the soil water reservoir kept losing water from soil evaporation, but it was not refilled with water from groundwater. More severe cavitation occurred in lateral roots as the hydraulic conductivity loss in shallow roots increased from 85% to approximate 95%. When the winter rainfall arrived, the lateral roots could not recover quickly because of the more intense cavitation during the dry period. Thus, HR serves as a protection mechanism to prevent hydraulic failure during dry season and to allows lateral roots to quickly respond when soil water becomes available.

Scenario 2: Different Soil Textures

We selected 21 soil textures located in USDA textural triangle (Figure 4.3) and used ROSETTA [*Schaap et al.*, 2001] to predict the van Genuchten parameters associated with each soil texture (Table 4.2).. Across the 21 simulations, only the van Genuchten parameters were changed, while the plant parameters of rooting depth and xylem cavitation (vulnerability curve) were kept the same. While previous studies have revealed that plants in different soil textures have different strategies of rooting depth and cavitation resistance, we assumed this was not the case to better constrain this sensitivity analysis.

Soil properties influenced water retention and movement, which further impacted the water availability of plants. Monthly transpiration rates varied by up to 127% across the 21 soil textures (Figure 4.4). During the wet season before May, the site was energy-limited condition. Nearly all the soil types could provide enough water to meet the transpiration demand. No obvious differences in wet-season transpiration were induced by soil texture variation. However, precipitation diminished since May and conditions at the site became water-limited. The differences in dry-season transpiration from May to October were distinct (Figure 4.4). In general, the impacts of soil characteristics on transpiration were significant during dry season in water-limited condition. Such impacts were not obvious when energy was the major limitation.

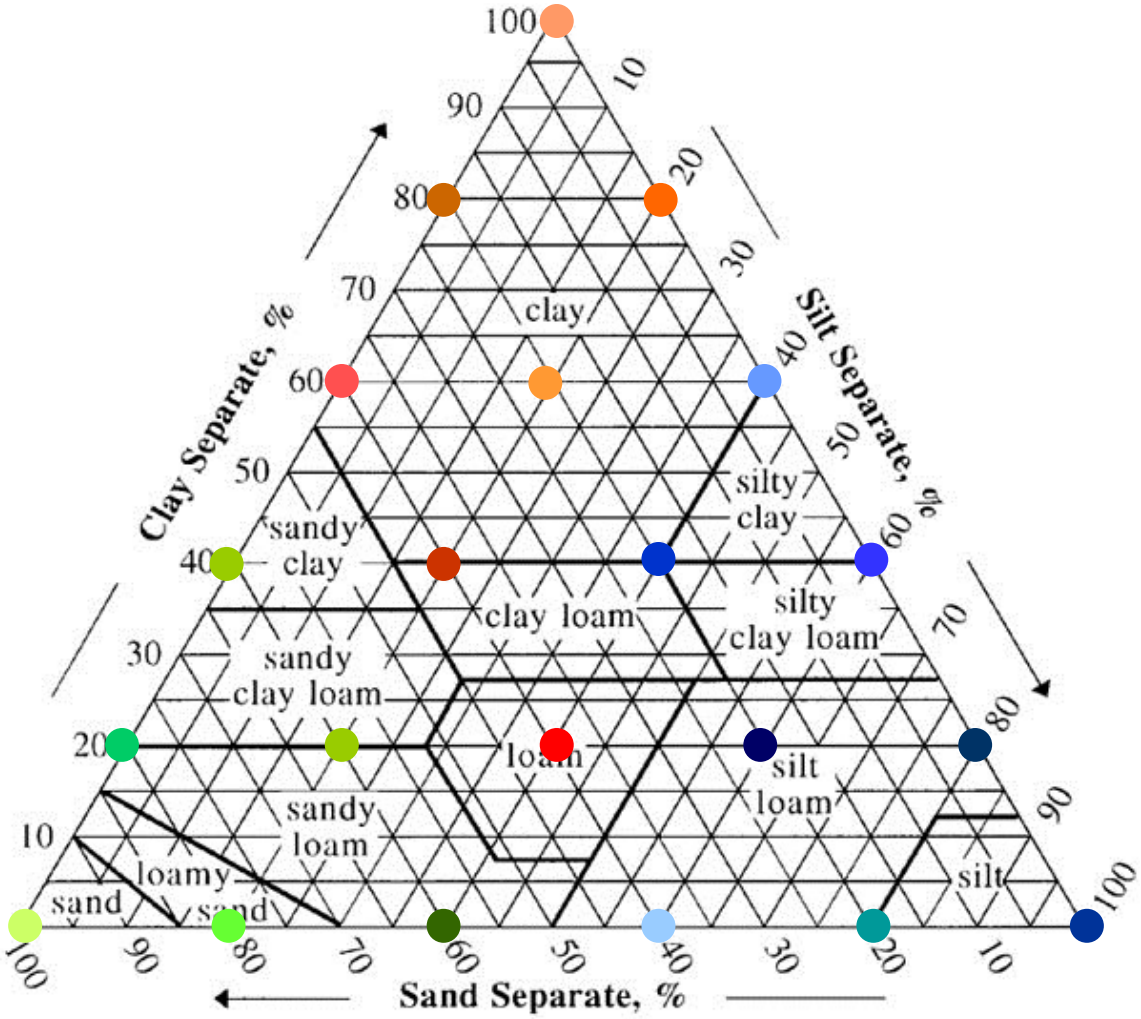

Figure 4.3 Twenty-one Soil Textures Used in Scenario 2. The dots showed the twenty-one soil textures which composed by different fractions of sand, silt and clay. Their locations in USDA soil textural triangle indicated their soil types.

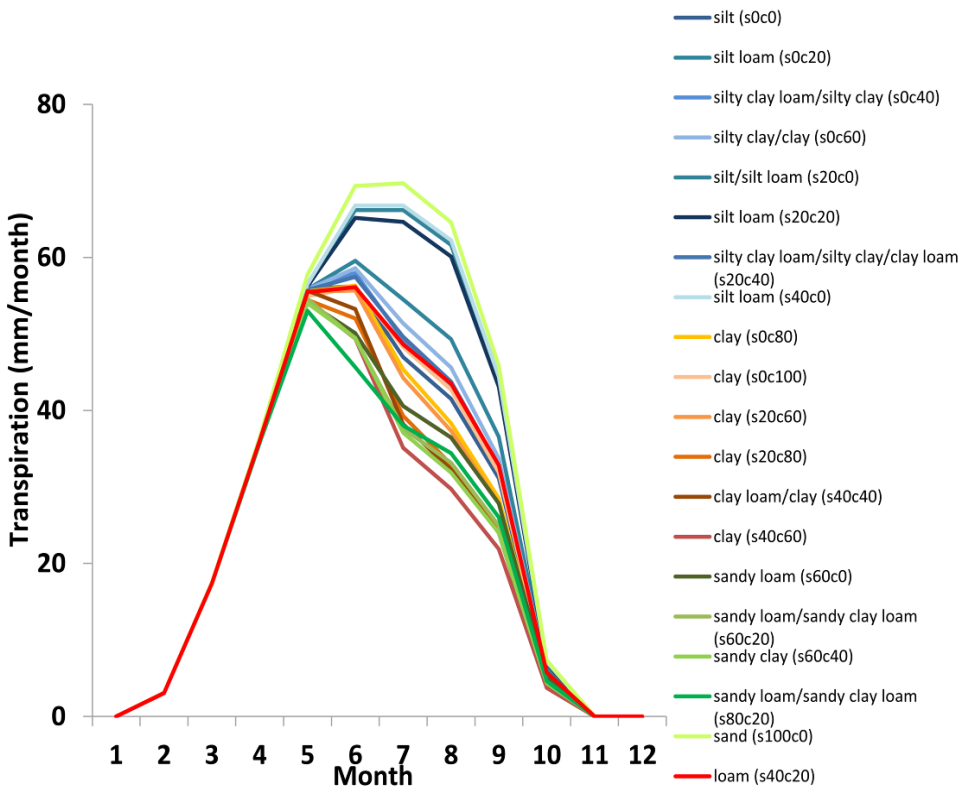

Figure 4.4 Monthly Transpiration Results with Twenty-one Soil Textures. The legend showed the soil texture with sand and clay fractions. For example, "s0c0" was 0% of sand (0%) and 0% of clay, and it indicated the soil is silt; "s0c20" was 0% of sand and 20% of clay, the rest 80% were silt. The differences among all soil textures were only significant in dry season from May to October when water was the major limit factor at Tonzi site.

Table 4.2 van Genuchten Parameters from ROSETTA Predication

Sand	Silt	Clay	Qr	Qs	alpha	n	Ks
0	0	100	0.11	0.50	1.59	1.15	18.45
0	20	80	0.11	0.53	1.99	1.18	17.09
0	40	60	0.11	0.53	1.69	1.27	25.53
0	60	40	0.10	0.51	1.13	1.44	10.36
0	80	20	0.08	0.47	0.73	1.59	9.11
0	100	0	0.04	0.58	1.41	1.62	37.99
20	0	80	0.10	0.48	2.07	1.13	13.66
20	20	60	0.10	0.49	2.10	1.21	17.73
20	40	40	0.09	0.47	1.21	1.39	12.53
20	60	20	0.07	0.43	0.49	1.64	15.02
20	80	0	0.04	0.52	0.68	1.69	101.06
40	0	60	0.09	0.44	2.94	1.14	14.32
40	20	40	0.08	0.43	2.26	1.27	6.91
40	40	20	0.06	0.41	0.97	1.50	9.94
40	60	0	0.03	0.46	0.75	1.62	139.54
60	0	40	0.08	0.39	2.63	1.20	18.30
60	20	20	0.06	0.39	2.60	1.36	18.79
60	40	0	0.02	0.42	2.81	1.43	89.98
80	0	20	0.07	0.36	2.24	1.45	25.74
80	20	0	0.03	0.40	5.14	1.78	130.31
100	0	0	0.05	0.38	3.44	4.42	1428.50

The water sources of transpiration were further examined. Three extreme cases were chosen to show their results in following figures. They were the three cases with 100% sand, 100% clay and 100% silt, correspondingly. The soil water retention curves of three soil types were depicted by the van Genuchten curves in Figure 4.5. The contributions of groundwater to transpiration were shown in Figure 4.6 (a), while the portions of transpiration from soil water were shown in Figure 4.6 (b). In the case with sandy soil, most water for transpiration was from groundwater. Because the large pores in sand hold water only when soil water potential was high and the hydraulic conductivity of sand was extremely high, the soil water was available for plant only after the rainfall pulses. Therefore, soil water uptake in sand soil only occurred immediately after the rainfall pulses in wet season. In contrast, in the other two cases with finer soils of clay and silt, soil water supported most transpiration. Groundwater uptake was much lower and it occurred mainly during the dry season. The relatively small pores in finer soil held more water when soil water potential was low, which provided the plants more available water in dry season than the coarse sand did. Among the three cases, the shallow soil water in clay supported highest portion of transpiration, while the deep groundwater in sand contributed to the largest portion of transpiration. The results suggest that plants in coarser soil may tend to explore relatively deep water source, while the plants in finer soil mainly depend on the shallow water source and only used the deep water source when necessary (i.e., the plants in silt and clay only used groundwater during the dry season when shallow soil water was not adequate). This result coincided with the findings in previous studies that the plants in coarser soil needed to develop

deeper root system to access deeper and more reliable water source than the plants in finer soil [*Hacke et al.*, 2000; *Sperry and Hacke*, 2002]. The study of global root distribution also showed that 95% of root biomass in deserts and arid shrublands located among "1.06±0.15 m on clay and loam soil and 1.90±0.53 m on sandy soil" [*Jackson et al.*, 2000; *Jackson et al.*, 1996]. Although the root distributions in all the cases of Scenarios 2 were the same, it is expected that, in reality, the plants in sandy soil would develop relatively deep root system as a rooting strategy to cope with the large demand of deep water source, while the plants in silt and clay soil would develop relatively shallow root system to exact shallow soil water at low soil water potential.

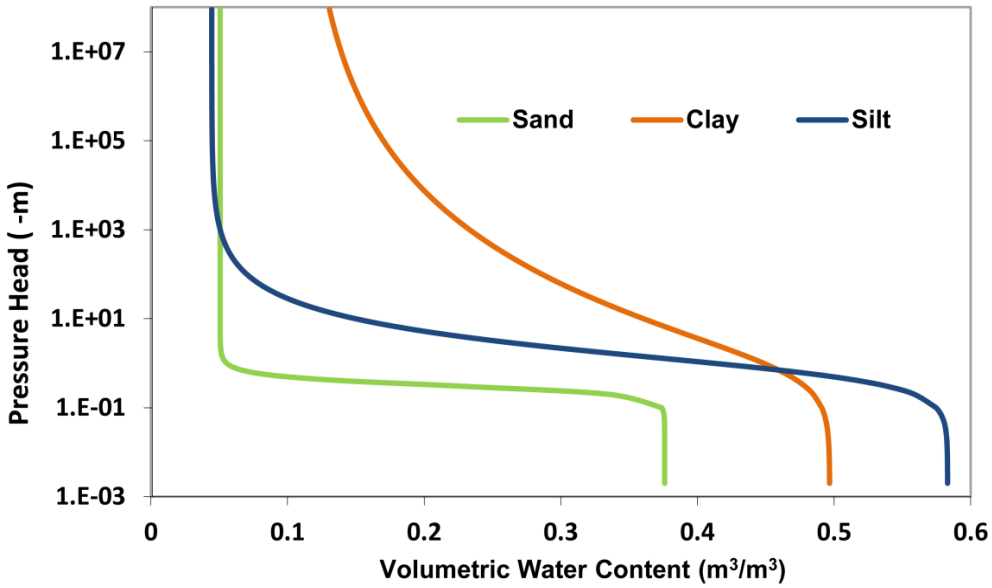

Figure 4.5 Soil Water Retention Curves for Three Represented Soils. The water retention curves of three cases with 100% sand, 100% clay and 100% silt were depicted by van Genuchten curves with the parameters predicated by ROSETTA.

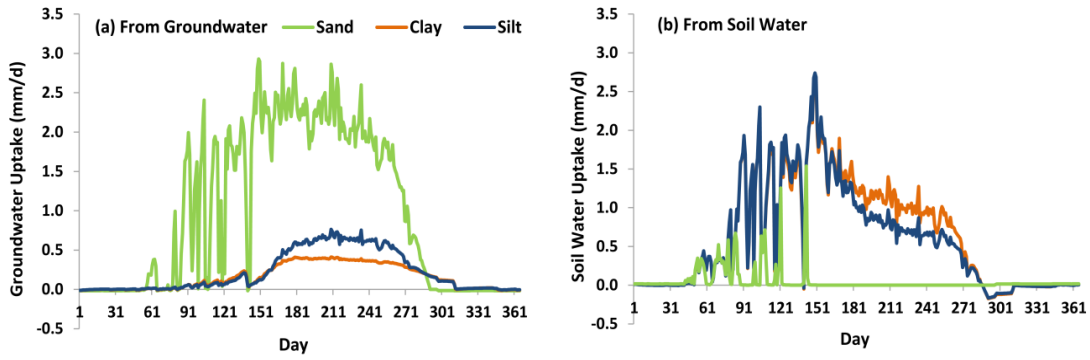

Figure 4.6 Contributions of Groundwater and Soil Water to Transpiration. (a) Daily groundwater uptake from the plants in three soils in Year 2002; (b) Daily soil water uptake from the plants in three soils. The plants in coarser soil tended to explore deeper water source, while the plants in finer soil used most water from shallower water source. Therefore, groundwater supported most transpiration of the plants in sand, while soil water contributed to most transpiration of the plants in clay.

The total soil water uptake was further explored to show the soil water uptake from different depths (10 cm, 30 cm, and 50 cm) in Figure 4.7. The soil water uptake from all three layers was very small in sandy soil. Clay is finer than silt. Thus, the plants in clay took more soil water from top 10 cm soil than in silt, while the plants in silt explored more water from deeper soil at 50 cm than in clay. It also demonstrated the previous finding that the plants in finer soil used more water in shallower soil layers. The negative values in plant water uptake from 30 and 50 cm indicated that hydraulic descent occurred during these days following the rain pulses. The phenomenon of hydraulic descent was obvious in the plants in clay and silt. However, hydraulic descent was very small in the plants in sandy soil. Water moved downward into deep soil through two pathways: percolation through soil itself, and hydraulic descent through plant roots. When large rainfall event commenced, the hydraulic conductivity of sand

was extremely high and formed a very effective pathway in sand itself to move water downward through percolation. Instead, downward water movement through hydraulic descent in roots was very slight at sandy site. The results indicated that the soil characteristics also influenced hydraulic redistribution.

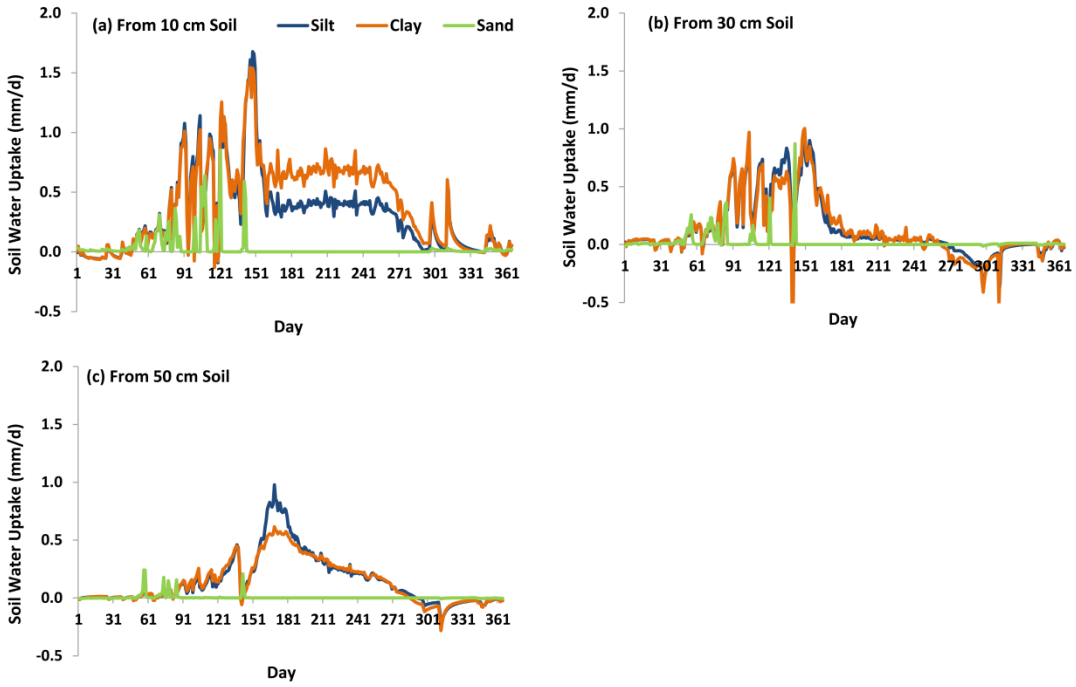

Figure 4.7 Soil Water Uptake from Three Soil Layers. (a) Soil water uptake from top 10 cm soil in Year 2002; (b) Soil water uptake from 30 cm soil; (c) Soil water uptake from 50 cm soil. The positive value indicated the roots took water from surrounding soil, while the negative value implied the roots released water into soil. The results showed the similar finding in Figure 4.6 that the plants in clay took more water from top 10 cm soil than the plants in silt did, while they took less water from deep 50 cm soil than the plants in silt did. The soil water uptake of the plants in sand was very small. In addition, the most negative soil water uptake from clay indicated that hydraulic descent was most significant at clay site. Hydraulic descent was not obvious in the plants in sand. Therefore, the soil textures also impacted HR that HR was more significant in the plants in finer soil.

The soil moisture and soil water potential in the top soil layer were shown in Figure 4.8. To focus on the impacts of soil characteristics on transpiration, the simulations in Scenario 2 did not include soil evaporation. Very low soil water content kept in sand due to its large pores and high hydraulic conductivity (Figure 4.8 (a)). However, the soil water potential in sand was relatively high (Figure 4.8 (b)) because the plants only took small amount of water from soil and soil evaporation was set to zero in model simulation. In contrast, the dry-season soil water potential in silt and clay was lower because the plants kept exacting water from soil during the dry season. A similar phenomenon was found in the study of Sperry and Hacke [2002]: finer textured soil was associated with lower soil water potential during drought. They also found the cavitation in the shallow roots was more severe at the loam site than at the sand site because of the lower soil potential at the loam site. In addition, previous studies revealed the plants in coarser soil had less cavitation resistance than the plants in finer soil [*Hacke et al.*, 2000; *Sperry and Hacke*, 2002]. This phenomenon could be explained by the results of Scenario 2: the plants in finer soil experienced lower soil water potential and they needed higher cavitation resistance to avoid severe cavitation in their roots; the plants in coarser soil needed roots with higher hydraulic conductivity to rapidly extract and transport soil water in coarser soil before water was fast evaporated or/and leaked. As a tradeoff, the higher root hydraulic conductivity was, the less cavitation resistance was. Therefore, comparing to the plants in finer soil, the plants in coarser soil may develop roots which were more vulnerable to cavitation, but had higher ability to absorb and transport water.

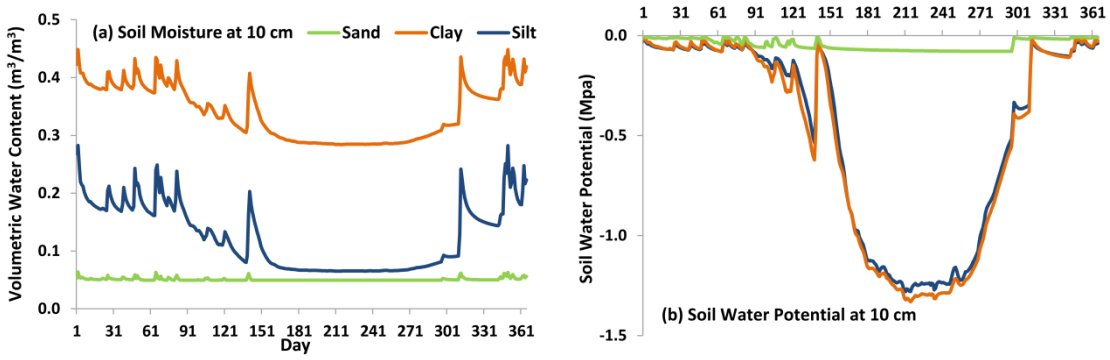

Figure 4.8 Soil Water Content and Soil Water Potential in Top 10 cm Soil. (a) Soil water content in top 10 cm soil in Year 2002; (b) Soil water potential. In Scenario 2, soil evaporation was set to zero in order to segregate the impacts of soil texture on transpiration and on soil evaporation. Therefore, without soil evaporation, the soil water potential shown in (b) was higher than reality. The soil water potential in clay was the lowest, indicating that the roots in clay experienced higher risk of cavitation and these roots were expected to develop more cavitation resistance to avoid extreme cavitation.

Scenario 3: Different Groundwater Depths

The results of Scenario 3 showed that the changes of groundwater depth had little influences on the whole system behaviors during the wet season until the beginning of May, but exhibited significant influences during the transitional season (the middle of May to June) and the dry season (July to October), at the time when the groundwater uptake largely occurred which was revealed from the previous model results. The shallower groundwater table was, the larger amount of groundwater was taken, since the shallower groundwater is more energetically favorable over the deep groundwater (Figure 4.9 (a)). The annual groundwater uptake ranged from 81 mm/yr (9 m water table), 88 mm/yr (7 m water table), 90 mm/yr (5 m water table) to 116 mm/yr (3 m water table). The shallower water table also led to higher rate of hydraulic lift during the dry season. The maximum daily hydraulic lift rate was from 1.4 mm/d (3 m water table), 1.1

mm/d (5 m water table), 0.6 mm/d (7 m water table) to 0.2 mm/d (9 m water table). The higher hydraulic lift in shallower water table case also promoted soil water uptake and transpiration during the dry season. In addition, the plants in shallower water table cases experienced less water stress and their roots in upper soil layers were more hydraulic active during dry season, which further promoted soil water uptake. Therefore, in shallower water table cases, the larger water uptake from both saturated layers and soil layers resulted to the higher transpiration rate during the transitional and dry seasons (Figure 4.9 (b)). During the wet season, the transpiration rates were nearly identical across all groundwater depths, but differed in the dry season when groundwater uptake and hydraulic lift largely occurred. Increasing the groundwater table from 9 m to 3 m promoted a 109 mm (60%) increase in transpiration for Year 2002, which implied that groundwater table changes may significantly influence the water and energy balances.

Previous understanding believed the relatively deep groundwater had very little influences on the surface water and energy processes *[Maxwell and Kollet, 2008]*. However, the presence of the deep-rooted plants may link the deep groundwater to the surface processes. The energy status of top soil layers were influenced by groundwater depth through the water use of plants and HR, especially during the transitional and dry periods (Figure 4.9 (c)). The deeper groundwater was, the lower soil water potential was during the dry season.

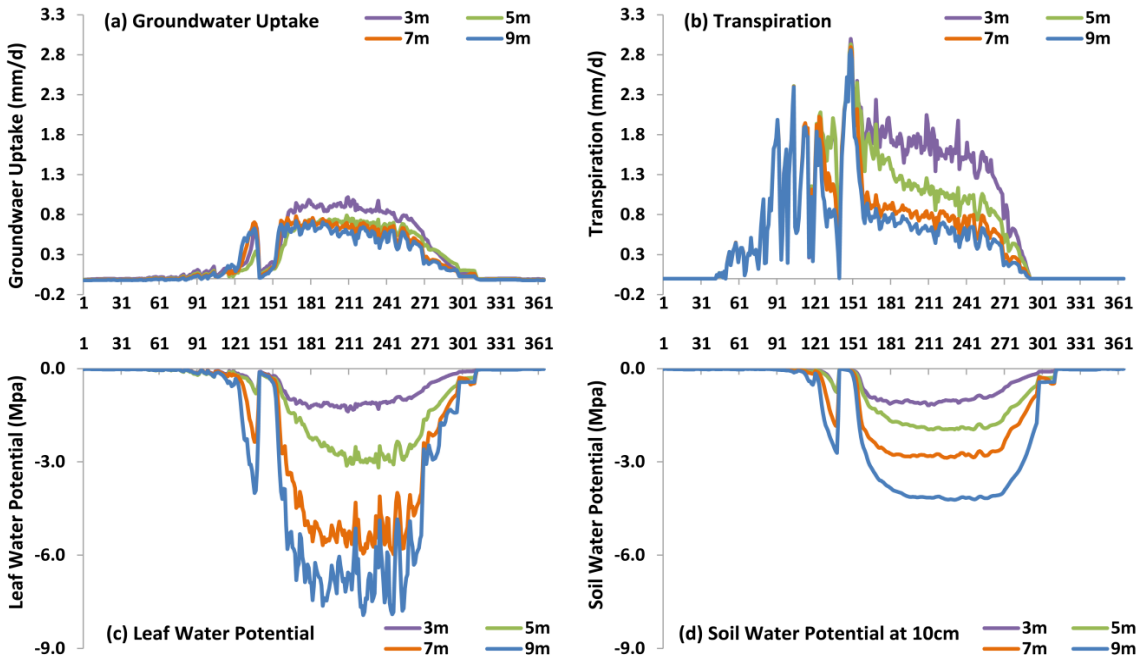

Figure 4.9 Scenario 3 Results with Four Groundwater Depths. (a) Groundwater uptake rate during the oak active season in Year 2002; (b) Transpiration difference; (c) Leaf water potential changes; (d) Soil water potential at top 10 cm soil. The results showed that the changes of groundwater depth had more significant influences on the whole system behaviors during the dry season than during the wet season, because dry season was the time when large amount groundwater was used to support plant water demand.

Meanwhile, the shallower groundwater level led to less severe plant water stress. The lowest leaf water potential increased from -8 Mpa (9 m water table), -6 Mpa (7 m water table), -3 Mpa (5 m water table) to -1.2 Mpa (3 m water table) in the dry season (Figure 4.9 (d)). The monthly averaged leaf water potential results for each case during oak active season were shown in Figure 4.10. For each month, R^2 value of the linear regression between leaf water potential and groundwater depth was shown in Table 4.3. During the dry season from June to October when groundwater contributed to most transpiration, the leaf water potential and the groundwater depth showed significant

linear relationships. In wet season when transpiration was mainly supported by soil water, the linear relationships were less significant with the lower R^2 values. For example, in March, more than 95% of transpiration was from soil water. Therefore, the R^2 value of the linear regression was only 0.04 in March, indicating there was no linear relationship between leaf water potential and groundwater depth. However, in August, nearly 80% of transpiration was contributed by groundwater. Thus, R^2 value of the linear regression was 0.99 only in August, indicating the significant linear relationship between leaf water potential and groundwater depth. In short, the linear regression analysis indicated that the leaf water potential closely related to the plant water uptake pattern that the groundwater depth largely controlled the leaf water potential dynamics during the dry season when groundwater uptake was dominant, while it had little relationship with the leaf water potential dynamics during the wet season when most transpiration was from soil water.

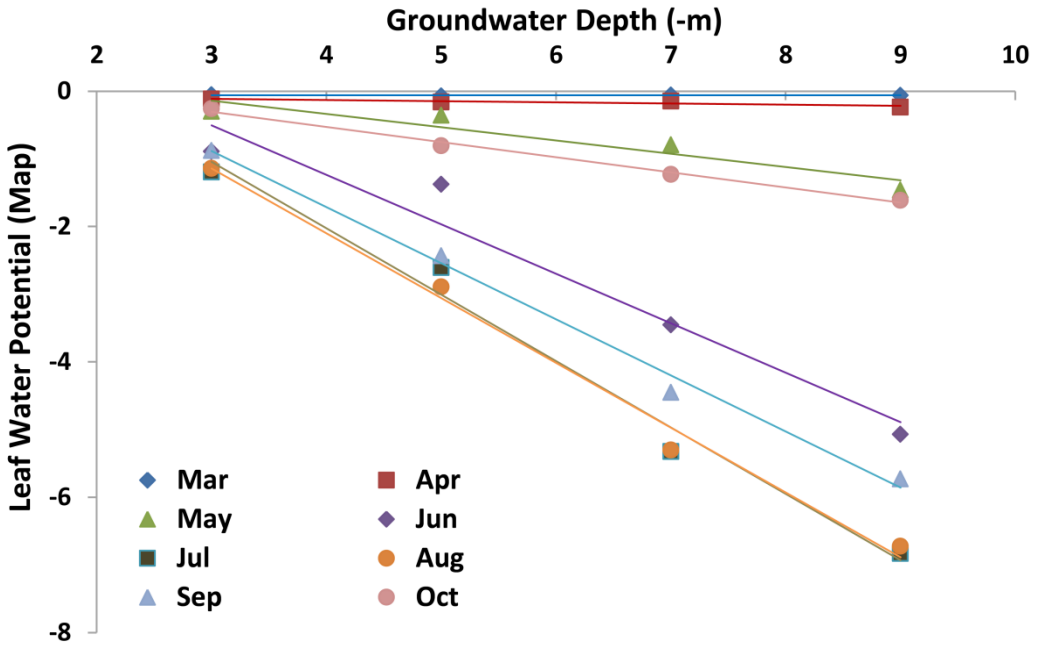

Figure 4.10 Linear Regression between Monthly Leaf Water Potential and Groundwater Depth. The results of trend lines were shown in Table 4.3. Leaf water potential linearly related to groundwater depth during the dry season when groundwater uptake was dominant, while they had little relationship during the wet season when most transpiration was from soil water.

Table 4.3 Linear Regression between Leaf Water Potential and Groundwater Depth

March	y = -0.0006x - 0.06	$R^2 = 0.04$
April	y = -0.02x - 0.06	$R^2 = 0.79$
May	y = -0.20x + 0.45	$R^2 = 0.89$
June	y = -0.73x + 1.68	$R^2 = 0.95$
July	y = -0.98x + 1.90	$R^2 = 0.98$
August	y = -0.96x + 1.73	$R^2 = 0.99$
September	y = -0.83x + 1.60	$R^2 = 0.99$
October	y = -0.22x + 0.37	$R^2 = 0.99$

(x: Groundwater depth (m); y: Leaf water potential (Mpa))

Scenario 4: Different Root Distributions

Root distribution is a key variable in modeling the carbon, water and nutrient fluxes in soil-plant-atmosphere continuum [*Jackson et al.*, 1996]. The results of more root fraction reaching groundwater (Figure 4.11) were similar to the Scenario 3 results with shallower groundwater table. More groundwater root fraction resulted to the smaller total root resistance for the groundwater-root-reference point path in Scenario 4, while shallower groundwater table led to the smaller energy consumption of groundwater uptake in Scenario 3. Both changes in resistance and energy can generate the similar results that the groundwater uptake increases (Figure 4.11 (a)). Since the groundwater uptake occurred mainly during the transitional period and the dry season.

The effects of more root fraction in groundwater also became obvious during these seasons. The increasing in groundwater root fraction (from 10% to 50%) largely increased the annual groundwater uptake from 77 mm/yr (10% tap roots), 112 mm/yr (20% tap roots), 140 mm/yr (30% tap roots), 177 mm/yr (40% tap roots), to 202 mm/yr (50% tap roots). The annual transpiration increased from 179 mm to 290 mm, with 62% increasing (Figure 4.11 (b)). The higher root fraction in groundwater promoted hydraulic lift from groundwater to the top dry soil layers. The maximum daily hydraulic lift rate was from 1.0 mm/d (50% tap roots), 0.8 mm/d (40% tap roots), 0.5 mm/d (30% tap roots), 0.3 mm/d (20% tap roots) to 0.2 mm/d (10% tap roots). More groundwater was lifted to soil layers through HR. But the soil water uptake did not increase significantly, because of lower root fractions in soil layers. The root fractions also impacted soil water potential in the top soil layer because of the changes in root water uptake and HR (Figure 4.11 (c)). Soil water potential at 10 cm was higher in cases with a higher percentage of tap roots. More tap roots also resulted in higher leaf water potentials during the dry period (Figure 4.11 (d)). The lowest leaf water potential increased from -8 Mpa (10% tap roots), -4 Mpa (20% tap roots), -2.7 Mpa (30% tap roots), -2 Mpa (40% tap roots) to -1.5 Mpa (50% tap roots) in dry season, which were huge changes in leaf water potential. Therefore, both tap root fraction in Scenario 4 and groundwater depth in Scenario 3 impacted the dry-season leaf water potential.

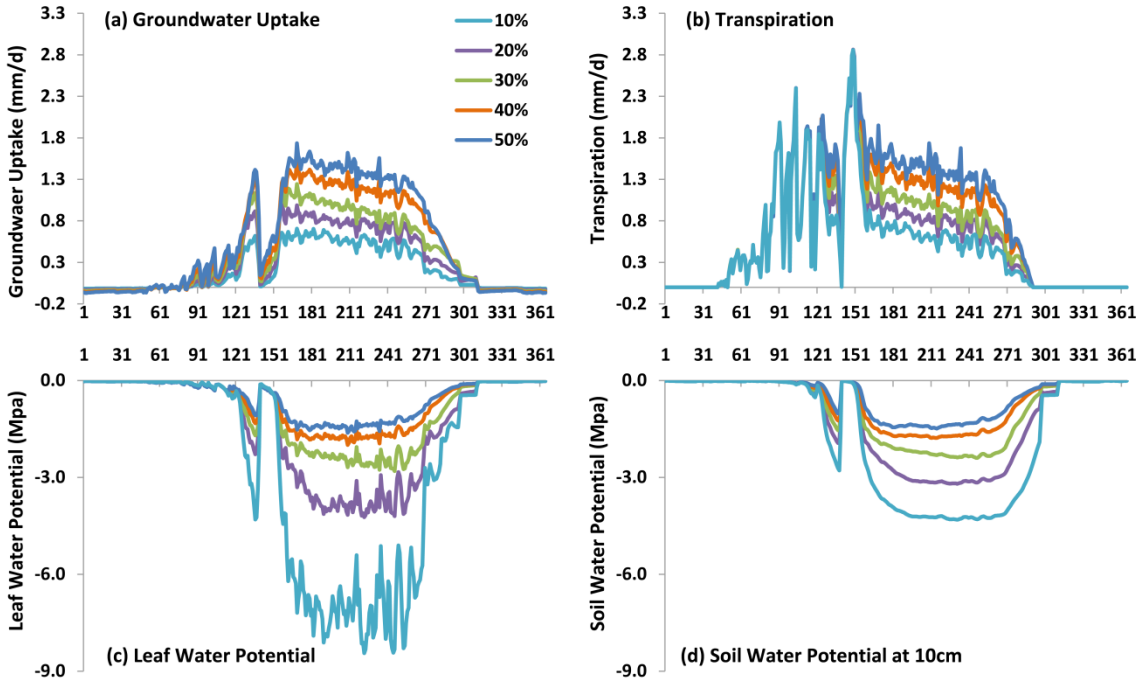

Figure 4.11 Scenario 4 Results with Different Percentages of Tap Roots. (a) Groundwater uptake rate during the oak active season in Year 2002; (b) Transpiration difference; (c) Leaf water potential changes; (d) Soil water potential at top 10 cm soil. The results were similar to the results of changing groundwater depth in Figure 4.9, because both more tap roots (in Scenario 4) and shallower water table (in Scenario 3) led to the smaller energy consumption of groundwater uptake.

Conclusions

The four scenarios address how plant characteristics (Scenario 1 and 4), soil (Scenario 2) and groundwater (Scenario 3) impacted the dynamics of the whole GSPAC system. Several ecohydrological impacts of HR were demonstrated in Scenario 1, such as promoting transpiration, preventing extreme cavitation in shallow roots during dry season, and distributing precipitation into deeper layers to limit water loss through soil

evaporation. Scenario 1 indicated that the impacts of HR on the whole GSPAC system had obvious seasonal trend since hydraulic lift mainly occurred during the dry season and hydraulic descent usually happened during the wet season following the rainfalls. Hydraulic lift was the main mechanism to promote transpiration, while hydraulic descent was the critical process to change soil moisture dynamics, especially the soil moisture in deeper soil layers. Therefore, the impacts of HR on transpiration were obvious in dry season and the changes of soil moisture were significant during wet season. HR was highly influenced by groundwater fluctuations and plant root distributions (Scenario 3 and 4), because groundwater was the major source of hydraulic lift and the roots forms the pathway of HR.

The results of Scenario 2 generally matched the hypotheses proposed by Sperry and Hacke [2002] that the plants in finer soil experienced lower soil moisture and tended to extract water from shallower soil layer, compared to the plants in coarser soil. The results further indicated that the plants in coarser sandy soil were expected to develop deeper roots with higher root hydraulic conductance, which led the deeper roots to be more vulnerable to cavitation. Soil texture impacted HR, which was more obvious in finer soil than in coarser soil. The impacts of soil texture on GSPAC dynamics also showed the seasonal changes that the changes of transpiration caused by soil texture mainly happened during dry season when water was limited. Therefore, it may expect that the influences of soil types on water and energy dynamics were more significant in arid and semi-arid regions rather than wet areas. The plant characteristics, such as root to leaf area ratio, xylem cavitation resistance and root distribution, were expected to change

in different soil textures to develop strategies for efficient plant water use. Such changes were not included in Scenario 2, but the model developed in Chapter II and III had corresponding components to depict these plant characteristics. Therefore, the model could be used to explore more complex GSPAC system responses to soil texture in future.

The changes related to groundwater fluctuation (Scenario 3) had distinct influences during the transitional and dry periods. The vegetation could adjust their root distributions (Scenario 4) to adapt the external groundwater changes. However, Scenario 3 and 4 also implied that plant water stress during the dry season closely related to groundwater depth and tap root fraction. The groundwater uptake acted as a protection mechanism for plant to survive during the dry period. The deeper groundwater and less tap roots resulted to severer plant water stress. Therefore, if the groundwater drawdown became too deep for plant to access, or if the rate of groundwater table decline was much faster than the plant root allocation rate [*Naumburg et al.*, 2005], the severe water stress would risk the vegetation survival. In addition, hydraulic redistribution acted as another plant protection mechanism. Through HR, groundwater was lifted to recharge the top dry soil layers and lateral roots. HR prevented the hydraulic dysfunction of GSPAC and kept the lateral roots active (Scenario 1). Thus the water table decline also impacted HR, which also led to risks to vegetation survival.

Pollacco and Mohanty [2012] estimated the uncertainties in inverting the water fluxes from the remote sensing retrieved topsoil moisture and evapotranspiration. They found the uncertainty increases as climate becomes drier, soil texture is coarser, root

goes deeper and groundwater depth goes shallower. Under those situations, soil moisture and transpiration decoupled that the topsoil moisture was no longer representative of root zone soil moisture [*Pollacco and Mohanty*, 2012]. Such findings can be explained by the scenario results in this chapter. Scenario 2 indicated that the plants in coarser soil tended to use deeper water source than the plants in finer soil did. In coarser soil, the plant transpiration links more closely to the deep soil moisture, rather than to the topsoil moisture. Therefore, the topsoil moisture of coarser soil retrieved from remote sensing is not enough to indicate the whole root zone soil moisture and evapotranspiration, which would increase the uncertainties in inverting the water fluxes in the study of Pollacco and Mohanty [2012]. Scenario 3 indicated that if the groundwater table rises, the plant tended to use more groundwater rather than soil water. Therefore, the soil moisture decoupled with transpiration. The uncertainty in inverting the water fluxes increases when groundwater table rises. Scenario 4 implied that if the plants grow more deep roots, they tended to use more groundwater rather than shallow soil water. Thus, the topsoil moisture could not represent the root zone soil moisture in this case. In addition, our model revealed that the plants mainly depended on groundwater during dry seasons and took more water from soil during wet seasons. Thus, the transpiration mainly linked to groundwater during dry season, while mainly coupled with soil moisture during wet season. These results explained why the uncertainties in inverting the water fluxes in the study of Pollacco and Mohanty [2012] increased when the climate goes drier.

The four scenarios in this chapter the linkages between groundwater, soil and plant. The changes in one of these components led to different responses in various time

periods. The results in all scenarios showed the distinct seasonal-responses. Most impacts were significant only during dry season, except the impacts of hydraulic descent on soil moisture were more obvious during wet season. The scenarios also implied that the impacts of groundwater, soil, plant and atmosphere were integrated together to impact energy and water dynamics. However, the scenario tests in Chapter IV only focused on one factor each time. The models developed in Chapter II and III allowed integrating the implications of these factors together. In future, the model can be used to conduct simulations with the combination of various factors to test the whole system dynamics of GSPAC.

CHAPTER V

MAPPING POTENTIAL GROUNDWATER DEPENDENT ECOSYSTEMS*

Introduction

Multiple ecosystems in semi-arid regions are likely to be stressed by the increasing pressures of climate, land use, and population change [*Baldwin et al.*, 2003; *Smith et al.*, 2003]. Groundwater-dependent ecosystems (GDEs), typically vegetative communities that rely on the surface or subsurface expression of groundwater, are especially sensitive to these changes. Greater understanding of GDEs will enable more informed management strategies as changes are observed. While previous studies have been able to identify and monitor individual GDEs, much remains to be done to document their collective spatial distribution, influence on the water balance, and response to changing water availability. The purpose of this study is to develop a method to map GDEs using existing geospatial and remote sensing datasets and apply this method to create state and aquifer scale maps in Texas.

GDEs in the USA occur in a number of potentially stressed ecoregions, particularly the Great Basin in Nevada [*Naumburg et al.*, 2005; *Steinwand et al.*, 2006], the Edwards Plateau in Texas [*Jackson et al.*, 1999; *McElrone et al.*, 2004], the Sonoran Desert in Arizona [*Scott et al.*, 2008b], and in California, the Owens Valley [*Elmore et*

---

* Reprinted with permission from "Mapping Potential Groundwater-Dependent Ecosystems for Sustainable Management" by Gou, S., S. Gonzales and G. Miller, 2014. *Ground Water*, doi: 10.1111/gwat.12169, Copyright 2014 by John Wiley and Sons.

al., 2003; *Goedhart and Pataki*, 2010] and the foothills [*Miller et al.*, 2010] and riparian meadows of the Sierra Nevadas [*Loheide and Gorelick*, 2005; 2007; *Loheide et al.*, 2009; *Lowry et al.*, 2011]. Two distinct types of groundwater-dependent ecosystems are significant for sustainable groundwater development [*Eamus et al.*, 2006]: 1) biota living in and around springs, groundwater-fed wetlands, and riparian zones, all of which rely on the surface expression of groundwater; and 2) vegetation with root access to deeper (>2 m) stores of water which require the subsurface presence of groundwater. A third class of GDEs, subsurface microbial communities, is also recognized. While these populations and the processes they facilitate are environmentally significant, they are substantially different in their character and thus will not be included in this study. We considered the vegetation belongs to the first two types of GDEs in this study, and have referred to them as "lowland GDEs" and "upland GDEs", correspondingly. Eamus et al. [2006] also suggested that the vegetation may rely on groundwater if it meets one or more of the following criteria: 1) the groundwater or the capillary fringe is within the vegetation rooting depth; 2) significant surface expressions of groundwater are present (e.g. springs), and the vegetation associated with these expressions is different from other nearby vegetation; 3) the vegetation, or a portion of it, remains green and physiologically active during extended dry periods; 4) the vegetation shows slow seasonal changes in leaf area index while others do not; 5) the vegetation exhibits lower water stress than the nearby vegetation without accessing groundwater; 6) the annual transpiration is significantly larger than the annual rainfall and run-on rate; and 7) daily

or seasonal changes in groundwater depths are observed, not due to lateral flow or percolation.

Table 5.1 shows the wide variety of known phreatophyte species in the southwestern United States. Within Texas, at least six phreatophyte species have been identified; two in karst upland areas (juniper and live oak), one in deep upland soils (mesquite), and three lining riparian zones (willow, salt cedar, and giant reed, *Arundo donax*).

Table 5.1 Selected Studies of Known Phreatophytes in the Southwestern U.S.

Source	Location		Species
McElrone et al. [2003]	Texas, karst uplands		Juniper (*Juniperus ashei*) and live oak (*Quercus fusiformis*)
Wilcox et al. [2006]	Texas	Riparian zones	Saltcedar (*Tamarix chinensis, Tamarix ramosissima*)
		Karst uplands	Ashe juniper (*Juniperus ashei Buchholz*)
		Deep soils	Mesquite (*Prosopis glandulosa Torr. var. glandulosa*)
Schaeffer et al. [2000]	Arizona, stream channels		Willow (*Salix goodingii Ball*) and cottonwood (*Populus fremontii Wats*.)
Scott et al. [2008b]	Arizona, savannas		Velvet mesquite (*Prosopis velutina Woot*.)
Miller et al. [2010]	California, savannas		Blue Oak (*Quercus douglasii*)
Steinwand et al. [2006]	California, scrubland		Rabbitbrush (*Chysothamnus nauseosus*), Nevada saltbush (*Atriplex lentiformis ssp. torreyi*), and greasewood (*Sarcobatus vermiculatus*)
Loheide et al. (2005, 2007)	California, riparian zones		Wet-meadow vegetation (sedges, rushes, and some other herbaceous species))
Martinet et al. [2009]	New Mexico, riparian zones		Cottonwood (*Populous deltoids spp*. wislizeni), salt cedar (*Tamarix chinesis*), Russian olive (*Elaeagnus angustifolia*), mesquite (*Prosopis pubescens*), saltbush (*Atriplex L. spp.*)

Two prior approaches have been used to predict the presence or absence of GDEs in a given region. The most common is the creation of an index based on key factors linking GDEs and abiotic factors, such as pedological, morphological, hydrological, and climate characteristics [*Bertrand et al.*, 2012]. Based on these existing datasets, some studies created index values for small watersheds; for example, studies had been conducted at the hydrologic unit code -12 (HUC-12, subwatersheds with the average area of ~40 mile^2) scale [*Howard and Merrifield*, 2010] and the HUC-6 (basins with the average area of ~10,000 mile^2) scale [*Brown et al.*, 2010]. This method can highlight areas with high index values which indicate the areas host large numbers of GDEs. The results can provide useful information to incorporate GDEs into groundwater management at large scale. However, the previous GDE index systems had only considered the factors related to the lowland GDE types (gaining streams, springs, riparian zones, potential groundwater-fed wetlands and perennial lakes) and did not include the factors linked with the deep-rooted, upland phreatophytes. In addition, the index approach considered watershed scale areas of interest (e.g., HUC-12) as the smallest estimation units. Thus, the detailed information on GDE distributions within a watershed was unavailable.

Alternate approaches directly identified potential GDEs based on their own specific characteristics or behaviors, such as relatively slower changes in their physiological activity than that of nearby, non-GDE plants. Various remote sensing based indices, such as Normalized Difference Vegetation Index (NDVI), Normalized Difference Wetness Index (NDWI) and MODIS Enhanced Vegetation Index (EVI), have

been used to detect such GDE characteristics. Based on the changes in NDVI and NDWI response to water-limiting conditions, Barron et al. [2012] identified potential GDEs in Western Australia using Landsat imagery. Dresel et al. [2010] combined three remote sensing measures, including the NDVI data derived from Landsat images, the changes of MODIS EVI, and the remote sensing based classification, to identify GDEs in Australia. GIS modeling can further improve remote sensing based GDE identification methods. Combining remote sensing derived NDVI, vegetation greenness and soil moisture, and the GIS modeled groundwater and landscape wetness information, Münch and Conrad [2007] classified the potential GDEs for a 2400 km^2 region in South Africa.
These remote sensing based approaches can provide more detailed GDE distribution than the index system approach. However, the previous studies did not consider the impacts of vegetation density and plant phenology on NDVI dynamics. The potential biases need to be addressed when NDVI dynamics was used to identify plant groundwater use. The combination of various remote sensing measures may ameliorate these biases. In addition, the remote sensing based approaches usually needed high quality images combined with additional calculations and careful user interpretation. Therefore, they were typically used only for GDE identification at small scales.

Our study aims to combine the best features of both approaches to address the different management needs found at various scales and to produce a more holistic assessment. At the large state/province scale, a GIS-based GDE index approach was used to generally identify which areas contained considerable numbers of both lowland and upland GDEs. The GDE index approach highlighted the critical areas where water

and ecosystem managers should consider GDEs in their planning. For these critical areas, a remote sensing-based approach was developed to provide more thorough information about the spatial location of GDEs. Thus, the objectives of this study are to: 1) develop a GIS-based method to estimate a GDE index value for each subregion in Texas; 2) propose a remote sensing-based method to delineate detailed GDE distributions for the area highlighted in objective 1); and 3) analyze the impacts of various factors on GDE distribution, including vegetation types, soil depth, and landforms. These mapping efforts represent a key step towards providing groundwater managers and modelers with the information they need to assess GDEs at different scales.

Methods

We mapped GDEs based on the criteria proposed by Eamus et al.(2006) using a two-step approach: at the state scale, a GIS-based method was first used to calculate a *GDE index* for each state subdivision, i.e., groundwater management area (GMA) or hydrologic unit code-6 (HUC-6) sized watershed in Texas. We chose GMAs and HUCs for GDE index estimation because these areas are the spatial scales used for groundwater and watershed management in Texas [*TWDB*, 2012]. Using publically available data, the GIS-based method served as a screening tool to identify critical regions with a high potential to host a significant number of GDEs. Next, at the aquifer/basin scale, a remote sensing method was applied to a critical region in order to identify ecosystems that

exhibit the physiological hallmarks of groundwater dependence. This method provided detailed, smaller scale information on GDE distributions.

GDE Index Method for State/Province Scales

The criteria proposed by Eamus et al. [2006], especially the first two criteria (see Introduction), mainly focus on two aspects—whether the groundwater is accessible by vegetation, and whether the vegetation's dynamics are associated with the available groundwater. Therefore, we created a new *GDE index* system, which combined two categories of GDE indicators—vegetative and hydrological. The vegetative indicators denoted the vegetation with high potential to be GDEs based on *ecosystem type*, while the hydrological indicators identified the areas where groundwater is most likely to be accessed by ecosystems. To derive these indicators, a GIS database was established with a variety of geospatial information on Texas topography, hydrology, and ecology, including previously generated data on springs [*Brune*, 1975; *USGS*, 2012b], wetlands [*USFWS*, 2012; *USGS*, 2012a], landuse/landcover [*USGS*, 2012a], vegetation types [*TPWD*, 2012], base flow index [*Wolock*, 2003], gaining/losing streams [*Slade et al.*, 2000], HUCs [*USGS*, 2012b], and GMAs [*TWDB*, 2012].

The vegetative indicators included representation of groundwater-fed wetlands and phreatophytes, which represented dominant ecosystem types of lowland and upland GDEs. The lowland GDEs in the riparian zones and around the springs were excluded in the estimation of the vegetative indicators, since our analysis suggested that their areas were insignificant when compared to the total area of wetlands and phreatophytes (see

Results and Discussions). Groundwater-fed wetlands were specified based on wetland types in National Wetland Inventory of U. S. Fish and Wildlife Service [2012] and included all non-coastal wetland types: freshwater emergent wetland and freshwater forested/shrub wetland. In some inland areas not covered by the National Wetland Inventory, wetland locations were derived from the USGS National Land Cover Database [2012a], and the emergent herbaceous wetlands and woody wetlands in these areas were considered to be groundwater-fed wetlands. To identify potential upland GDEs, the vegetation belonging to phreatophytic species was identified from vegetation cover data based on the list of species known to occur in the southwestern US (Table 5.1). The *vegetative index* was calculated for each state subdivision (GMA or HUC-6) (Equation 5.1).

$$\text{Vegetative Index} = \frac{\text{Phreatophyte Area} + \text{Wetland Area}}{\text{Total Subdivision Area}} \tag{5.1}$$

A higher vegetative index value denoted that the area had more of the ecosystem types that are likely to use groundwater. However, in some areas, groundwater is too deep to be accessed by these ecosystems. In that case, even though the dominant vegetation belongs to the phreatophytic species, they may not be groundwater dependent. Therefore, a hydrological indicator was introduced to show the areas where groundwater is accessible by ecosystems. Ideally, the hydrological indicators should include the information on the location and depth of near surface water tables. However, this information is unavailable in many regions. Instead, we used the USGS Baseflow Index (BFI) was used as a surrogate hydrological indicator of regional groundwater-

surface water interactions. BFI is a measure of the contribution of baseflow to a stream's overall flow and was produced by USGS based on their stream gaging data [*Wahl and Wahl*, 2007; *Wolock*, 2003]. It also included some spring flows contributing to the streams [*Wahl and Wahl*, 1995]. A high BFI shows a high proportion of total flow coming from more reliable groundwater sources, which implies a high potential that groundwater presented to land surface or water table rised near land surface to contribute to streamflow.

The USGS BFI data used in this study were point-based estimates created from and assigned to individual USGS streamgages, rather than the spatially interpolated grids that were also available [*Wolock*, 2003]. In some cases, a HUC-6 watershed contained multiple USGS streamgages with different BFI values, while in others, a HUC-6 watershed did not have any stream gages or had stream gages not reporting BFI values. For the watersheds with multiple USGS stream gages, BFI values were averaged. For the watersheds without data, a BFI value was assigned based on the average BFI value of the larger HUC-4 watershed where the HUC-6 watershed resides (e.g., Upper Beaver, HUC 111001, was assigned the average BFI value for North Canadian, HUC 1110). For each GMA, a BFI value was determined to be the area weighted average of corresponding HUC-6s' BFI values (Equation 5.2). The area of a specific HUC-6 within a certain GMA was calculated in ArcGIS.

$$\mathrm{GMA_j\_BFI} = \frac{\sum_{i=1}^{n} \mathrm{HUC_i\_BFI} \times \mathrm{Area\ of\ HUC_i\ within\ GMA_j}}{\mathrm{Total\ Area\ of\ GMA_j}} \tag{5.2}$$

Finally, a *GDE index* was developed to integrate both vegetative and hydrological indices. For each state subdivision (GMA or HUC-6), the *vegetative index* was multiplied by the *hydrological index (regional BFI)* to calculate the *GDE Index* of each specific area:

$$GDE\ Index = Vegetative\ Index \times Hydrological\ Index \tag{5.3}$$

The two indices were combined multiplicatively, such that if one index was not satisfied then another index could not compensate for it. Both hydrological and vegetative indices need to be above zero in order for an area to be identified as potentially hosting a GDE. Multiplying the two indices yielded zero if one of the indices was not satisfied, which eliminated some directly. When both indices were above zero, those areas with higher multiplication results implied a higher potential to host GDEs. Efforts to sustainably manage groundwater in areas with high GDE indices should focus attention on these vulnerable ecosystems as potential groundwater consumers.

Remote Sensing-based Method at Aquifer Scale

For regions identified as highly likely to contain GDEs, more accurate information about the spatial distribution of GDE was needed to support sustainable groundwater management. The exercise was not straightforward; many factors combined together to impact GDE distribution, such as plant characteristics, climate, soil, and geology. Not all the plants belonging to the phreatophytic species depend on groundwater. For example, if a mesquite was on deep soil and the local precipitation was adequate to support its water use, this mesquite may only rely on water stored in deep

soil from rainfall events, rather than using groundwater. However, even in the same climate regime, another mesquite may be located on shallow soil with a lower available water content. Under such conditions, a mesquite may need to access deeper groundwater to support its water use. Even though the two mesquites were the same species under the same climate, they may be different in groundwater dependency. Additionally, different, yet co-occurring, species may have different levels of groundwater dependence. For example, if a live oak is located in upland area with shallow water table, this live oak may access groundwater using its deep roots, while shallow-rooted grasses around it may not access groundwater directly. Therefore, we needed to develop a more complex method, based on remote sensing data, to detect the physiological signatures of groundwater dependent vegetation.

The criteria of Eamus et al. [2006] were also applied to guide the GDE identification using remote sensing. Two of these criteria can be assessed by analyzing remote sensing data: (1) A proportion of the vegetation that uses groundwater remains green and physiologically active during extended dry periods, and (2) The vegetation that accesses groundwater exhibits lower seasonal changes in leaf area index than the other nearby vegetation does. In addition, Tweed et al. [2007] highlighted a third criterion for GDE identification: (3) Vegetation with low inter-annual variability of vegetation photosynthetic activity is likely to access groundwater.

To assess these criteria remotely, the Normalized Difference Vegetation Index (NDVI) was chosen as an indicator. NDVI is widely used to monitor vegetation cover and biomass production. It is sensitive to leaf area index change until a full vegetation

cover has been reached [*Carlson and Ripley*, 1997] and provides useful information about vegetation physiological function under clear weather conditions [*Tweed et al.*, 2007; *Wang et al.*, 2004]. Two different remote sensing products from Landsat 7 Enhanced Thematic Mapper (ETM+) and MODIS were used to relate vegetation NDVI variability to groundwater use (Figure 5.1). Landsat ETM+ has relatively high spatial resolution, which helps to discern the fine scale distribution of GDEs, while MODIS has relatively high temporal resolution, enabling it to capture NDVI changes of vegetation within short time periods.

We selected the Edwards Aquifer region, belonging to GMA 10, as case study area for the remote sensing-based methods. This area hosts three known phreatophytic species: live oak (*Quercus fusiformis*), ashe juniper (*Juniperus ashei*), and mesquite (*Prosopis glandulosa*) [*McElrone et al.*, 2004; *Wilcox et al.*, 2006]. Numerous springs appear along the Balcones fault zone. The data from National Land Cover Database [*USGS*, 2012a] showed that the dominant plant functional types were shrublands (48% of total natural vegetative areas), grasslands (22%), evergreen forests (20%), deciduous forests (8%) and woody wetlands (1%). Data from Web Soil Survey [*USDA*, 2013] showed that 57% of the Edwards Aquifer region has shallow soil s(average depth of 45 cm), and the remaining 43% has deep soils (>200 cm). The region also has a subtropical to semi-arid climate. Precipitation is highly variable in time, but is generally highest in May and September. In July and August, the precipitation is usually low, while the potential evapotranspiration is high. The precipitation is "out of phase" with potential evapotranspiration during this period. This implies that GDEs are most likely to rely on

groundwater during July and August. Therefore, satellite imagery from July was used in the analyses relating to Criteria One and Three.

During the extended summer dry season, vegetation with high NDVI values was considered to be physiologically active, indicating that there was a high likelihood it was using groundwater (Criterion One). To verify the first criterion remotely, Landsat ETM+ images (30×30 meters) from July 2002 were used; these images were high quality and relatively cloud-free. The NDVI value of each pixel was calculated (Equation 5.4). Since we only considered the natural vegetation in this study, the pixels representing urban areas, water, farmlands, and pastures were removed from the NDVI results based on land cover data from USGS [2012a].

$$NDVI_j = \frac{(NIR_j - R_j)}{(NIR_j + R_j)} \tag{5.4}$$

where, j is the jth vegetation pixel, NIR_j and R_j refers to the spectral reflectance measurements in the near-infrared and red regions, respectively.

We chose an unsupervised classification technique, K-means, to cluster the NDVI results into five groups. K-means is a widely used algorithm to automatically classify the data into K clusters according to their similarity [*MacQueen*, 1967]. Unlike supervised classification methods, this unsupervised classification technique does not need prior knowledge to define training sets. Instead, it attempts to find the underlying cluster structure automatically [*Canty*, 2007], thus it was suitable for our region of interest, which lacked previous studies of GDEs. We conducted the K-means classification in ENVI software (version 4.8) (Canty 2007), which we used to classify

the pixels into five groups according to the similarity of their NDVI values. We then calculated the average NDVI value of the pixels in each group and assigned each group a value from 1 (the group containing the lowest average NDVI value) to 5 (highest NDVI group).

Vegetation exhibiting low seasonal changes in leaf area index over a whole year may also access groundwater (Criterion Two). For each vegetation pixel, the standard deviation in NDVI across a year-long time series was calculated by equation (5.5).

$$SD_j = \sqrt{\frac{1}{n}\sum_{t=1}^{n}(NDVI_{t,j} - NDVI_{mean,j})^2} \tag{5.5}$$

where, n is the number of time-series satellite images, j is the jth vegetation pixel, $NDVI_{t,j}$ is the NDVI value of the jth pixel at time t, $NDVI_{mean}$ is the mean NDVI value of the jth pixel for the n images. A low NDVI standard deviation implies that the vegetation pixel had slow changes in leaf area during the study period.

MODIS NDVI products (MOD13Q1, 250×250 meters), collected every 16 days in Year 2011, were used to analyze the seasonal NDVI changes over the whole year. The dry year 2011 was chosen for the analysis because Year 2009 and Year 2010 were also dry years, minimizing the potential impacts of antecedent soil moisture on vegetation dynamics. As in the previous analyses, urban areas, water, farmlands and pastures were also removed. The K-means technique was then applied to cluster the seasonal NDVI standard deviation into five groups. Five groups were assigned the values from 1 (the group with highest average seasonal NDVI standard deviation) to 5 (lowest NDVI SD).

Higher group values indicated that the vegetation located within a pixel had relatively higher potential to be using groundwater.

A similar method was used to identify the vegetation with low inter-annual changes in leaf area index (Criterion Three). The MOD13Q1 data (250×250 meters), from images taken in July for each year from 2002 to 2011, were used to calculate the inter-annual NDVI standard deviation value for each natural vegetative pixel. The results were also clustered into five groups using the K-means algorithm and assigned from 1 (the group with highest average inter-annual NDVI standard deviation) to 5 (lowest NDVI SD). Both results from the MODIS-based analyses in Criteria Two and Three were further resampled in ArcGIS to change the cell size from 250×250 meters to 30×30 meters resolution to correlate to the spatial resolution of Landsat ETM+.

Each criterion yielded a dataset containing potentially unique information to identify GDEs. However, each criterion still had its own disadvantages, which centered on its biases in regard to certain plant functional types (see Results and Discussion). To overcome these, we merged all three datasets from Criteria One, Two and Three using the raster calculator in GIS. The assigned values (1 to 5) were summed for each pixel and the resulting sum had the values ranging from 3 to 15. Using the K-means algorithm, these values were further classified into five GDE likelihood groups of the final results—very likely to be GDEs (the group with highest average values), likely to be GDEs, about as likely as not to be GDEs, unlikely to be GDEs and very unlikely to be GDEs (the group with lowest average values).

Results and Discussion

GDE Index at the State/Province Scale

We estimated the *GDE index* for each GMA and HUC-6 in Texas. Phreatophytes clustered in the middle regions of Texas, from the High Plains through the Central Great Plains and Edwards Plateau to the Southern Texas Plains. Live oak and mesquite were the two dominant phreatophyte species (Figure 5.1a). Other phreatophytes, including cottonwood, saltceder, and willow oak, were found in riparian areas. The woody wetlands and the emergent herbaceous wetlands were mainly found in eastern Texas (Figure 5.1b). A large number of these wetlands were located in riparian areas, where they may be fed by shallow groundwater. The regions with the highest *vegetative index* were located in central Texas. BFI values indicated that the streams in central and eastern Texas had high baseflow ratios (Figure 5.1c). Correspondingly, the highest *hydrological index* values were also found in the central Texas.

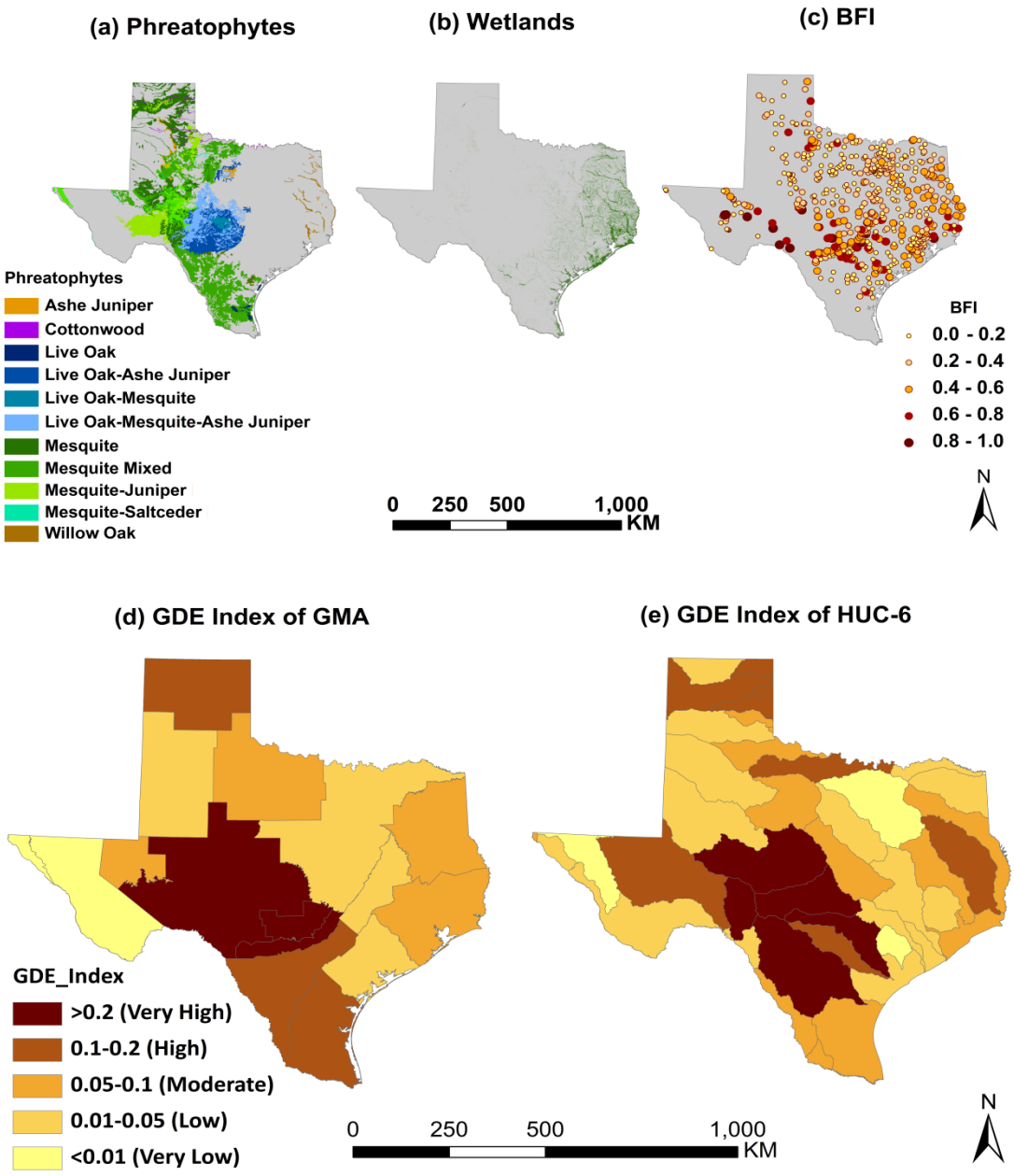

Figure 5.1 GDE Index. Developed by integrating the *vegetative* and *hydrological indicators* (a,b,c) for each GMA (d) and HUC-6 (e) watershed. Darker areas indicate a higher likelihood of supporting significant numbers of GDEs.

GMAs 7, 9 and 10 had the highest *GDE index* values, indicating they had the highest potential to contain GDEs (Figure 5.1d). The HUC-6 basins with the highest *GDE index* values were the Colorado River and the Neuces River (Figure 5.1e). The BFI values in these regions ranged from 0.3 to 0.45, and they are underlain by a number of major aquifers, including the Edwards, Edwards-Trinity, Trinity, Ogallala, Pecos Valley and Seymour. Karsted carbonate rocks and other permeable formations in these areas are known to produce numerous springs, including the two largest: Comal and San Marcos. These areas were almost fully covered by phreatophytic plant species, with wetlands scattered in the riparian areas and around the large springs, making upland GDEs the dominant type. Plans for sustainable groundwater management need to address the groundwater use of potential GDEs and the risks of disturbances on GDEs, such as the land use changes, groundwater over-extraction and climate change. In addition, managers in some specific areas need to consider the influence of GDEs on public water supplies, including the potential changes to groundwater recharge and baseflow that may result from their presence or expansion [*Wilcox*, 2002b].

Remote Sensing-based Results in the Edwards Aquifer Region

Results Using the Three Groundwater-Dependence Criteria

Each criterion captured the groundwater use potential of different plant functional types. Table 5.2 shows the percentages of each plant functional type, as classified into likelihood groups (with 5 being the highest). If one plant functional type had the largest portion in the highest likelihood group and the smallest portion in the

lowest likelihood group, it was considered as the type has the highest likelihood to use groundwater, such as the wetland in Criterion One.

Table 5.2 Plant Functional Types Captured by Each Criterion

Plant Functional Types	Percentage of Each Type (%)					
	Criterion 1		Criterion 2		Criterion 3	
	Highest Likelihood (5)	Lowest Likelihood (1)	Highest Likelihood (5)	Lowest Likelihood (1)	Highest Likelihood (5)	Lowest Likelihood (1)
Deciduous Forest	10*	42	13	4	27	9
Evergreen Forest	4	43	23	2	36	6
Shrubland	2	67	14	8	11	18
Grasslands/ Herbaceous	2	78	9	16	10	26
Wetlands	36	22	28	11	28	9
Total Vegetation Covered Areas	3	62	15	8	17	16

(* Percentage was calculated as 10%=Deciduous Forest in Group 5/Total Deciduous Forest×100%. Other percentages were calculated in the same way.)

Criterion One identified the areas with high NDVI values in the dry summer (Figure 5.2a). The pixels in the highest likelihood group (group 5) had an NDVI value greater than 0.5, similar to the 0.35 to 0.5 range suggested by Barron et al. [2012]. Wetlands were identified as the plant functional type most likely to use groundwater. In contrast, a large portion of the grasslands (78%) was classified into the lowest likelihood group. These grasslands likely depend only on soil water. There were 10% of deciduous forests classified into the highest likelihood group, while only 4% of evergreen forests were included into this group. The different results between deciduous and evergreen forests may because of vegetation density rather than differences in their groundwater

dependency; NDVI is tightly related to the vegetation density [*Carlson and Ripley*, 1997; *Purevdorj et al.*, 1998]. Van Auken et al. [1981] found that in central Texas, the evergreen forests had significantly lower density and species richness than the deciduous forests. Therefore, Criterion One can exclude some non-GDEs with low NDVI in the dry season because they did not access groundwater, but it may also ignore some GDEs with low NDVI due to their low density, such as the evergreen forests. The similar problem occurred for the shrublands due to their low canopy coverage. Only 2% of total shrublands were included in the highest likelihood group.

Criterion Two indicated areas with slow seasonal changes in NDVI for a dry year (Figure 5.2b). As compared to Criterion One, more areas (15% of the total vegetation covered areas) were classified into the highest likelihood group and much fewer areas (8%) were in the lowest likelihood group (Table 5.2); obvious increases occurred in the number of both evergreen forests and shrublands in the highest likelihood group. Wetlands were still the type with the highest potential to use groundwater, while grasslands were still the type with the lowest groundwater use potential. Criterion Two focused on the rate of change in NDVI rather than the NDVI value itself, which eliminated the impacts of vegetation density on NDVI in Criterion One. The percentage of the deciduous forests in the highest likelihood group (13%) only increased slightly. Due to their growth pattern and phenological stages, the deciduous forests essentially exhibited faster seasonal NDVI changes compared to the evergreen forests. Therefore, Criterion Two may ignore some GDEs with faster seasonal NDVI changes due to their essential seasonal growth pattern rather than their dependence on groundwater.

However, Criterion Two still had its own advantage to capture the species which may access groundwater at times outside of the dry season, while Criteria One and Three only analyzed the NDVI variability in dry periods to distinguish vegetation with different water use patterns.

The third criterion analysis indicated areas with low inter-annual changes in NDVI in dry seasons for multiple years (Figure 5.2c). By using only the satellite images collected in July, each plant functional type in the images was at a consistent phenological stage for every year. It eliminated the impacts of plant growth pattern on NDVI standard deviation in Criterion Two. Focusing on the responses of vegetation in various precipitation conditions during the dry season, Criterion Three segregated the effects of annual variations in precipitation from the impact of vegetation growth patterns and phenological stages. Compared to the results of Criterion Two, more deciduous forests (27%) were classified into the highest likelihood group. Grasslands still had the lowest potential to use groundwater based on Criterion Three. Evergreen forests had the highest groundwater use potential in Criterion Three, rather than wetlands as identified in Criteria One and Two.

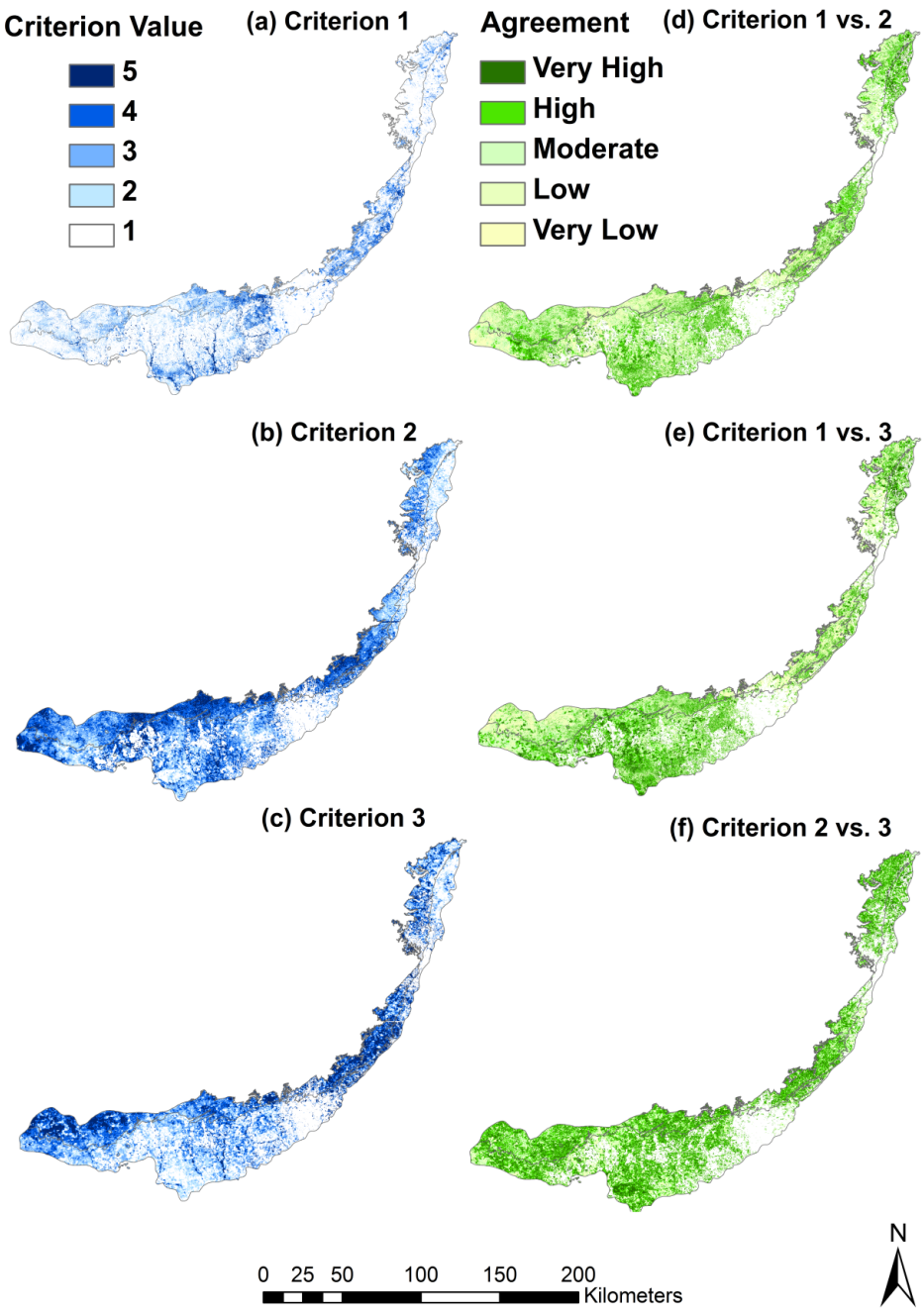

Figure 5.2 Remote Sensing Results Using Three GDE Criteria. The left three figures show the individual results from the three criteria, shown in blue. The areas with higher criterion values imply the higher probability of containing GDEs. These three results were synthesized together to generate the five likelihood groups in Figure 5.3. The right three figures show the relationship between each two criteria, shown in green. The areas with the highest agreement imply the two criteria had the same results in these areas.

We analyzed the results to determine if the three criteria each contained distinct information on GDEs. For one vegetation pixel, if two criteria yielded the same results, we considered that these criteria had the highest agreement. For example, if both Criteria One and Two classified a pixel into Group 5, they had highest agreement in this pixel; if they classified the pixel into Groups 1 and 5, they had the lowest agreement. Similarity maps for each pair of criteria are shown in Figure 5.2 (parts d, e, and f). The results indicated that Criteria One and Two had the highest agreement over wetlands, and the lowest agreement in shrublands. Therefore, if the results of Criteria One and Two were summed, their combination would strengthen the final results in wetlands and would help ameliorate the disadvantage of Criterion One in shrublands. Criteria One and Three also had the highest agreement in wetlands, but the lowest agreement in evergreen forests s; Criteria Two and Three had the highest agreement in deciduous forests s, but the lowest agreement in the wetlands s. In general, Criteria One and Two had the most distinct results (Figure 5.2d): 14% of the total vegetation cover had the highest agreement and 9% had the lowest. Criteria Two and Three had the most similar results (Figure 5.2f), with 27% in this highest agreement category and 2% in the lowest agreement category.

Combination of Three Criteria

Across the Edwards Aquifer, the sum of the three criteria ranged from 3 to 15. The K-means algorithm was used to find classification thresholds for the five groups—very likely to be GDEs (values ranging from 12 to 15), likely to be GDEs (10 to 11),

about as likely as not to be GDEs (8 to 9), unlikely to be GDEs (6 to 7) and very unlikely to be GDEs (3 to 5). The five groups, from "Very Likely" to "Very Unlikely," were 8%, 19%, 32%, 26%, and 15% of total natural vegetation covered areas, respectively (Figure 5.3). The group "Very Likely to be GDEs" was further divided into lowland and upland GDEs. Potential GDEs within 200 meters from a stream or within 500 meters around a spring or a wetland were classified as lowland GDEs. The analysis showed that 11% of the potential GDEs belonged to lowland category, with 8% occurring in riparian zones and around springs and 3% in other groundwater-fed wetlands. The remaining 89% of the potential GDEs were located in uplands, indicating that they were the dominant GDE category in the Edwards Aquifer region.

For the areas very likely to contain GDEs, we examined vegetation types, the soil depth, and the landforms to determine whether or not the remote sensing results coincided with our understanding of important GDE characteristics. While water table depths for surficial, unconfined aquifers were not available for this area, the soil data from Web Soil Survey [*USDA*, 2013] indicated that more than 99% of the study area had a water table deeper than 2 meters. Therefore, in order for vegetation to access groundwater in this area, it must possess a deep root system;. Previous studies have found that live oak, ashe juniper and mesquite are able to develop such rooting patterns [*McElrone et al.*, 2004; *Wilcox*, 2002b].

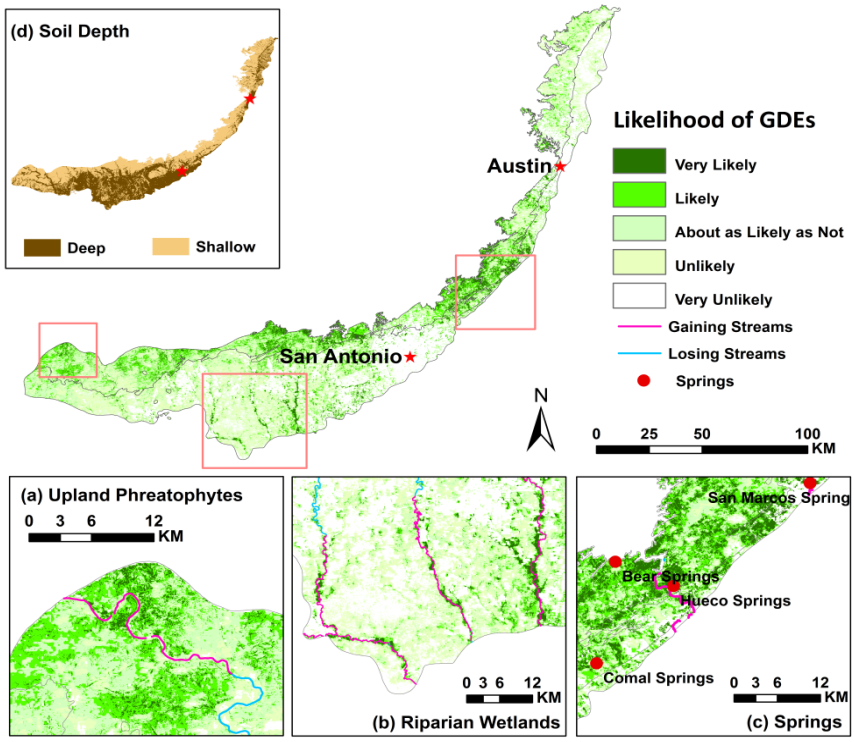

Figure 5.3 GDE Mapping in the Edwards Aquifer Using the Remote Sensing Method. Three areas were highlighted to show that GDEs were most likely to be found around springs, along the streams, and in the upland where groundwater is accessible by phreatophytes. The figure on the left corner showed the soil depth of the Edwards Aquifer region; deep soil refers to that with depths over 200 cm. A large number of pixels classified as "Very Likely to Contain GDEs" (shown in dark green color) were found on shallow soils over carbonate rocks, while the remaining were associated with deep alluvial soils.

In the Edwards Aquifer region, live oaks and ashe juniper dominated 45% of total natural vegetation, and mesquite dominated 47% [*TPWD*, 2012]. However, 81% of the potential GDEs were live oak-ashe juniper parks/woods, while only 14% were mesquite dominated forests and shrublands. We further determined that a large fraction of potential GDEs (75%) were located on shallow soils, where live oaks and ashe junipers are chiefly found (Mesquite may be located on both shallow and deep soils.)

Why is this significant? Shallow soil areas had the average soil depth of 45 cm, which places significant limits on soil water storage. As a result, vegetation may need to access groundwater to complement its water use, especially during the dry season. However, deep soil areas had depths greater than 200 cm, creating with large storage reservoirs which may be used to buffer the impacts of droughts and low rainfall periods. Therefore, plants on shallow soils exhibited a higher potential to use groundwater than those on deep soils.

Landform type was also correlated with areas highly likely to support GDEs; 66% of potential GDEs were located on ridges with shallow soils weathered from limestone, and 9% were located on plains covered by shallow soils, also weathered from limestone (Figure 5.3a and c). The remaining GDEs were found on deep soils, mainly near streams (Figure 5.3b) with alluvial deposits: 10% on flood plains 12% on stream terraces and their erosion remnants, and 3% on paleoterraces.

In the Edwards Aquifer region, the total area potentially hosting GDEs was 840 km^2. Assuming 90 mm/year of groundwater is consumed by GDEs, based on literature estimates [*Orellana et al.,* 2012], a total of 2.0×10^{10} gallons of groundwater is used by the potential GDEs every year in the Edwards aquifer region. For comparison, this rate of water consumption is nearly 30% of the annual net groundwater use of the City of San Antonio [*TWDB*, 2013b], indicating the significance of GDEs to groundwater management.

Conclusions

We proposed a methodological framework to identify potential groundwater dependent ecosystems and applied it to map GDEs in Texas. To address the different management requirements at various scales, we developed a two-step approach for the state/province scale using GIS and the aquifer/basin scale using remote sensing-based techniques. We produced state scale *GDE index* maps for GMAs and HUC-6s in Texas and aquifer/basin scale, 30×30 meter resolution maps of potential GDEs distributions in the Edwards Aquifer region. The *GDE index* maps aimed to identify critical regions with vulnerable GDEs. These GDE index maps indicated that areas in central Texas, which host streams with high baseflow ratios, numerous springs, large areas of phreatophyte species, and groundwater-fed wetlands, had a high potential to contain a significant amount of GDEs.

The remote sensing-based analysis aimed to identify GDEs for more specific management and study; in this case, the Edwards Aquifer region was used as a demonstration of the method. Three criteria were developed, and these captured the physiologic signature of groundwater use associated with different plant functional types. Analysis of the criteria showed that each had identifiable biases when assessing plant groundwater use. Criterion One captured the potential groundwater use of wetlands, but failed to capture it in shrublands and evergreen forests, due to the impact of their low vegetation density on NDVI. This disadvantage was eliminated by Criterion Two, but Criterion Two failed to capture the deciduous forests due to their relatively fast

seasonal changes in their leaf areas. These impacts were mitigated by Criterion Three, but Criterion Three failed to capture the groundwater use potential of wetlands. Three criteria were combined together to ameliorate their disadvantages and yield a final detailed map of the locations of potential GDEs. The results indicated that not all plants belonging to phreatophyte species or within wetlands were groundwater dependent. Only 9% of the total phreatophytes and 31% of woody and herbaceous wetlands were classified as having the highest potential to use groundwater. Soil depth and landforms were found to be the critical factors impacting vegetation groundwater use. Of potential GDEs, 75% were found on ridges and plains with shallow soils. The remaining 25% of potential GDEs were located on soils deeper than 200 cm, and these were mainly associated with streams.

The proposed methods had several limitations. In the GDE index method, phreatophytes, woody wetlands and emergent herbaceous wetlands were considered as the *vegetative indicators*. However, this assumption led to overestimation of the potential GDEs, as compared to the independent remote sensing-based results. In some instances, the overestimated *vegetative index* values may have overwhelmed the effect of the *hydrological index* on the overall *GDE index*. In the remote sensing-based method, due to the relatively coarse spatial resolution of the satellite images from Landsat ETM+ and MODIS, vegetation pixels with mixed vegetation coverage (e.g., phreatophytes mixed with bare soil or grasses) may have NDVI changes that do not accurately reflect the actual vegetation water use pattern. Also, the Criteria Two and Three results from MODIS data were resampled to 30×30 meters resolution, which produced some loss of

information. Finally, due to the lack of previous GDE studies in our study area, future field studies are needed to fully verify the results produced by the remote sensing method.

In summary, this two-step approach can provide useful GDE information for decision makers. The general understanding of the occurrence of GDEs gained from *GDE index* maps can help groundwater managers screen areas and integrate the consideration of GDEs into management practices. Detailed GDE distributions obtained from remote sensing provides researchers with a guiding tool for the study of GDEs, indicating priority areas for field-based assessment and monitoring. The results can also be used in numerical models intended to simulate the groundwater use of GDEs and their potential impacts on water supply, including the tools developed by the Texas Groundwater Availability Modeling program [*TWDB*, 2013a]. In addition, the remote sensing-based method highlights the potential to use satellites to remotely monitor GDE dynamics and health under changing hydrological and climatological conditions.

CHAPTER VI

SUMMARY

The interactions between groundwater and vegetation have received more attention in recent years because of the potential impacts of groundwater extraction and climate changes on the health of groundwater dependent ecosystems (GDEs), and the potential influence of GDE groundwater consumption on anthropogenic water availability. GDEs act as a critical linkage to tightly couple groundwater, soil and atmosphere dynamics. The efforts to explore GDEs and their complex interactions and feedbacks in water and energy dynamics from local and regional scale to global scale can provide valuable information for sustainable water and ecosystem management under the stresses of increasing water demand and climate change. This dissertation aimed to improve the understanding of the plant-groundwater interactions from plant scale, local scale to large regional scale.

Several useful tools were developed to address different objectives in the studies of plant-groundwater interactions. The plant scale model developed in Chapter II was a physically-based modeling tool, which proposed new functions for the simulations of root water uptake, hydraulic redistribution (HR) and plant water stress. This model was used to test the basic mechanism of plant groundwater use and demonstrated good performance in capturing transpiration, soil moisture and leaf water stress. It provided a new 1-D GDE modeling module, which could be easily incorporated into spatial distributed land surface models to represent GDEs. Chapter III proposed an example

how to incorporate the plant scale model in Chapter II into land surface model. These new functions were implemented into a groundwater-land surface model, ParFlow.CLM. The modified ParFlow.CLM was tested in long term simulation to prove its performance in capturing temporal and spatial water and energy dynamics. This model can be used to simulate the impacts of GDEs on groundwater and baseflow in large scale, which can provide information about the effects of removing/restoring GDEs on regional water balance. It can also be used to simulate the interactions and feedbacks of GDEs and atmosphere, which can help understand the impacts of GDE groundwater use on climate prediction and the potential risks of GDEs caused by climate change. The two models in Chapter II and III have other utilizations in scientific studies and resource management. For example, Chapter IV provided an example how these models could be used to test the impacts of potential decreasing of water table. It also highlighted the potential to use these models to understand field data collected from various sites with different soil types. In Chapter V, a remote sensing based framework was proposed to identify GDE distribution at large scale. The method should prove useful for land mangers needing to prioritize conservation and restoration efforts. It also highlighted the potential to document the change in GDEs through time using satellite data. In addition, the combination of the model in Chapter III and the GDE identification method in Chapter V could provide powerful tools for future groundwater management. For example, the GDE map generated using the method in Chapter V could be used as the input land cover data with GDEs and non-GDEs for the model in Chapter III, and the model could simulate how these GDEs impact local and regional water availability of human. The

model could also simulate how groundwater extraction and drought influence GDE health and distribution, which could be monitored by the method in Chapter V using remote sensing.

Using these modeling and mapping tools, this dissertation revealed a series of important scientific findings.

- The model in Chapter II demonstrated that the linear relationship between the loss of hydraulic conductance in roots and the changes of stomatal conductance can be used to simulate plant water stress, which highlighted a new and tractable modeling method for future studies of plant water stress. Both HR and plant groundwater use acted as short-term protection mechanisms for the blue oaks at the Tonzi site, which prevented hydraulic dysfunction in GSPAC during dry season. However, if the oaks relied too much on these protections, they could use more groundwater and waste valuable soil water.
- The study in Chapter III further explored that plant groundwater use was tightly related to plant soil water use. The blue oaks at Tonzi site switched to use more groundwater when soil water was depleted. This finding highlighted an interesting critical point that the starting time of groundwater use occurred when surface soil water content dropped around the point of inflection in soil water retention curve. In addition, it also highlighted that plant water source switched temporally, which implied that the soil moisture memories at different depths linked to atmosphere at different time. This finding could have implications in future studies of land surface-climate model in climate prediction. The model in

Chapter III was capable of capturing the detailed processes of both hydraulic lift and hydraulic descent in both tree active and dormant seasons. The detailed information on HR revealed the time and driving forces of HR: hydraulic lift usually occurred during dry seasons, while hydraulic descent happened following the rainfall pulses. The magnitude of hydraulic descent did not only depend on precipitation, but also related to potential gradients among layers. Hydraulic descent could move water from even small rainfalls into deeper soils, which could have important ecohydrological impacts in arid areas.

- The scenario tests in Chapter IV examined the influences of HR, soil textures, groundwater and root distribution on the whole GSPAC system. The HR scenario demonstrated several ecohydrologcial impacts of HR found in previous model and field studies, including increasing dry season transpiration, preventing hydraulic dysfunction, and moving precipitation into deeper soil. The scenario with different soil textures generally matched the findings in previous studies that, comparing to the plants in coarser soil, the plants in finer soil used more water in shallower soil layer, experienced lower soil potential, had more severe cavitation in shallow roots, and were expected to develop the roots with less hydraulic conductivity but more cavitation resistance. More tap roots accessing groundwater and shallower groundwater table had the similar impacts because groundwater uptake was less energy consuming in these cases. All four scenarios in Chapter IV highlighted that these impacts had distinct seasonal changes

between dry and wet seasons, which implied climate was also a critical factor to control GSPAC system.

- The GDE distribution identified in Chapter V revealed that GDEs were most likely to locate in shallow soil areas in Edwards Aquifer region in Texas. The GDEs in deep soil areas were usually near streams.

These scientific findings can be used to guide water and ecosystem management in future. For example, the GDE identification in Chapter V could be used to find the hotspots where GDEs had high risks due to surrounding groundwater extraction. Using the model in Chapter III to simulate the impacts of groundwater extraction on GDEs could help optimize the location of groundwater extraction. Another example is based on the findings in Chapter IV that the decreasing of water table had severe impacts on GDE water use only during dry seasons. It provided information to optimize the timing of groundwater extraction.

This dissertation also suggested two specific questions for future research: 1) How do groundwater uptake and soil water uptake link together? More evidence from other sites is needed to examine whether the point of inflection in soil water retention curve relates to the shift from soil water uptake to groundwater uptake. If so, how do the different climates, soil textures, plant characteristics, and groundwater depth combine together to impact the switch of plant water sources? 2) How do the soil moisture memories at different depths link to atmosphere through transpiration at different times? This phenomenon may impact long-term soil moisture and ET simulation and further

impact climate prediction. It is needed to test the magnitude of such impacts to determine whether future land surface-climate models should address this problem.

REFERENCES

Amenu, G. G., and P. Kumar (2008), A model for hydraulic redistribution incorporating coupled soil-root moisture transport, *Hydrol. Earth Syst. Sci.*, *12*(1), 55-74.

Anyah, R. O., C. P. Weaver, G. Miguez-Macho, Y. Fan, and A. Robock (2008), Incorporating water table dynamics in climate modeling: 3. Simulated groundwater influence on coupled land-atmosphere variability, *J. Geophys. Res.*, *113*(D7), D07103., doi: 10.1029/2007JD009087.

Atchley, A. L., and R. M. Maxwell (2011), Influences of subsurface heterogeneity and vegetation cover on soil moisture, surface temperature and evapotranspiration at hillslope scales, *Hydrogeol. J.*, *19*(2), 289-305.

Baldocchi, D. D. (2012), Tonzi and Vaira Ranches Document (AmeriFlux Site: Ione, CA). *http://nature.berkeley.edu/biometlab/pdf/tonzi%20site%20document.pdf. Accessed December, 2012.*

Baldocchi, D. D., and L. K. Xu (2007), What limits evaporation from Mediterranean oak woodlands - The supply of moisture in the soil, physiological control by plants or the demand by the atmosphere?, *Adv. Water Resour.*, *30*(10), 2113-2122.

Baldocchi, D. D., L. Xu, and N. Kiang (2004), How plant functional-type, weather, seasonal drought, and soil physical properties alter water and energy fluxes of an oak–grass savanna and an annual grassland, *Agr. Forest Meteorol.*, *123*(1), 13-39.

Baldocchi, D. D., Q. Chen, X. Chen, S. Ma, G. Miller, Y. Ryu, J. Xiao, R. Wenk, and J. Battles (2010), The Dynamics of Energy, Water, and Carbon Fluxes in a Blue Oak

(Quercus douglasii) Savanna in California, *Ecosystem Function in Savannas: Measurement and Modeling at Landscape to Global Scales*. edited by Michael J. Hill and Niall P. Hanan and published by CRC/Taylor and Francis. pp 135-151. Boca Raton, FL.

Baldwin, C. K., F. H. Wagner, and U. Lall (2003), Water Resources, in *Rocky Mountain/Great Basin Regional Climate-Change Assessment. Report for the U.S. Global Change Research Program.*, edited by F. H. Wagner, pp. 79-112, Utah State University, Logan, UT.

Barron, O. V., Emelyanova, I., Van Niel, T. G., Pollock, D. and Hodgson, G. (2012), Mapping groundwater-dependent ecosystems using remote sensing measures of vegetation and moisture dynamics, *Hydrol. Process*. doi: 10.1002/hyp.9609.

Bauerle, T., J. Richards, D. Smart, and D. Eissenstat (2008), Importance of internal hydraulic redistribution for prolonging the lifespan of roots in dry soil, *Plant, Cell Environ.*, *31*(2), 177-186.

Bertrand, G., N. Goldscheider, J. M. Gobat, and D. Hunkeler (2012), Review: From multi-scale conceptualization to a classification system for inland groundwater-dependent ecosystems, *Hydrogeol. J.*, *20*(1), 1-21.

Bleby, T. M., A. J. McElrone, and R. B. Jackson (2010), Water uptake and hydraulic redistribution across large woody root systems to 20 m depth, *Plant Cell Environ.*, *33*(12), 2132-2148.

Brown, J., L. Bach, A. Aldous, A. Wyers, and J. DeGagné (2010), Groundwater-dependent ecosystems in Oregon: an assessment of their distribution and associated threats, *Front. Ecol. Environ.*, *9*(2), 97-102.

Brune, G. (1975), Major and Historical Springs of Texas., *Texas Water Development Board Report 189. http://www.twdb.texas.gov/publications/reports/numbered_reports/doc/R189/Report189.asp. Accessed December, 2011.*

Burgess, S. S., M. A. Adams, N. C. Turner, and C. K. Ong (1998), The redistribution of soil water by tree root systems, *Oecologia*, *115*(3), 306-311.

Busch, D. E., N. L. Ingraham, and S. D. Smith (1992), Water-uptake in woody riparian phreatophytes of the southwestern United States-A stable isotope study, *Ecol. Appl.*, *2*(4), 450-459.

Butler Jr, J. J., G. J. Kluitenberg, D. O. Whittemore, S. P. Loheide II, W. Jin, M. A. Billinger, and X. Zhan (2007), A field investigation of phreatophyte-induced fluctuations in the water table, *Water Resour. Res.*, *43*(2), W02404, doi:10.1029/2005WR004627.

Caldwell, M. M., and J. H. Richards (1989), Hydraulic lift: water efflux from upper roots improves effectiveness of water uptake by deep roots, *Oecologia*, *79*(1), 1-5.

Caldwell, M. M., T. E. Dawson, and J. H. Richards (1998), Hydraulic lift: consequences of water efflux from the roots of plants, *Oecologia*, *113*(2), 151-161.

Canadell, J., R. B. Jackson, J. R. Ehleringer, H. A. Mooney, O. E. Sala, and E. D. Schulze (1996), Maximum rooting depth of vegetation types at the global scale, *Oecologia*, *108*(4), 583-595.

Canty, M. J. (2007), *Image analysis, classification and change detection in remote sensing: with algorithms for ENVI/IDL*, CRC Press. Boca Raton, FL.

Carlson, T. N., and D. A. Ripley (1997), On the relation between NDVI, fractional vegetation cover, and leaf area index, *Remote Sens. Environ.*, *62*(3), 241-252.

Chen, Q., D. D. Baldocchi, P. Gong, and T. E. Dawson (2008), Modeling radiation and photosynthesis of a heterogeneous savanna woodland landscape with a hierarchy of model complexities, *Agr. Forest Meteorol.*, *148*(6), 1005-1020.

Chen, X., and Q. Hu (2004), Groundwater influences on soil moisture and surface evaporation, *J. Hydrol.*, *297*(1), 285-300.

Chen, X. Y., Y. Rubin, S. Y. Ma, and D. D. Baldocchi (2008), Observations and stochastic modeling of soil moisture control on evapotranspiration in a Californian oak savanna, *Water Resour. Res.*, *44*(8), doi: W08409 10.1029/2007wr006646.

Cochard, H., and M. T. Tyree (1990), Xylem dysfunction in quercus - vessel sizes, tyloses, cavitation and seasonal-changes in embolism, *Tree Physiol.*, *6*(4), 393-407.

Cowan, I. (1965), Transport of water in the soil-plant-atmosphere system, *J. Appl. Ecol.*, 221-239.

Dai, X. P., X. Zeng, and C. D. Dickinson (2001), The Common Land Model (CLM): Technical documentation and user's guide. *http://igwmc.mines.edu/short-course/ParFlow/clm_user_guide.pdf. Accessed August, 2010.*

Dawson, T. E. (1993), Hydraulic lift and water-use by plants - implications for water-balance, performance and plant-plant interactions, *Oecologia*, *95*(4), 565-574.

Dawson, T. E. (1996), Determining water use by trees and forests from isotopic, energy balance and transpiration analyses: The roles of tree size and hydraulic lift, *Tree Physiol.*, *16*(1-2), 263-272.

Dawson, T. E., and J. S. Pate (1996), Seasonal water uptake and movement in root systems of Australian phraeatophytic plants of dimorphic root morphology: A stable isotope investigation, *Oecologia*, *107*(1), 13-20.

Domec, J.-C., J. Warren, F. Meinzer, J. Brooks, and R. Coulombe (2004), Native root xylem embolism and stomatal closure in stands of Douglas-fir and ponderosa pine: mitigation by hydraulic redistribution, *Oecologia*, *141*(1), 7-16.

Domec, J. C., F. G. Scholz, S. J. Bucci, F. C. Meinzer, G. Goldstein, and R. Villalobos-Vega (2006), Diurnal and seasonal variation in root xylem embolism in neotropical savanna woody species: impact on stomatal control of plant water status, *Plant Cell Environ.*, *29*(1), 26-35.

Doody, T. M., and R. G. Benyon (2011), Direct measurement of groundwater uptake through tree roots in a cave, *Ecohydrology*, *4*(5), 644-649.

Dresel, P. E., R. Clark, X. Cheng, M. Reid, J. Fawcett, and D. Cochraine (2010), Mapping Terrestrial Groundwater Dependent Ecosystems: Method Development and Example Output, edited, Victoria Department of Primary Industries, Melbourne, VIC, Australia.

http://vro.depi.vic.gov.au/dpi/vro/vrosite.nsf/pages/lwm_mapping_terrestrial_gwater_dep_ecosystems_pdf/$FILE/mapping_terrestrial_gwater_dep_ecosystems_fp_toc.pdf. Accessed March, 2011.

Eamus, D., and R. Froend (2006), Groundwater-dependent ecosystems: the where, what and why of GDEs, *Aust. J. Bot.*, *54*(2), 91-96.

Eamus, D., R. Froend, R. Loomes, G. Hose, and B. Murray (2006), A functional methodology for determining the groundwater regime needed to maintain the health of groundwater-dependent vegetation, *Aust. J. Bot.*, *54*(2), 97-114.

Ehleringer, J., and T. Dawson (1992), Water uptake by plants: perspectives from stable isotope composition, *Plant, Cell Environ.*, *15*(9), 1073-1082.

Elmore, A. J., J. F. Mustard, and S. J. Manning (2003), Regional patterns of plant community response to changes in water: Owens Valley, California, *Ecological Applications*, *13*(2), 443-460.

Emerman, S. H., and T. E. Dawson (1996), Hydraulic lift and its influence on the water content of the rhizosphere: an example from sugar maple, Acer saccharum, *Oecologia*, *108*(2), 273-278.

Fan, Y., and G. Miguez-Macho (2010), Potential groundwater contribution to Amazon evapotranspiration, *Hydrol. Earth Syst. Sci.*, *14*(10), 2039-2056.

Fan, Y., G. Miguez-Macho, P. Weaver, R. Walko, and A. Robock (2007), Incorporating water table dynamics in climate modeling: 1. Water table observations and equilibrium water table simulations, *J. Geophys. Res.*, *112*(D10), D10125, doi: 10.1029/2006JD008111.

Feddes, R. A., P. Kowalik, and H. Zaradny (1978), *Simulation of field water use and crop yield*, Centre for Agricultural Publishing and Documentation., Wageningen.

Feddes, R. A., et al. (2001), Modeling root water uptake in hydrological and climate models, *Bull. Am. Meteorol. Soc.*, *82*(12), 2797-2809.

Federer, C. A. (1979), Soil-plant-atmosphere model for transpiration and availability of soil-water, *Water Resour. Res.*, *15*(3), 555-562.

Ferguson, I. M., and R. M. Maxwell (2010), Role of groundwater in watershed response and land surface feedbacks under climate change, *Water Resour. Res.*, *46*, W00f02, doi: 10.1029/2009wr008616.

Foken, T. (2008), The energy balance closure problem: An overview, *Ecol. Appl.*, *18*(6), 1351-1367.

Forrester, J. W. (2007), System dynamics - a personal view of the first fifty years, *System Dynamics Review*, *23*(2-3), 345-358.

Gardner, W. (1960), Dynamic aspects of water availability to plants, *Soil Sci.*, *89*(2), 63.

Gardner, W. R. (1965), Dynamic aspects of soil-water availability to plants, *Annu. Rev. Plant Physio.*, *16*, 323, doi: 10.1146/annurev.pp.16.060165.001543.

Gardner, W. R., and C. F. Ehlig (1962), Impedance to water movement in soil and plant, *Science*, *138*(3539), 522, doi: 10.1126/science.138.3539.522.

Goedhart, C. M., and D. E. Pataki (2010), Ecosystem effects of groundwater depth in Owens Valley, California, *Ecohydrology*, *4*(3), 458-468.

Gou, S., and G. Miller (2013), A groundwater-soil-plant-atmosphere continuum approach for modeling water stress, uptake, and hydraulic redistribution in phreatophytic vegetation, *Ecohydrology*, doi: 10.1002/eco.1427.

Gusev, Y. M., and O. N. Nasonova (2002), The simulation of heat and water exchange at the land-atmosphere interface for the boreal grassland by the land-surface model SWAP, *Hydrol. Processes*, *16*(10), 1893-1919.

Gutowski Jr, W. J., C. J. Vörösmarty, M. Person, Z. Ötles, B. Fekete, and J. York (2002), A coupled land-atmosphere simulation program (CLASP): Calibration and validation, *J. Geophys. Res.*, *107*(D16), 4283, doi: 10.1029/2001JD000392.

Hacke, U. G., J. S. Sperry, B. E. Ewers, D. S. Ellsworth, K. V. R. Schafer, and R. Oren (2000), Influence of soil porosity on water use in Pinus taeda, *Oecologia*, *124*(4), 495-505.

Howard, J., and M. Merrifield (2010), Mapping groundwater dependent ecosystems in California, *PloS one*, *5*(6), e11249. doi: 10.1371/journal.pone.0011249.

Hultine, K., D. Williams, S. Burgess, and T. Keefer (2003), Contrasting patterns of hydraulic redistribution in three desert phreatophytes, *Oecologia*, *135*(2), 167-175.

Hultine, K., R. Scott, W. Cable, D. Goodrich, and D. Williams (2004), Hydraulic redistribution by a dominant, warm-desert phreatophyte: Seasonal patterns and response to precipitation pulses, *Funct. Ecol.*, *18*(4), 530-538.

Huxman, T. E., B. P. Wilcox, D. D. Breshears, R. L. Scott, K. A. Snyder, E. E. Small, K. Hultine, W. T. Pockman, and R. B. Jackson (2005), Ecohydrological implications of woody plant encroachment, *Ecology*, *86*(2), 308-319.

Ishikawa, C. M., and C. Bledsoe (2000), Seasonal and diurnal patterns of soil water potential in the rhizosphere of blue oaks: evidence for hydraulic lift, *Oecologia*, *125*(4), 459-465.

Jackson, R. B., J. S. Sperry, and T. E. Dawson (2000), Root water uptake and transport: using physiological processes in global predictions, *Trends Plant Sci.*, *5*(11), 482-488.

Jackson, R. B., L. A. Moore, W. A. Hoffmann, W. T. Pockman, and C. R. Linder (1999), Ecosystem rooting depth determined with caves and DNA, *Proc. Nat. Acad. Sci. U.S.A.*, *96*(20), 11387-11392.

Jackson, R. B., J. Canadell, J. R. Ehleringer, H. A. Mooney, O. E. Sala, and E. D. Schulze (1996), A global analysis of root distributions for terrestrial biomes, *Oecologia*, *108*(3), 389-411.

Jiang, X., G. Y. Niu, and Z. L. Yang (2009), Impacts of vegetation and groundwater dynamics on warm season precipitation over the Central United States, *J. Geophys. Res*, *114*, D06109, doi: 10.1029/2008JD010756.

Jones, J. E., and C. S. Woodward (2001), Newton-Krylov-multigrid solvers for large-scale, highly heterogeneous, variably saturated flow problems, *Adv. Water Resour.*, *24*(7), 763-774.

Kollet, S. J., and R. M. Maxwell (2006), Integrated surface-groundwater flow modeling: A free-surface overland flow boundary condition in a parallel groundwater flow model, *Adv. Water Resour.*, *29*(7), 945-958.

Kollet, S. J., and R. M. Maxwell (2008), Capturing the influence of groundwater dynamics on land surface processes using an integrated, distributed watershed model, *Water Resour. Res.*, *44*(2), W02402, doi: 10.1029/2007WR006004.

Koster, R. D., and M. J. Suarez (2001), Soil moisture memory in climate models, *J. Hydrometeorol.*, *2*(6), 558-570.

Laio, F., A. Porporato, L. Ridolfi, and I. Rodriguez-Iturbe (2001), Plants in water-controlled ecosystems: active role in hydrologic processes and response to water stress-II. Probabilistic soil moisture dynamics, *Adv. Water Resour.*, *24*(7), 707-723.

Laio, F., S. Tamea, L. Ridolfi, P. D'Odorico, and I. Rodriguez-Iturbe (2009), Ecohydrology of groundwater-dependent ecosystems: 1. Stochastic water table dynamics, *Water Resour. Res.*, *45*, doi: W0541910.1029/2008wr007292.

Lautz, L. K. (2008), Estimating groundwater evapotranspiration rates using diurnal water-table fluctuations in a semi-arid riparian zone, *Hydrogeol. J.*, *16*(3), 483-497.

Lawrence, D. M., P. E. Thornton, K. W. Oleson, and G. B. Bonan (2007), The partitioning of evapotranspiration into transpiration, soil evaporation, and canopy evaporation in a GCM: Impacts on land-atmosphere interaction, *J. Hydrometeorol.*, *8*(4), 862-880.

Lee, J. E., R. S. Oliveira, T. E. Dawson, and I. Fung (2005), Root functioning modifies seasonal climate, *Proc. Nat. Acad. Sci. U.S.A.*, *102*(49), 17576-17581.

Lewis, D., and R. H. Burgy (1964), The Relationship between Oak Tree Roots and Groundwater in Fractured Rock As Determined by Tritium Tracing, *J. Geophys. Res.*, *69*(12), 2579-2588.

Liang, X., Z. Xie, and M. Huang (2003), A new parameterization for surface and groundwater interactions and its impact on water budgets with the variable infiltration capacity (VIC) land surface model, *J. Geophys. Res.*, *108*(D16), 8613, doi: 10.1029/2002JD003090.

Loheide, S. P. (2008), A method for estimating subdaily evapotranspiration of shallow groundwater using diurnal water table fluctuations, *Ecohydrology*, *1*(1), 59-66.

Loheide, S. P., and S. M. Gorelick (2005), A local-scale, high-resolution evapotranspiration mapping algorithm (ETMA) with hydroecological applications at riparian meadow restoration sites, *Remote Sens. Environ.*, *98*(2), 182-200.

Loheide, S. P., and S. M. Gorelick (2007), Riparian hydroecology: a coupled model of the observed interactions between groundwater flow and meadow vegetation patterning, *Water Resour. Res.*, *43*(7). W07414, doi:10.1029/2006WR005233.

Loheide, S. P., J. J. Butler, and S. M. Gorelick (2005), Estimation of groundwater consumption by phreatophytes using diurnal water table fluctuations: A saturated-unsaturated flow assessment, *Water Resour. Res.*, *41*(7), doi: W07030 10.1029/2005wr003942.

Loheide, S. P., R. S. Deitchman, D. J. Cooper, E. C. Wolf, C. T. Hammersmark, and J. D. Lundquist (2009), A framework for understanding the hydroecology of impacted wet meadows in the Sierra Nevada and Cascade Ranges, California, USA, *Hydrogeol. J.*, *17*(1), 229-246.

Lowry, C. S., S. P. Loheide II, C. E. Moore, and J. D. Lundquist (2011), Groundwater controls on vegetation composition and patterning in mountain meadows, *Water Resour. Res.*, *47*(10), W00J11, doi:10.1029/2010WR010086.

Ludwig, F., T. E. Dawson, H. de Kroon, F. Berendse, and H. H. Prins (2003), Hydraulic lift in Acacia tortilis trees on an East African savanna, *Oecologia*, *134*(3), 293-300.

Ma, S. Y., D. D. Baldocchi, L. K. Xu, and T. Hehn (2007), Inter-annual variability in carbon dioxide exchange of an oak/grass savanna and open grassland in California, *Agr. Forest Meteorol.*, *147*(3-4), 157-171.

MacQueen, J. (1967), Some methods for classification and analysis of multivariate observations, paper presented at Proceedings of the fifth Berkeley symposium on mathematical statistics and probability, California, USA.

Martinet, M. C., E. R. Vivoni, J. R. Cleverly, J. R. Thibault, J. F. Schuetz, and C. N. Dahm (2009), On groundwater fluctuations, evapotranspiration, and understory removal in riparian corridors, *Water Resour. Res.*, *45*(5), W05425, doi:10.1029/2008WR007152.

Matzner, S. L., K. J. Rice, and J. H. Richards (2001), Intra-specific variation in xylem cavitation in interior live oak (Quercus wislizenii A. DC.), *J. Exp. Bot.*, *52*(357), 783-789.

Maxwell, R. M., and N. L. Miller (2005), Development of a coupled land surface and groundwater model, *J. Hydrometeorol.*, *6*(3), 233-247.

Maxwell, R. M., J. K. Lundquist, J. D. Mirocha, S. G. Smith, C. S. Woodward, and A. F. Tompson (2011), Development of a coupled groundwater-atmosphere model, *Mon. Weather Rev.*, *139*(1), 96-116.

McElrone, A. J., W. T. Pockman, and R. B. Jackson (2003), The contribution of deep roots to the water cycle: Seasonal patterns of water uptake and hydraulic lift from below 7 m on the Edwards Plateau, Texas, *Eos Trans. AGU, Fall Meet. Suppl.*, *84*(46), Abstract H32C-0581.

McElrone, A. J., W. T. Pockman, J. Martinez-Vilalta, and R. B. Jackson (2004), Variation in xylem structure and function in stems and roots of trees to 20 m depth, *New Phytol.*, *163*, 507-517.

Meinzer, F. C., M. J. Clearwater, and G. Goldstein (2001), Water transport in trees: current perspectives, new insights and some controversies, *Environ. Exp. Bot.*, *45*(3), 239-262.

Meinzer, F. C., J. L. Andrade, G. Goldstein, N. M. Holbrook, J. Cavelier, and S. J. Wright (1999), Partitioning of soil water among canopy trees in a seasonally dry tropical forest, *Oecologia*, *121*(3), 293-301.

Mendel, M., S. Hergarten, and H. Neugebauer (2002), On a better understanding of hydraulic lift: a numerical study, *Water Resour. Res.*, *38*(10), 1183, doi: 10.1029/2001WR000911.

Miguez-Macho, G., and Y. Fan (2012a), The role of groundwater in the Amazon water cycle: 2. Influence on seasonal soil moisture and evapotranspiration, *J. Geophys. Res.: A.(1984–2012)*, *117*(D15), doi: 10.1029/2012JD017540.

Miguez-Macho, G., and Y. Fan (2012b), The role of groundwater in the Amazon water cycle: 1. Influence on seasonal streamflow, flooding and wetlands, *J. Geophys. Res.: A. (1984–2012)*, *117*(D15), doi: 10.1029/2012JD017539.

Miller, G. R. (2009), Measuring and Modeling Interactions Between Groundwater, Soil Moisture, and Plant Transpiration in Natural and Agricultural Ecosystems, University Of California, Berkeley.

Miller, G. R., X. Chen, D. Baldocchi, and Y. Rubin (2010), Groundwater uptake by woody vegetation in a Mediterranean oak savanna, *Water Resour. Res.*, *46*, W10503, doi: 10.1029/2009WR008902.

Miller, G. R., X. Y. Chen, Y. Rubin, S. Y. Ma, and D. D. Baldocchi (2010a), Groundwater uptake by woody vegetation in a semiarid oak savanna, *Water Resour. Res.*, *46*, W10503, doi:10.1029/2009wr008902.

Miller, G. R., X. Y. Chen, Y. Rubin, S. Y. Ma, and D. D. Baldocchi (2010b), Groundwater uptake by woody vegetation in a semiarid oak savanna, *Water Resour. Res.*, *46*, W10503, doi: 10.1029/2009wr008902.

Miller, G. R., J. M. Cable, A. K. McDonald, B. Bond, T. E. Franz, L. X. Wang, S. Gou, A. P. Tyler, C. B. Zou, and R. L. Scott (2012), Understanding ecohydrological connectivity in savannas: a system dynamics modelling approach, *Ecohydrology*, *5*(2), 200-220.

Münch, Z., and J. Conrad (2007), Remote sensing and GIS based determination of groundwater dependent ecosystems in the Western Cape, South Africa, *Hydrogeol. J.*, *15*(1), 19-28.

Naumburg, E., R. Mata-Gonzalez, R. G. Hunter, T. McLendon, and D. W. Martin (2005), Phreatophytic vegetation and groundwater fluctuations: A review of current research and application of ecosystem response modeling with an emphasis on Great Basin vegetation, *Environ. Manage.*, *35*(6), 726-740.

Neumann, R. B., and Z. G. Cardon (2012), The magnitude of hydraulic redistribution by plant roots: a review and synthesis of empirical and modeling studies, *New Phytol.*, *194*(2), 337-352.

Newman, B. D., B. P. Wilcox, S. R. Archer, D. D. Breshears, C. N. Dahm, C. J. Duffy, N. G. McDowell, F. M. Phillips, B. R. Scanlon, and E. R. Vivoni (2006), Ecohydrology of water-limited environments: A scientific vision, *Water Resour. Res.*, *42*(6), W06302, doi:10.1029/2005wr004141.

Newman, E. I. (1969), Resistance to water flow in soil and plant .i. soil resistance in relation to amounts of root - theoretical estimates, *J. Appl. Ecol.*, *6*(1), 1, doi: 10.2307/2401297.

Niu, G. Y., Z. L. Yang, R. E. Dickinson, L. E. Gulden, and H. Su (2007), Development of a simple groundwater model for use in climate models and evaluation with Gravity Recovery and Climate Experiment data, *J. Geophys. Res*, *112*, D07103, doi:10.1029/2006JD007522.

Oliveira, R. S., T. E. Dawson, S. S. O. Burgess, and D. C. Nepstad (2005), Hydraulic redistribution in three Amazonian trees, *Oecologia*, *145*(3), 354-363.

Orellana, F., P. Verma, S. P. Loheide II, and E. Daly (2012), Monitoring and modeling water-vegetation interactions in groundwater-dependent ecosystems, *Rev. Geophys.*, *50*(3), RG3003, doi: 10.1029/2011RG000383.

Osuna, J. L. (2011), Drought Tolerance in Quercus douglasii in the California Mediterranean Savanna: A study of photosynthetic functional responses, limitations, and changes during annual seasonal drought, University Of California, Berkeley.

Pockman, W. T., J. S. Sperry, and J. W. Oleary (1995), Sustained and significant negative water-pressure in xylem, *Nature*, *378*(6558), 715-716.

Pollacco, J. A., and B. P. Mohanty (2012), Uncertainties of water fluxes in soil-vegetation-atmosphere transfer models: Inverting surface soil moisture and evapotranspiration retrieved from remote sensing, *Vadose Zone J.*, *11*(3). doi:10.2136/vzj2011.0167

Porporato, A., F. Laio, L. Ridolfi, and I. Rodriguez-Iturbe (2001), Plants in water-controlled ecosystems: active role in hydrologic processes and response to water stress-III. Vegetation water stress, *Adv. Water Resour.*, *24*(7), 725-744.

Purevdorj, T., R. Tateishi, T. Ishiyama, and Y. Honda (1998), Relationships between percent vegetation cover and vegetation indices, *Int. J. Remote Sens.*, *19*(18), 3519-3535.

Quijano, J. C., P. Kumar, D. T. Drewry, A. Goldstein, and L. Misson (2012), Competitive and mutualistic dependencies in multispecies vegetation dynamics enabled by hydraulic redistribution, *Water Resour. Res.*, *48*(5), W05518, doi:10.1029/2011WR011416.

Rihani, J. F., R. M. Maxwell, and F. K. Chow (2010), Coupling groundwater and land surface processes: Idealized simulations to identify effects of terrain and subsurface heterogeneity on land surface energy fluxes, *Water Resour. Res.*, *46*(12), W12523, doi: 10.1029/2010WR009111.

Rose, K., R. Graham, and D. Parker (2003), Water source utilization by Pinus jeffreyi and Arctostaphylos patula on thin soils over bedrock, *Oecologia*, *134*(1), 46-54.

Ryel, R. J., M. M. Caldwell, C. K. Yoder, D. Or, and A. J. Leffler (2002), Hydraulic redistribution in a stand of Artemisia tridentata: evaluation of benefits to transpiration assessed with a simulation model, *Oecologia*, *130*(2), 173-184.

Ryel, R. J., A. Leffler, M. Peek, C. Ivans, and M. Caldwell (2004), Water conservation in Artemisia tridentata through redistribution of precipitation, *Oecologia*, *141*(2), 335-345.

Saliendra, N. Z., J. S. Sperry, and J. P. Comstock (1995), Influence of leaf water status on stomatal response to humidity, hydraulic conductance, and soil drought in Betula occidentalis, *Planta*, *196*(2), 357-366.

Schaap, M. G., F. J. Leij, and M. T. van Genuchten (2001), ROSETTA: a computer program for estimating soil hydraulic parameters with hierarchical pedotransfer functions, *J. Hydrol.*, *251*(3-4), 163-176.

Schaeffer, S., D. G. Williams, and D. C. Goodrich (2000), Transpiration of cottonwood/willow forest estimated from sap flux, *Agr. Forest Meteorol.*, *105*, 257-270.

Scott, R. L., W. L. Cable, and K. R. Hultine (2008a), The ecohydrologic significance of hydraulic redistribution in a semiarid savanna, *Water Resour. Res.*, *44*(2), W02440, doi: 10.1029/2007wr006149.

Scott, R. L., W. L. Cable, T. E. Huxman, P. L. Nagler, M. Hernandez, and D. C. Goodrich (2008b), Multiyear riparian evapotranspiration and groundwater use for a semiarid watershed, *J. Arid Environ.*, *72*(7), 1232-1246.

Slade, R. M., J. T. Bentley, and D. Michaud (2000), Results of Streamflow Gain-Loss Studies in Texas, With Emphasis on Gains From and Losses to Major and Minor Aquifers, *U.S. Geological Survey-Open-File Report 02-068*.

Smith, J. B., R. Richels, and B. Miller (2003), The Potential Consequences of Climate Variability and Change for the Western United States, in *Climate Change Impacts on the United States*, edited, U. S. Climate Change Science Program, Washington, D. C.

Sperry, J., J. Donnelly, and M. Tyree (1988), A method for measuring hydraulic conductivity and embolism in xylem, *Plant, Cell Environ.*, *11*(1), 35-40.

Sperry, J. S. (2000), Hydraulic constraints on plant gas exchange, *Agr. Forest Meteorol.*, *104*(1), 13-23.

Sperry, J. S., and M. T. Tyree (1988), Mechanism of water stress-induced xylem embolism, *Plant Physiol.*, *88*(3), 581-587.

Sperry, J. S., and N. Z. Saliendra (1994), Intra-plant and inter-plant variation in xylem cavitation in betula-occidentalis, *Plant Cell Environ.*, *17*(11), 1233-1241.

Sperry, J. S., and U. G. Hacke (2002), Desert shrub water relations with respect to soil characteristics and plant functional type, *Funct. Ecol.*, *16*(3), 367-378.

Sperry, J. S., N. N. Alder, and S. E. Eastlack (1993), The effect of reduced hydraulic conductance on stomatal conductance and xylem cavitation, *J. Exp. Bot.*, *44*(263), 1075-1082.

Sperry, J. S., V. Stiller, and U. G. Hacke (2003), Xylem hydraulics and the soil-plant-atmosphere continuum: Opportunities and unresolved issues, *Agron. J.*, *95*(6), 1362-1370.

Sperry, J. S., F. R. Adler, G. S. Campbell, and J. P. Comstock (1998), Limitation of plant water use by rhizosphere and xylem conductance: results from a model, *Plant Cell Environ.*, *21*(4), 347-359.

Sperry, J. S., U. G. Hacke, R. Oren, and J. P. Comstock (2002), Water deficits and hydraulic limits to leaf water supply, *Plant Cell Environ.*, *25*(2), 251-263.

Steinwand, A. L., R. F. Harrington, and D. Or (2006), Water balance for Great Basin phreatophytes derived from eddy covariance, soil water, and water table measurements, *J. Hydrol.*, *329*(3-4), 595-605.

Tamea, S., F. Laio, L. Ridolfi, P. D'Odorico, and I. Rodriguez-Iturbe (2009), Ecohydrology of groundwater-dependent ecosystems: 2. Stochastic soil moisture dynamics, *Water Resour. Res.*, *45*, doi: W0542010.1029/2008wr007293.

Texas Parks and Wildlife Department (TPWD) (2012), The Vegetation Types of Texas, edited, Texas Parks and Wildlife Department, Austin, TX.

Texas Water Development Board (TWDB) (2012), Groundwater Management Areas in Texas (GMA), edited.

Texas Water Development Board (TWDB) (2013a), Groundwater Availability Models. Texas Water Development Board. Austin, TX., *http://www.twdb.state.tx.us/groundwater/models/gam/index.asp. Accessed June, 2013.*

Texas Water Development Board (TWDB) (2013b), Historical Water Use Estimates. Texas Water Development Board. Austin, Texas. *http://www.twdb.state.tx.us/waterplanning/waterusesurvey/estimates/. Accessed June, 2013.*

Tweed, S. O., M. Leblanc, J. A. Webb, and M. W. Lubczynski (2007), Remote sensing and GIS for mapping groundwater recharge and discharge areas in salinity prone catchments, southeastern Australia, *Hydrogeol. J.*, *15*(1), 75-96.

Tyree, M. T. (1997), The Cohesion-Tension theory of sap ascent: current controversies, *J. Exp. Bot.*, *48*(315), 1753-1765.

Tyree, M. T., and J. S. Sperry (1989), Vulnerability of xylem to cavitation and embolism, *Annu. Rev. Plant Physiol. Plant Mol. Biol.*, *40*, 19-38.

Tyree, M. T., B. Sinclair, P. Lu, and A. Granier (1993), Whole shoot hydraulic resistance in quercus species measured with a new high-pressure flowmeter, *Annales Des Sciences Forestieres*, *50*(5), 417-423.

U.S. Department of Agriculture (USDA) (2013), *Soil Survey Staff, Natural Resources Conservation Service, United States Department of Agriculture. Web Soil Survey. http://websoilsurvey.nrcs.usda.gov/. Accessed October, 2013.*

U.S. Fish and Wildlife Service (USFWS) (2012), National Wetlands Inventory website. U.S. Department of the Interior, Fish and Wildlife Service, Washington, D.C. *http://www.fws.gov/wetlands/. Accessed December, 2012.*

U.S. Geological Survey (USGS) (2012a), National Land Cover Database (NLCD 2006), edited, U.S. Department of the Interior, U.S. Geological Survey, Reston, VA.

U.S. Geological Survey (USGS) (2012b), National Hydrography Dataset (NHD), edited, U.S. Department of the Interior, U.S. Geological Survey, Reston, VA.

Van Auken, O., A. Ford, and J. Allen (1981), An ecological comparison of upland deciduous and evergreen forests of central Texas, *Am. J. Bot.*, 1249-1256.

van Genuchten, M. T. (1980), A closed-form equation for predicting the hydraulic conductivity of unsaturated soils, *Soil Sci. Soc. Am. J.*, *44*(5), 892-898.

Vincke, C., and Y. Thiry (2008), Water table is a relevant source for water uptake by a Scots pine (Pinus sylvestris L.) stand: Evidences from continuous evapotranspiration and water table monitoring, *Agr. Forest Meteorol.*, *148*(10), 1419-1432.

Wahl, K. L., and T. L. Wahl (1995), Determining the Flow of Comal Springs at New Braunfels, Texas, *Texas Water '95, American Society of Civil Engineers, August 16-17, 1995, San Antonio, TX*.

Wahl, T. L., and K. L. Wahl (2007), BFI: A Computer Program for Determining an Index to Base Flow, edited, U.S. Department of the Interior, Bureau of Reclamation, Lakewood, CO.

Wang, E. L., and C. J. Smith (2004), Modelling the growth and water uptake function of plant root systems: a review, *Aust. J. Agric. Res.*, *55*(5), 501-523, doi: 10.1071/ar03201.

Wang, G. L. (2011), Assessing the potential hydrological impacts of hydraulic redistribution in Amazonia using a numerical modeling approach, *Water Resour. Res.*, *47*, W02528, doi: 10.1029/2010wr009601.

Wang, Q., J. Tenhunen, N. Q. Dinh, M. Reichstein, T. Vesala, and P. Keronen (2004), Similarities in ground-and satellite-based NDVI time series and their relationship to physiological activity of a Scots pine forest in Finland, *Remote Sens. Environ.*, *93*(1), 225-237.

White, J. W., E. R. Cook, J. R. Lawrence, and B. Wallace S (1985), The DH ratios of sap in trees: Implications for water sources and tree ring DH ratios, *Geochim. Cosmochim. Acta*, *49*(1), 237-246.

White, W. N. (1932), A method of estimating groundwater supplies based on discharge by plants and evaporation from soil - results of investigations in Escalante Valley, Utah, *Water Supply Paper Report Number 659 A, edited by U.S. Geol. Surv.*

Wilcox, B. P. (2002), Shrub control and streamflow on rangelands: A process based viewpoint, *J. Range Manag.*, 55, 318-326.

Wilcox, B. P., M. K. Owens, W. A. Dugas, D. N. Ueckert, and C. R. Hart (2006), Shrubs, streamflow, and the paradox of scale, *Hydrol. Process.*, *20*(15), 3245-3259.

Wilson, K., A. Goldstein, E. Falge, M. Aubinet, D. Baldocchi, P. Berbigier, C. Bernhofer, R. Ceulemans, H. Dolman, and C. Field (2002), Energy balance closure at FLUXNET sites, *Agr. Forest Meteorol.*, *113*(1), 223-243.

Wolock, D. M. (2003), Base-flow index grid for the conterminous United States: U.S. Geological Survey Open-File Report 03-263, edited, U.S. Geological Survey, Lawrence, KS.

Xu, L. K., and D. D. Baldocchi (2003), Seasonal trends in photosynthetic parameters and stomatal conductance of blue oak (Quercus douglasii) under prolonged summer drought and high temperature, *Tree Physiol.*, *23*(13), 865-877.

Yeh, P. J., and E. A. Eltahir (2005), Representation of water table dynamics in a land surface scheme. Part I: Model development, *J. Clim.*, *18*(12), 1861-1880.

York, J. P., M. Person, W. J. Gutowski, and T. C. Winter (2002), Putting aquifers into atmospheric simulation models: An example from the Mill Creek Watershed, northeastern Kansas, *Adv. Water Resour.*, *25*(2), 221-238.

Zeng, X. (2001), Global vegetation root distribution for land modeling, *J. Hydrometeorol.*, *2*(5), 525-530.

Zeng, X. B., Y. J. Dai, R. E. Dickinson, and M. Shaikh (1998), The role of root distribution for climate simulation over land, *Geophys. Res. Lett.*, *25*(24), 4533-4536.

Zheng, Z., and G. Wang (2007), Modeling the dynamic root water uptake and its hydrological impact at the Reserva Jaru site in Amazonia, *J. Geophys. Res.*, *112*(G4), doi: 10.1029/2007JG000413.